IVW - Schriftenreihe Band 60

Institut für Verbundwerkstoffe GmbH - Kaiserslautern

Li Chang

Friction and Wear of Nanoparticle Filled Polymer Composites

Bibliografische Information Der Deutschen Bibliothek

Die Deutsche Bibliothek verzeichnet diese Publikation in der Deutschen Nationalbibliografie; detaillierte bibliografische Daten sind im Internet über <http://dnb.ddb.de> abrufbar.

Bibliographic information published by Die Deutsche Bibliothek

Die Deutsche Bibliothek lists this publication in the Deutsche Nationalbibliografie; detailed bibliographic data is available in the Internet at <http://dnb.ddb.de>.

Herausgeber: Institut für Verbundwerkstoffe GmbH
Prof. Dr.-Ing. Alois K. Schlarb
Erwin-Schrödinger-Straße
TU Kaiserslautern, Gebäude 58
67663 Kaiserslautern
http://www.ivw.uni-kl.de

Verlag: Institut für Verbundwerkstoffe GmbH

Druck: Technische Universität Kaiserslautern
ZBT – Abteilung Foto-Repro-Druck

D 386

Als Manuskript gedruckt. Printed in Germany.

ISSN 1615-021X
ISBN 3-934930-56-5

Friction and Wear of Nanoparticle Filled Polymer Composites

Vom Fachbereich Maschinenbau und Verfahrenstechnik
der Technischen Universität Kaiserslautern
zur Erlangung des akademischen Grades

Doktor-Ingenieur (Dr.-Ing.)

genehmigte Dissertation

vorgelegt von

M.S. Li Chang

aus China

Tag der mündlichen Prüfung: 23. Aug. 2005

Prüfungsvorsitzender:
1. Berichterstatter: Prof. Dr.-Ing. Dietmar Eifler
2. Berichterstatter: Prof. Dr. Zhong Zhang
3. Berichterstatter: Prof. Dr.-Ing. Dr. h.c. Klaus Friedrich

D386

Acknowledgement

The present work was completed between February 2002 and June 2005 at the Institute for Composite Materials (IVW GmbH), University of Kaiserslautern, Germany.

First of all, I would like to express my gratitude to Prof. Dr.-Ing. Dr.h.c. Klaus Friedrich and Prof. Dr. Zhong Zhang for their scientific support and concern about the progress of my study. I am thankful to Prof. Dr-Ing. Dietmar Eifler for accepting the presidency of the examination committee.

I am grateful to the IVW for providing me the opportunity of working in an outstanding environment. I would like to express my appreciation to IVW staff and especially to my colleagues of Division II for their perfect and friendly help in my work and life.

I am thankful to MSc.-Ing Hui Zhang for his help and preparation of materials. Many thankful also to Mr. Stefan Schmitt, and Mr. Hermann Giertzsch for their useful help in experiments. I wish also to thank Prof. Dr. Minzhi Rong from Zhongshan University, China, for the interesting scientific discussions and helpful suggestions.

This work is dedicated in love to my wife Xiaozheng and my parents for their patience and support.

Kaiserslautern, August 2005 Li Chang

Abstract

The use of polymers subjected to various tribological situations has become state of the art. Owing to the advantages of self-lubrication and superior cleanliness, more and more polymer composites are now being used as sliding elements, which were formerly composed of metallic materials only. The feature that makes polymer composites so promising in industrial applications is the opportunity to tailor their properties with special fillers. The main aim of this study was to strength the importance of integrating various functional fillers in the design of wear-resistant polymer composites and to understand the role of fillers in modifying the wear behaviour of the materials. Special emphasis was focused on enhancement of the wear resistance of thermosetting and thermoplastic matrix composites by nano-TiO_2 particles (with a diameter of 300nm).

In order to optimize the content of various fillers, the tribological performance of a series of epoxy-based composites, filled with short carbon fibre (SCF), graphite, PTFE and nano-TiO_2 in different proportions and combinations, was investigated. The patterns of frictional coefficient, wear resistance and contact temperature were examined by a pin-on-disc apparatus in a dry sliding condition under different contact pressures and sliding velocities. The experimental results indicated that the addition of nano-TiO_2 effectively reduced the frictional coefficient, and consequently the contact temperature, of short-fibre reinforced epoxy composites. Based on scanning electron microscopy (SEM) and atomic force microscopy (AFM) observations of the worn surfaces, a positive rolling effect of the nanoparticles between the material pairs was proposed, which led to remarkable reduction of the frictional coefficient. In particular, this rolling effect protected the SCF from more severe wear mechanisms, especially in high sliding pressure and speed situations. As a result, the load carrying capacity of materials was significantly improved. In addition, the different contributions of two solid lubricants, PTFE powders and graphite flakes, on the tribological performance of epoxy nanocomposites were compared. It seems that graphite contributes to the improved wear resistance in general, whereas PTFE can easily form a transfer film and reduce the wear rate, especially in the running-in period. A combina-

tion of SCF and solid lubricants (PTFE and graphite) together with TiO_2 nanoparticles can achieve a synergistic effect on the wear behaviour of materials.

The favourable effect of nanoparticles detected in epoxy composites was also found in the investigations of thermoplastic, e.g. polyamide (PA) 6,6 matrix. It was found that nanoparticles could reduce the friction coefficient and wear rate of the PA6,6 composite remarkably, when additionally incorporated with short carbon fibres and graphite flakes. In particular, the addition of nanoparticles contributed to an obvious enhancement of the tribological performances of the short-fibre reinforced, high-temperature resistant polymers, e.g. polyetherimide (PEI), especially under extreme sliding conditions.

A procedure was proposed in order to correlate the contact temperature and the wear rate with the frictional dissipated energy. Based on this energy consideration, a better interpretation of the different performance of distinct tribo-systems is possible. The validity of the model was illustrated for various sliding tests under different conditions. Although simple quantitative formulations could not be expected at present, the study may lead to a fundamental understanding of the mechanisms controlling friction and wear from a general system point of view. Moreover, using the energy-based models, the artificial neural network (ANN) approach was applied to the experimental data. The well-trained ANN has the potential to be further used for online monitoring and prediction of wear progress in practical applications.

Kurzfassung

Die Verwendung von Polymeren im Hinblick auf verschiedene tribologische Anwendungen entspricht mittlerweile dem Stand der Technik. Aufgrund der Vorteile von Selbstschmierung und ausgezeichneter Sauberkeit werden polymere Verbundwerkstoffe immer mehr als Gleitelemente genutzt, welche früher ausschließlich aus metallischen Werkstoffen bestanden. Die Besonderheit, die polymere Verbundwerkstoffe so vielversprechend für industrielle Anwendungen macht, ist die Möglichkeit ihre Eigenschaften durch Zugabe von speziellen Füllstoffen maßzuschneidern. Das Hauptziel dieser Arbeit bestand darin, die Wichtigkeit der Integration verschiedener funktionalisierter Füllstoffe in den Aufbau polymerer Verbundwerkstoffe mit hohem Verschleißwiderstand aufzuzeigen und die Rolle der Füllstoffe hinsichtlich des Verschleißverhaltens zu verstehen. Hierbei lag besonderes Augenmerk auf der Verbesserung des Verschleißwiderstandes bei Verbunden mit duromerer und thermoplastischer Matrix durch die Präsenz von TiO_2-Partikeln (Durchmesser 300nm).

Das tribologische Verhalten epoxidharzbasierter Verbunde, gefüllt mit kurzen Kohlenstofffasern (SCF), Graphite, PTFE und nano-TiO_2 in unterschiedlichen Proportionen und Kombinationen wurde untersucht, um den jeweiligen Füllstoffgehalt zu optimieren. Das Verhalten von Reibungskoeffizient, Verschleißwiderstand und Kontakttemperatur wurde unter Verwendung einer Stift-Scheibe Apparatur bei trockenem Gleitzustand, verschiedenen Kontaktdrücken und Gleitgeschwindigkeiten erforscht. Die experimentellen Ergebnisse zeigen, dass die Zugabe von nano-TiO_2 in kohlenstofffaserverstärkte Epoxide den Reibungskoeffizienten und die Kontakttemperatur herabsetzen können. Basierend auf Aufnahmen der verschlissenen Oberflächen durch Rasterelektronen- (REM) und Rasterkraftmikroskopie (AFM) trat ein positiver Rolleffekt der Nanopartikel zwischen den Materialpaaren zum Vorschein, welcher zu einer beachtlichen Reduktion des Reibungskoeffizienten führte. Dieser Rolleffekt schützte insbesondere die SCF vor schwerwiegenderen Verschleißmechanismen, speziell bei hohem Gleitdruck und hohen Geschwindigkeiten. Als Ergebnis konnte die Tragfähigkeit dieser Materialien wesentlich verbessert werden. Zusätzlich wurde die Wirkung zweier fester Schmierstoffe (PTFE-Pulver und Graphit-Flocken) auf die

tribologische Leistungsfähigkeit verglichen. Es scheint, daß Graphit generell zur Verbesserung des Verschleißwiderstandes beiträgt, wobei PTFE einen Transferfilm bilden kann und die Verschleißrate insbesondere in der Einlaufphase reduziert. Die Kombination von SCF und festen Schmierstoffen zusammen mit TiO_2-Nanopartikeln kann einen Synergieeffekt bei dem Verschleißverhalten der Materialien hervorrufen.

Der positive Effekt der Nanopartikel in Duromeren wurde ebenfalls bei den Untersuchungen von Thermoplasten (PA 66) gefunden. Die Nanopartikel konnten den Reibungskoeffizienten und die Verschleißrate der PA 66-Verbunde herabsetzen, wobei zusätzlich Kohlenstofffasern und Graphit-Flocken enthalten waren. Die Zugabe von Nanopartikeln trug offensichtlich auch zur Verbesserung der tribologischen Leistungsfähigkeit von SCF-verstärkten, hochtemperaturbeständigen Polymeren (PEI) insbesondere unter extremen Gleitzuständen, bei. Es wurde eine Methode vorgestellt, um die Kontakttemperatur und die Verschleißrate mit der durch Reibung dissipierten Energie zu korrelieren. Diese Energiebetrachtung ermöglicht eine bessere Interpretation der verschiedenen Eigenschaften von ausgewählten Tribo-Systemen. Die Gültigkeit dieses Models wurde für mehrere Gleittests unter verschiedenen Bedingungen erklärt.

Vom generellen Blickpunkt eines tribologischen Systems aus mag diese Arbeit zu einem fundamentalen Verständnis der Mechanismen führen, welche das Reibungs- und Verschleißverhalten kontrollieren, obwohl hier einfache quantitative (mathematische) Zusammenhänge bisher nicht zu erwarten sind. Der auf energiebasierenden Modellen fußende Lösungsansatz der neuronalen Netzwerke (ANN) wurde darüber hinaus auf die experimentellen Datensätze angewendet. Die gut trainierten ANN's besitzen das Potenzial sie in der praktischen Anwendungen zur Online-Datenauswertung und zur Vorhersage des Verschleißfortschritts einzusetzen.

List of Abbreviations and Symbols

Abbreviation	
AFM	Atomic force microscope
ANNs	Artificial neural networks
B-o-R	Block-on-Ring
DMTA	Dynamic-mechanical-thermo analyzer
IF	Inorganic fullerene-like
PA	Polyamide
PEI	Polyetherimide
PEEK	Polyetheretherketone
PEN	Polyethylenenaphthalate
PMMA	Polymethyl methacrylate
POM	Polyoxymethylene
P-o-D	Pin-on-Disk
PPS	Polyphenylene sulfide
PTFE	Polytetrafluoroethylene
SCF	Short carbon fibre
SEM	Scanning electron microscope
SFRP	Short fibre-reinforced polymer
SGF	Short glass fibre
SPM	Scanning probe microscopy
TFL	Transfer Film Layer
WDX	Wavelength dispersive X-ray
XPS	X-ray photoelectron spectroscopy

Symbols

a	[m]	Radius of the real contact area
A_n	[m^2]	Nominal contact area
B		Coefficient of determination
c	[J/gK]	Specific heat capacity
E_d	[J]	Frictional dissipated energy
f_0	[Ncm^3/g]	Mass fraction of oxide film
F_N	[N]	Normal load
h	[mm]	Indentation depth
Δh	[nm]	Height loss of specimen
HU	[MPa]	Universal hardness
k*	[mm^3/Nm]	Wear factor
k_1, k_2	[W/mK]	Thermal conductivities of surfaces 1 and 2
k_b	[W/mK]	Thermal conductivity of the body
l_1, l_2	[m]	Equivalent distances from surface to heat sinks
L	[m]	Sliding distance
L_P		Pelcet parameter
Δm	[mg]	Mass loss of specimen
M		Number of test data
$O(p^{(i)})$		*i*th predicted property characteristic
$O^{(i)}$		*i*th measured value
p	[MPa]	Normal pressure
q_f	[W/m^2s]	Friction power intensity
Q_f	[W]	Rate of frictional heat supply from contact area
t	[s]	Test time

T_b	[K]	Bulk temperature
T_0	[K]	Ambient temperature of remote heat sink
v	[m/s]	Sliding velocity
w_s	[mm^3/Nm]	Specific wear rate
w_t	[nm/s]	Time-related depth wear rate
w_v	[mm^3]	Wear volume loss of specimen
α	[m]	Half width of the Hertzian contact
δ_g	[m]	Sliding amplitude
κ	[m^2/s]	Thermal diffusivity
μ		Frictional coefficient
ρ	[g/cm^3]	Density
ρ_0	[g/cm^3]	Average density of oxides

1 State of the Art

1.1 Introduction

Tribology is the study of the friction, wear and lubrication of interacting surfaces in relative motion. The direct motivation of the study was the saving of energy and materials in industrial applications. In practice, tribology is a varied and diffuse topic associated with the development of industrial technology. Recent developments of tribology have brought about new problems and materials such as polymer, ceramics, composites materials etc [1,2]. The present chapter presents a review and analysis of the development in this field during the last few decades. Special emphasis is placed on recent efforts in enhancing the wear performance of composites filled with inorganic nanoparticles, which has been recognized as an important topic of scientific research and has been received considerable attention recently.

Over the past decades, polymer composites have been increasingly applied as structural materials in the aerospace, automotive and chemical industries, providing lower weight alternatives to traditional metallic materials. A number of these applications are concentrated on tribological components, such as gears, cams, bearings and seals, where the self-lubrication of polymers is of special advantages. The feature that makes polymer composites so promising in industrial applications is the possibility of tailoring their properties with special fillers. For instance, short fibre reinforcements, such as carbon, glass and aramid fibres, have been successfully used to improve the strength and therefore the load carrying capacity of polymer composites subjected to various wear modes [3-6]. Solid lubricants, such as PTFE, graphite and MoS_2, have proved to be generally helpful in reducing the frictional coefficient and consequently wear rate [7-9]. Nevertheless, further effort is still under way to explore other fields of application for these materials and further enhance their properties for more extreme loading and environmental conditions [10]. Nano-scale inorganic particles have recently come under consideration, suggesting that this method is promising for new methods of wear-resistant materials even at very low filler content (about 1~4vol.%) [11,12]. Fig.1.1 shows schematically the possible principles of design in the composition of wear-resistant polymer composites [10]. In the following sections,

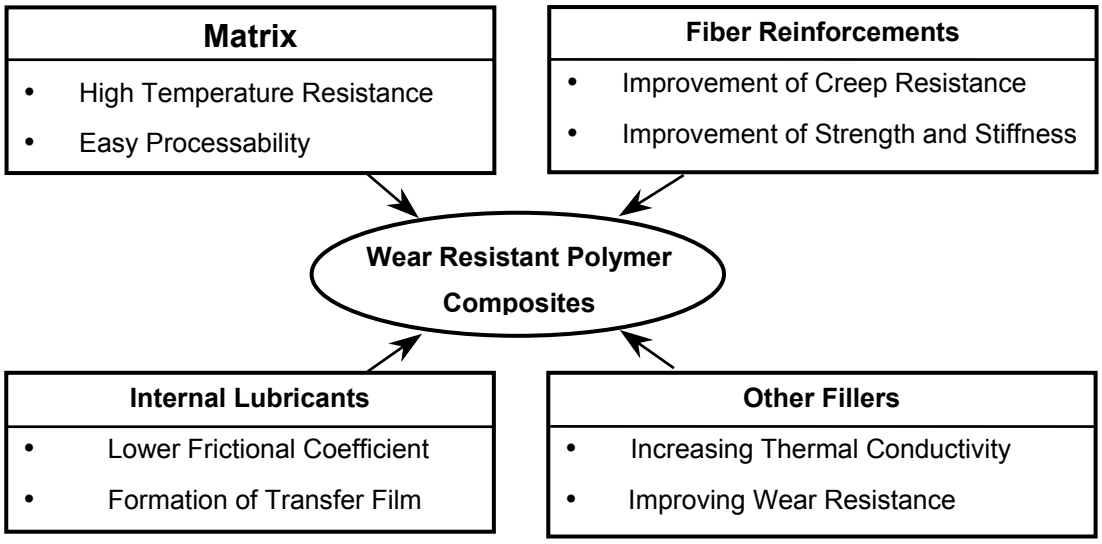

Figure 1.1: Schematic presentation of how to design the composition of wear resistant polymer composites.

developments in the design of these tribo-materials are briefly reviewed. All cases discussed here relate mainly to the sliding wear behaviour of polymer composite specimens against polished steel counterparts.

In order to characterize the wear behaviour of polymers in the laboratory, standard tests are used, corresponding to real service conditions. The pin-on-disk and block-on-ring tests are two commonly applied configurations according to ASTM wear testing standards [13]. These tests allow ranking of the most important tribological property of materials, the specific wear rate, which is determined by the equation,

$$W_s = \frac{\Delta m}{\rho F_N L} \qquad [mm^3/N{\cdot}m] \qquad (1.1)$$

in which F_N is the normal load applied on the specimen during sliding, $\triangle m$ is the specimen's mass loss, ρ is the density of the specimen, and L is the total sliding distance. It should be borne in mind, however, that tribological properties are generally not real material parameters, but depend on the system in which these materials have to function [10,14,15]. In order to evaluate the wear behaviour of materials under different sliding conditions, i.e. various contact pressures and sliding speeds, the time-related depth wear rate, W_t, is frequently used,

$$W_t = k^* \cdot pv = \frac{\Delta h}{t} \qquad [m/s] \qquad (1.2)$$

in which k^* is called the wear factor, which is the same as the specific wear rate determined by equation 1.1, p is the normal pressure, v is the sliding velocity, t is the test time and $\triangle h$ is the height loss of the specimen. In this equation, the wear factor, k^* is supposed to be a material parameter corresponding to the alteration of the product of pv factors. Based on the equation, the pv factor could be considered as a tribological criterion of the load-carrying capacity for bearing materials, and results in two evaluation parameters [4]: (i) the basic wear factor, k^*, which remains constant in a certain range of pv factor, and (ii) the "limiting pv", above which the increase of the wear rate of materials is too rapid to be applied. The general objectives in the design of wear-resistant polymer composites are to reduce the basic wear factor k^* and to enhance the "limiting pv" value.

1.2 Applications of Conventional Fillers

1.2.1 Sliding Wear of Short Fibre-Reinforced Polymer Composites

Various short fibres are known to considerably enhance not only the mechanical properties but also the tribological performance of polymer composites. Moreover, in comparison with continuous fibre-reinforced polymers, short fibre-reinforced polymer (SFRP) composites have the advantage of rapid, lower-cost processability by injection/compression moulding or by extrusion [16]. In general, the beneficial effect on the wear behaviour of polymer composites by short fibres is attributed to a reduced ability of ploughing, tearing and other non-adhesive components of wear [17,18]. A schematic illustration of the wear process of the SFRP is represented in Fig.1.2 [4], depicted by the characteristic micrographs of worn surfaces of epoxy matrix composite filled with short carbon fibre (SCF)/PTFE/graphite. The following stages of wear mechanisms can be recognized: (a) matrix wear and fibre thinning, (b) fibre breakage, (c) interfacial debonding, and (d) fibre peeling-off. The last two stages occur sequentially, i.e. interfacial debonding is followed by the removal of fibres. As a result, the exposed fibre would be easily removed by the asperities of the counterface with a large mass, leaving a void on the worn surfaces.

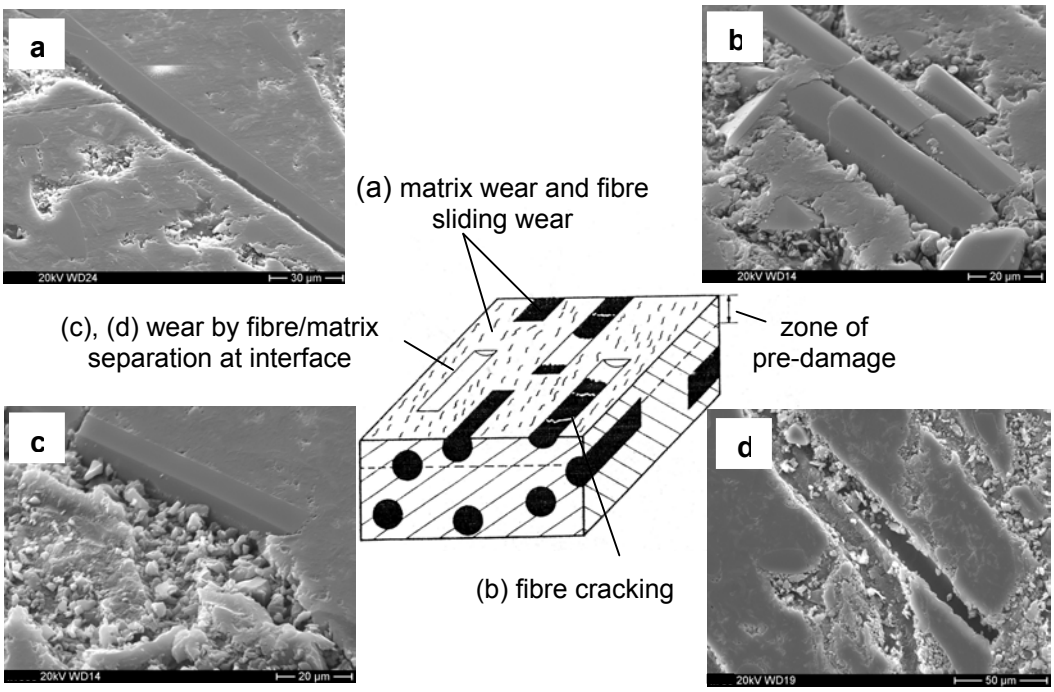

Figure 1.2: A schematic illustration of the wear process of fibre-reinforced epoxy composite: (a) matrix wear and fibre thinning, (b) fibre fracture and matrix/fibre interfacial debonding, and (c) fibre removal.

For randomly oriented SFRP, the type of fibre has a significant effect on the tribological properties. For instance, short carbon fibres (SCF) have been reported to be more effective than short glass fibres (SGF) in improvement of the wear resistance of various polymers [18,19]. This can be explained by the different wear mechanisms introduced by the two types of fibre. For SCF reinforced polymers wear occurs mainly by fibre thinning and fibre breakage whereas fibre pulverization and abrasive processes are much reduced in comparison with SGF reinforced materials. Beside, the ability of SCF to transfer a smooth carbon film onto the counterface and its contribution to the improved thermal conductivity of the composites may also lead to superior wear performance of materials [20,21].

To optimise wear performance, the influence of SCF volume fraction has been studied in various polymeric systems. Fig.1.3 shows the dependence of the specific wear rate on the volume contents of the SCF of three polymers, polyetheretherketone (PEEK) [17], polyethylenenaphthalate (PEN) [18] and epoxy. It is evident that a con-

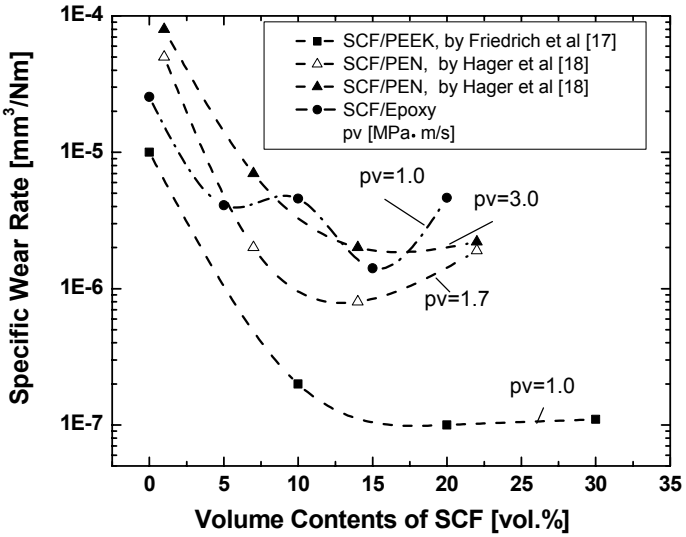

Figure 1.3: Influence of short carbon fibre reinforcement on the sliding wear behaviour of various polymeric matrices.

tent of 10~20vol.% of SCF exhibits an optimum effect in all these cases. With a further increase in the amount of carbon fibres, however, the wear rate of the composites dose not change efficiently.

Recently, the influence of interfacial bonding between fibre and matrix on the wear behaviour of SCF reinforced epoxy composites, was investigated by Zhang et al [22]. It was found that the wear resistance of SFRP could be enhanced under lower *pv* conditions by using carbon fibre treated by either an air oxidation or a cryogenic treatment, which resulted in improved fibre-matrix interfacial bonding. However, negative effects may occur at higher *pv* values, due to fibre damage after the oxidation treatment. Cryogenic treatment showed better performance in this case.

Voss and Friedrich [18] recognised the significance of fibre orientation with respect to the sliding plane. They found that when the fibres in the core region of mouldings were aligned orthogonally to the sliding plane (normal direction), the wear resistance was significantly better than when the skin fibres were at the worn surface (parallel or anti-parallel direction). This outstanding tribological behaviour of normally orientated fibres was attributed to the reduction of fibre breakage and pulverization. However, it has been indicated by other researchers that normally orientated fibres may suffer

the risk of server wear or sudden seizure, which is related to an abrupt increase of friction as well as contact temperature [23]. When designing high wear-resistant materials it is necessary to take all these factors into consideration. Combining favourable factors, e.g. orientation and type of fibres, may lead to further improvements or to so-called 'synergistic' effects [24].

1.2.2 Effects of Solid Lubricants: Development of Transfer Film Layer

The importance of "transfer film" for the tribological performances of polymers has long been realised and widely studied [7]. When polymers slide against metal surfaces or other harder counterfaces, material transfer generally occurs, and sometimes continuous films can develop in certain wear processes. These films thereafter act as soft shields for the polymers from the harder asperities they contact, resulting in adhesive wear by the "like-on-like" sliding pairs. As a result, wear loss can be dramatically reduced [7, 25]. It is agreed that the tribological characteristics of the transfer film are mostly determined by the bonding strength between the transfer film and counterface, as well the morphology of the film depending on the sliding conditions.

In order to achieve a uniform and continuous transfer film, solid lubricants e.g. graphite and PTFE are commonly used [26,27]. The lubricating effects of these materials result from their special band or layer molecular structure, which makes them relatively free to slip over each other and transfer to the metallic counterface [14, 27]. As well as these two solid lubricants, some inorganic particles, e.g. TiO_2, SiC, MOS_2, and copper compounds (CuO, CuS, CuF_2), have also been used as lubricating fillers in different polymer matrices such as polytetrafluoroethylene (PTFE) [27-30], polyamide (PA) [31,32], PEEK [33], polyphenylene sulfide (PPS) [34-37] and polyoxymethylene (POM) [38], to improve the wear performance of transfer film by mechanical and/or chemical actions. For instance, Bahadur et al [28] observed a remarkable reduction in the wear rate of PTFE by using graphite, CuS etc. They attributed this reduction to the changes in the shape and size of the worn aggregates as well as their bonding to the counterface, which were conducive to the development of a uniform and coherent transfer film. Using XPS analysis, Gao [30] highlighted the effect of the tribo-chemical reaction of PTFE and its particle fillers on the formation of transfer film.

Zhao and Bahadur [35,36] also indicated that the tribo-chemical reaction between the fillers and the metallic counterface was needed for wear reduction in PPS. Schwartz and Bahadur [37] filled various particles in PPS and concluded that the formation of good transfer film as well as higher wear resistance was determined by the ability of particles to plastically deform and by the quality of the bond between filler and matrix.

Despite numerous studies, understanding of the growth of transfer films and their tribological behaviour in steady state is still limited owing to the lack of quantitative techniques [7]. Therefore, new methods and devices have recently been applied in this field in order to obtain more reliable material data of the transfer film. Schwartz and Bahadur [39,40] developed an interesting novel device to measure the tangential shear stress needed to peel the transfer film, which was taken as a measure of the bonding strength between transfer film and counterface. Friedrich et al [41] studied the mechanical properties of films by micro-hardness measurement, and accordingly evaluated the load-depth curves. Using the same method, Zhang et al [42] further compared the thickness of transfer films developed with different lubricants. It was noticed that transfer films developed with graphite were thinner and harder in comparison to those developed with PTFE. The former led to a lower frictional coefficient, especially under high pressures. To obtain the mechanical properties of thin transfer film independent of the metallic substrate, nano-techniques such as atomic force/friction force microscopy (AFM/FFM) and scanning probe microscopy (SPM) have recently been introduced to study highly localized damage and/or topographical changes of very thin film [43-46]. Such studies entailing high accuracy are expected to provide insight into failure mechanisms of thin transfer film and to be of help in better understanding the contribution of lubricants.

1.2.3 Synergistic Effects Between Inorganic Particles and Other Fillers

As mentioned already, the integration of various functional fillers is a traditional route to achieving high wear-resistant polymer composites [10]. It is well accepted that the overall behaviour of multiphase materials can be considered as a function of the respective contribution of each phase, which is also true with regard to wear properties. However, some special reactions between various fillers have been observed which

greatly influence the wear performance of polymer composites. In the selection of multi-fillers, it is of great importance to apply synergistic reactions and avoid negative ones.

Bahadur et al [47,48] added micron size CuS or CuO particles together with PTFE powders into short carbon fibre or glass fabric reinforced polyamide (PA). Neither CuS nor CuO alone contributed to the development of a good transfer film when combined with the fibres. However, the further incorporation of PTFE was very effective in the reduction of wear. The optimum wear-resistant composition was found to be PA with 25 vol.% CuO, 11.3 vol.% glass fabric, and 10 vol.% PTFE. A beneficial effect between PTFE powders and micron size CuS particles has also been found in PEEK systems [33]. It has been proposed that a chemical reaction occurs and thereby increases the adhesion of transfer film to the metallic counterpart. Wang et al [49] investigated the effect of MoS_2 micron particles on PA composites. Although MoS_2 particles alone did not result in a positive effect, an integration of MoS_2 particles with short-CF significantly improved the wear resistance of the material. It was believed that the synergistic action between carbon fibres and MoS_2 particles contributed to the formation of thin, uniform and continuous transfer film, although the dominating mechanism was unclear. Suzuki and his colleagues [50,51] demonstrated the synergism of a sputtered MoS_2 film and a PTFE composite (PTFE+glass-fibre+Mo), which dramatically enhanced the durability of the sputtered MoS_2 film and the friction performance of PTFE composites.

1.3 Nanoparticle Reinforcement

1.3.1 Effect of the Particle Size: from Micro- to Nanometre

When particle size is diminished to nanoscale, the wear performance of composites may be significantly different from that of micron particle filled systems [11]. Nanoparticle filled polymers, so-called polymer nanocomposites, are very promising materials for various applications. They are expected to partly replace polymers, polymer blends and their traditional composites in products produced by melt processing techniques. This prediction is justified by the improvements in properties without sac-

rificing the melt rheological properties. The major feature of polymer nanocomposites is their huge interfacial surface area, which may result in a peculiar physical network structure of three-dimensional interphase (well reviewed recently in [12]). Of special interest with respect to tribological performance, the use of nanoparticles is believed to have two other advantages [39,52,53]: i) the abrasiveness of hard nanoparticles decreases remarkably as the result of the reduction in angularity in comparison with micro-particles, and ii) the material removal of nanocomposites would be much less than that of conventional composites because the fillers have the same size as the segments of the surrounding polymer chains.

In general, fine particles seem to contribute better to the improvement of tribological properties under sliding wear conditions than larger particles. One example of this relationship was detected by Xue et al [54]. They found that various kinds of SiC particles, i.e. nano, micron and whisker, could reduce friction and wear when incorporated into a PEEK matrix at a constant filler content, e.g. 10wt.% (≈4vol.%). However, the nanoparticles resulted in the most effective reduction, which was attributed to their beneficial effect on the formation of a thin, uniform, and tenacious transfer film. Wang et al [55] investigated the influence of the size of ZrO_2 nanoparticles, varying from 10nm to 100nm. Effective reduction of the wear of filled PEEK by nanoparticles was observed only when the size of particle was below 15nm. Xing et al [56] recently compared the wear properties of spherical particle-filled epoxy when particle size varied from 120 to 510 nm. They also confirmed a similar trend, i.e. the smaller the particles used as fillers, the better was the wear resistance of the composites. However, opposite effects were observed by Tanaka [27] in a study of the wear performance of PTFE filled with TiO_2 and ZrO_2 particles. The TiO_2 was an agglomeration of fine particles of less than 300 nm in size, and the filler content was 20wt.% (≈12vol.%). The ZrO_2 particles applied ranged from several microns to about 50 μm, and the filler content was 40wt.% (≈20vol.%). It was found that both particles could significantly improve the wear resistance of PTFE, although the frictional coefficient was increased. The larger ZrO_2 particles performed better with regard to a reduction in wear, but at the same time displayed a higher frictional coefficient in comparison to the smaller ones. From the observation of worn surfaces it was deduced that, ZrO_2 resulted in a

greater abrasiveness against the steel counterpart than TiO_2, due to the larger particle size and probably the greater hardness of ZrO_2. It seems, at least for a PTFE matrix, that diminishing the particle size does not lead to improved wear resistance. More studies are reviewed in the following section regarding the influence of the volume of nanoparticles.

1.3.2 Influence of the Nanoparticle Volume Content

Up to the present, various inorganic nanoparticles, e.g. Al_2O_3, TiO_2, ZnO, CuO, SiC, ZrO_2, Si_3N_4, SiO_2, and $CaCO_3$, have been incorporated into PPS [39,40], PEEK [54,55,57-62], epoxy [52,53,56, 63-67], PMMA [68], and PTFE [69,70] matrices, to improve wear performance. In most cases, optimum nanoparticle filler contents could be identified at which maximal wear resistance of these polymers was found. It was noticed that the optimum filler content of the small particles was mostly in a range between 1 and 4 vol.%, except for PTFE matrix composites. Although in most of these studies the morphologies of nanoparticle dispersion were not provided in detail, it should be clear that high filler content leads to deterioration in wear properties, which may be due to a tendency of particle agglomeration. It is generally necessary

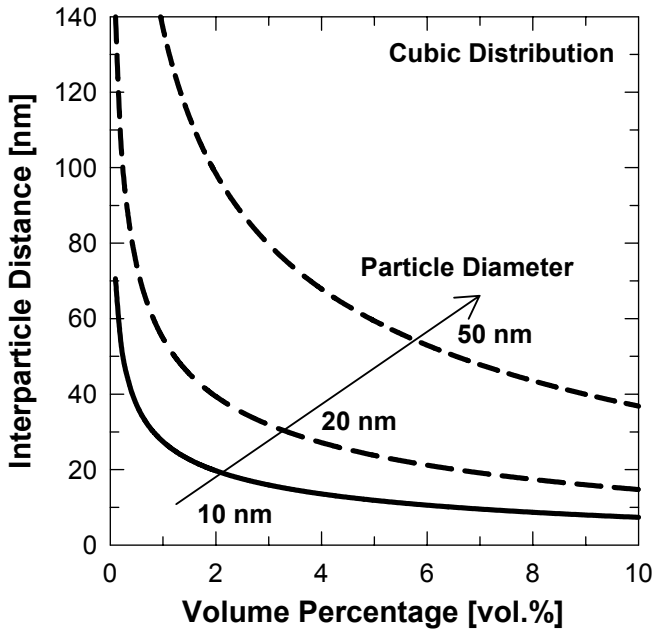

Figure 1.4: Correlations among nanoparticle diameter, inter-particle distance and volume percentage based on assumptions of spherical particle, cubic distribution and ideal dispersion.

that the nanoparticles are uniformly dispersed rather than agglomerated, in order to yield a good property profile. Agglomeration is considered a common problem of polymer nanocomposites, especially at higher nano-filler contents. Fig.1.4 illustrates the correlations among particle diameter, distance and volume content. Here the spherical particles were assumed to be in a cubic distribution situation with perfect dispersion in a polymer matrix [11]. It should be noted that agglomeration could easily occur for smaller particles at higher filler content due to the reduced inter-particle distance.

For PEEK matrix nanocomposites [49,50, 57-62], a small amount of inorganic nanoparticles, such as Si_3N_4, SiO_2, SiC, and ZrO_2, has been found to contribute to a reduction in frictional coefficient from about 0.4 for the neat matrix down to about 0.2. The dominating wear mechanisms were modified from adhesive and fatigue wear in case of the neat PEEK to a mild abrasive wear of the nanocomposites. However, with a further increase in nano-filler content, particle agglomeration occurred and resulted in severe abrasive wear, as observed on the worn surfaces [60]. A similar tendency was demonstrated by Bahadur et al [39,40] for PPS, filled with various kinds and amounts of nanoparticles. A 2 vol.% Al_2O_3 produced optimum reduction in the wear rate of the composites at two different surface roughnesses of the steel counterpart, i.e. *Ra*=60 and 100 nm. However, with roughness of *Ra*=27 nm, which was smaller than the particle size (33 nm on average), any amount of nanoparticles increased the wear rate. Very recently, nano-size TiO_2 and CuO particles have been found to reduce wear in PPS matrix composites, whereas ZnO and SiC exhibited an opposite effect [40]. Optimum wear resistance was again obtained with 2 vol.% of CuO or TiO_2. With measurement of the transfer film-counterpart bond strength in the peeling study, the increased bond strength with nanoparticles was taken as the main reason for the improvement in wear resistance of nanocomposites.

Sliding wear studies using inorganic nanoparticle filled epoxy have also been carried out recently [52,53,56,63-67]. It was found that well dispersed nanoparticles could significantly improve both the mechanical and the tribological properties of the thermosetting matrix composites. The incorporation of SiO_2 nanoparticles (9 nm), grafted

with another polymer (PAAM) to enhance the adhesion of the particle agglomerates with the surrounding epoxy resin matrix, was carried out by Zhang et al. [53,63]. The grafting polymerization technique not only increased the interfacial interaction between the nanoparticles and the matrix but also disintegrated the agglomerated nanoparticles. As a result, the frictional coefficient and wear rate of the material were effectively reduced by the treated nano-Si_3N_4 (<20nm) or nano-Al_2O_3 (3.8nm) at very low filler content (<1vol.%) [64,65]. Similarly, 300 nm TiO_2 contributed to improved wear resistance, by changing from severe abrasive wear to mild abrasive wear of the neat epoxy, due to the formation of a compacted transfer film [66].

Inorganic nanoparticles of ZnO and Al_2O_3 were recently incorporated into PTFE by Li et al [69] and Sawyer et al [70], respectively. It was found that the optimum filler content was relatively high, i.e. more than 10 vol.%. Although the nanoparticles were agglomerated together, as in the case of nano-Al_2O_3 [70], wear was significantly reduced. From the reviewers' point of view, the reason may be the soft nature of the PTFE matrix. The improved mechanical properties of PTFE, e.g. stiffness and creep resistance, by hard particles play a key role to such reduction in wear. Agglomerated nanoparticles have a similar function to that of micron sizes particles [27,28].

1.3.3 Integration of Nano-Particles with Traditional Fillers

To date, few efforts have been made towards the development of such composites by integrating inorganic nanoparticles with traditional fillers. Wang et al. [61] investigated the wear behaviour of PEEK based composites filled with both nano-SiC (80nm) and PTFE fillers. Although either of the fillers could successfully improve the wear performance of PEEK, the combination of two fillers actually lessened the improvement. It was believed by the authors that a chemical reaction between the SiC nanoparticles and PTFE resulted in this negative effect. In another case, however, Wetzel et al [66, 67] found that the combination of nano-Al_2O_3 (13nm) and micro-$CaSiO_3$ (4-15µm) induced some kind of synergistic effect and improved both the wear resistance and the stiffness of epoxy.

More systemic studies of the combinative effect of nanoparticles with short carbon fibre have been recently carried out by Zhang et al [71-74]. The tribological performance of a series of epoxy-based composites was investigated under dry sliding conditions, different contact pressures and various sliding velocities. The best wear-resistant composition was found to be a combination of nano-TiO_2 with conventional reinforcements. As an example, epoxy plus 15 vol.% graphite, 5 vol.% nano-TiO_2, and 15 vol.% SCF exhibited a specific wear rate of $3.2\times10^{-7}mm^3/Nm$ at a pressure of 1 MPa and a sliding speed of 1 m/s, which is more than 100 times lower than that of the neat epoxy. Investigations have been conducted with a constant amount of graphite and SCF, but with a varying content of nano-TiO_2 particles. When the nanoparticle content was either reduced to 2vol.% or increased to 8vol.%, the specific wear rates of the composites increased. Fig.1.5 illustrates the dependence of the specific wear rate of epoxy based composites with either 5 or 15 vol.% of both graphite and SCF, respectively, on the nano-TiO_2 content. A comparison to the epoxy filled with various amounts of nanoparticles only [61] is also given in this figure. It is interesting to note that a content of 4~6vol.% of nano-TiO_2 exhibited the optimum effect in all the three cases. On the basis of micro-observations with a scanning electron mi-

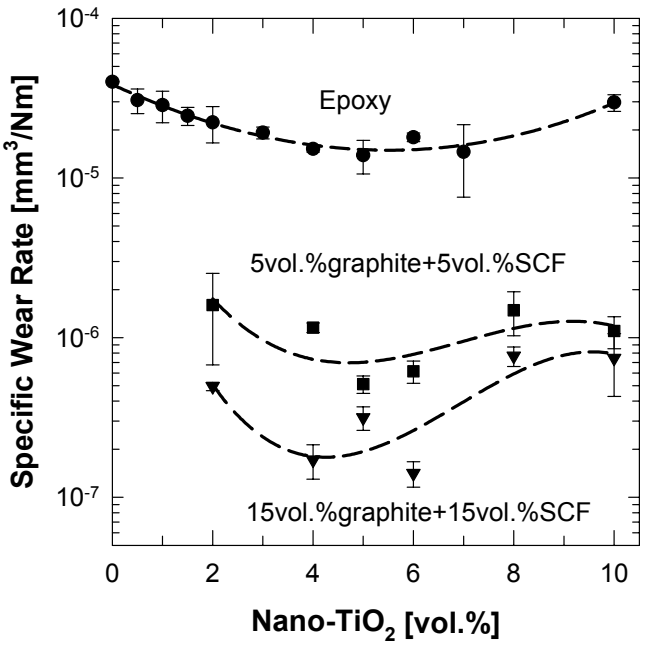

Figure 1.5: Dependence of the specific wear rate on the nano-TiO_2 content of epoxy nanocomposites. Wear conditions: normal pressure=1MPa; sliding velocity=1m/s; duration=20 hours; block-on-ring apparatus.

croscope (SEM) and an atomic force microscope (AFM) [74], the authors proposed a positive rolling effect of the nanoparticles between the material pairs. This effect was also described by others for WS_2 nanoparticle systems under mixed lubrication [75,76]. It is assumed that this effect reduces the frictional coefficient during sliding, as well as the shear stress and the contact temperature, especially in high sliding pressure and speed situations. Furthermore, the rolling effect seems also to protect the SCF from more severe wear mechanisms. As a result, the short carbon fibres can remain in the polymer matrix longer, providing high wear resistance of the composite. This favourable effect has also been observed in preliminary investigations of thermoplastic composites, e.g. PA 66 [77] and polyetherimide (PEI) matrices [78,79]. It was found that the wear resistance of both nanocomposites was remarkably improved especially under high *pv* conditions.

1.4 Wear Modelling: Analytical and Computational

It is a vital and continuing purpose in tribological studies to model the wear behaviours of contact materials, i.e. to establish the mathematical equations to predict the wear rate of materials with all the parameters in the system [80-83]. However, wear resistance is not an intrinsic property of materials but dependent on conditions and environments at contact. Therefore, each “mechanism” is treated individually [81]. In the following, however, only the three-body abrasive wear mechanism will be briefly reviewed.

1.4.1 Mechanism of Three-Body Abrasive Wear

Tribologists have recently paid increasing attention to three-body abrasion caused by particulate contaminants under wet and dry sliding conditions. When hard particles are interposed between two counterparts, it results in a three-body abrasive wear mode. This is in contrast with the two-body abrasive wear mode, which occurs when a pair of opposing surfaces interact abrasively by their hard asperities or rigidly held grits [84]. Until recently, the wear behaviour of these two modes of abrasive wear was thought to be very similar, although some significant differences were revealed

[14]. It has been found that the size of the additional particles plays a key role in modifying wear behaviour; reducing the particle size e.g. to a nanoscale level, may even enhance the tribological performances of materials. Most analysis assumes that this apparently lower wear rate is caused by the ability of the particles to roll on the surfaces - a rolling mechanism - which depends on their size, shape, hardness and sliding conditions [85]. For example, Iams et al [86] investigated the micro-abrasion of various particles, e.g., powered quartz, micron silicon carbide, and finely divided diamond, in a foil bearing with hydrodynamic film between 10 and 50 μm thick. It was found that the particles could roll or tumble through the gap and thus result in relatively little damage. Dwyer-Joyce et al [87] indicated that small particles tend to tumble through the contact region while larger particles plough through it. To make this low-wear regime operate on both surfaces, the ratio of the maximum particle dimension to the minimum film thickness must not exceed a critical value, which depends on particle shape and typically has an approximate value of 2.0. Accordingly, the wear rate was increased with an increase in abrasive particle size. Adachi et al [88,89] highlighted that the threshold value for the transition from three-body to two-body abrasion also depends on the hardness ratio between the ball and the specimen, although the reason for this dependence is unclear. Stachowiak et al [90] studied the effects of particles shape on three-body abrasive wear in both ball-on-plate and pin-on-disk tribo-meters. It was found that rolling (indentation) wear prevailed on the plate in the former machine, whereas both sliding and rolling were observed in the latter. In addition, the morphology of worn surfaces correlated well with the shape of particles.

Trezona et al [91] investigated the influence of test conditions on micro-scale abrasive wear behaviour. They found that grooving wear mechanisms dominated at high loads and low abrasive volume fractions, while the rolling mechanism played a significant role at low loads and high abrasive volume fractions. Similar observations were made by Stack and Mathew [92]. More recently, a significant beneficial effect was observed by Hutchings et al [93] in hybrid bearings in the presence of fine (< 5μm) anatase particles. The addition of small anatase particles to lubricating grease in hybrid rolling bearings was found to reduce wear and to provide enhanced lubrica-

tion, leading to lower running temperatures under high bearing loads. The improvement was attributed primarily to the formation of thin and relatively soft anatase film on ball surfaces. Nevertheless, it was also emphasised that free particles presenting within the thin lubricated film could enhance the potential for slip, and could thus reduce the coefficient of friction. Rapoport et al [75,76,94] found that nanoparticles can further improve the wear performance of lubricated wear couples. It was observed that inorganic fullerene-like (IF) nanoparticles, e.g., HN-WS_2 (120nm), could be used as solid lubricants and additives in liquid lubricants, and that the beneficial effect of IF nanoparticles increased with the applied load. The outstanding performance of the particles was attributed to their chemical inertness and hollow cage structure, which allowed them to roll rather than slide. Recently, the tribological performance of a series of epoxy-based composites reinforced with various quantities of short carbon fibres (SCF) and TiO_2 (300nm), and different amounts of solid lubricants, i.e. PTFE powders and graphite flakes, was investigated [71–74]. The best wear performance was found in a combination of TiO_2 with conventional reinforcements due to the remarkable reduction of the frictional coefficient, the consequent reduction in contact temperature, which was also explained by the rolling effect of the nanoparticles.

Therefore, the advantages produced by additional hard particles, particularly nanoparticles, can mainly be attributed to three effects: (i) reduction of the frictional coefficient owing to the rolling effect [74,75]; (ii) the lower abrasiveness of nanoparticles because of the remarkable reduction in their angularity in comparison with micro-particles [53]; (iii) the reinforcement on softer surfaces due to the embedding of hard, fine particles in worn surfaces [87, 90, 93]. However, three-body abrasion is very complex and depends on many variables, including particle characteristics such as size, hardness and shape, and counterpart properties such as surface topography and transfer films, as well sliding conditions. In order to fully characterise the wear mechanisms of nanoparticles, however, it is desirable to understand the roles of all these factors in wear and friction.

1.4.2 Wear Process Based on Energy Consideration

Because tribological properties are generally not real material parameters but depend on the tribo-system in which these materials have to function, some researchers have characterized the processes of friction and wear as energetic processes from a general system point of view. Attempts have been made to establish standard procedures in tribology that relate dissipated energy with wear loss in different sliding conditions [95-98]. Moreover, applying an energetic approach can directly correlate the three most important parameters of the tribo-system: frictional coefficient, wear rate and contact temperature.

The friction process is an energy process [99]. Nearly all the energy dissipated by friction appears as heat, generated at or very close to the rubbing surfaces. The local increase in temperature significantly influences both friction and the rate of wear. Numerous papers have been reported relating to the temperature rise at local contact asperities [100-104]. Commonly, two temperatures are of interest due to their great importance in the analysis of friction and wear: the mean or bulk surface temperature T_b and the local or flash temperature T_f. The bulk temperature T_b appears approximately a few tens of microns below the actual contact surface.

In almost all dry-sliding tests, when a steady state is reached, conduction is found to dominate, and convection and radiation effects may be neglected [104]. Therefore, it may be conveniently calculated by heat-conduction equations. For a quasi-stationary heat source at the contact area, the heat flow can be considered as a flow of thermal current through a thermal resistance, and by comparison with the corresponding electrical problem, which is easily shown as [101],

$$T_b = \frac{Q_f}{4ak_b} \tag{1.3}$$

in which, Q_f is rate of frictional heat supply from the real contact area, a is the radius of the circular area of the contact region, and k_b is the thermal conductivity of the body. In particular, for a pin-on-disk configuration, assume that both pin and disk are connected with the corresponding remote heat sinks of ambient temperature T_0. k_1

and k_2 are the thermal conductivities of the materials of the two contacting surfaces, and l_1 and l_2 are the equivalent lengths for the solids. A more general equation can be given by [103,104]:

$$T_b - T_0 = \frac{\mu F_N v}{A_n}\left[\frac{1}{\frac{k_1}{l_1}+\frac{k_2}{l_2}}\right] \tag{1.4}$$

in which, μ is the coefficient of friction in the steady stage, F_N is the applied normal load, v is the relative sliding velocity, and A_n is the nominal contact area. The complexity of the equation is contained in the equivalent depth. In particular, the latter depends not only on the geometry of heat flow but also on whether the heat flow is transient or steady–state according to speed conditions [100-103]. However, using experimental measurements it is possible to drive an accurate temperature map, which then has predictive power.

The flash temperature T_f occurs transiently at the tip of the individual contacting asperities, and is almost always higher than T_b. The T_f normally occurs over a small dimension (10^{-4}m or less) with a very short duration (10^{-3}s or less) [102]. This makes it difficult to measure the T_f through either a mathematical or experimental method. Archard [101,102] formulated a simplified presentation of the T_f, which allows estimation of the distribution of the temperature around the contact area. For example, under high-speed conditions, the maximum flash temperature T_{max}, occurring at the centre of heat source, was estimated to be 1.64 times larger than T_b. The temperature at the area of contact, is proportional to $y^{1/2}$, where y is the depth form the point to the heat source.

As the two responses of a tribo-system, friction and wear must be exactly related with each other in each state of contact, although a comprehensive simple relationship should not be expected. Some efforts have been expended to correlate the volumetric wear loss of first body with frictional work. Based on experimental results from unidirectional and bidirectional ball-on-flat tests, Huq et al [97] found that the wear volume is linearly related to dissipated energy i.e.:

$$w_v = \frac{A_n}{f_0 \rho_0} E_d \tag{1.5}$$

in which, A_n is the nominal contact area, f_0 is the mass fraction of oxide film which is oxygen, ρ_o is the average density of oxides formed at the real area of contact and E_d is the total dissipated energy. However, the power consumed by wear loss is normally difficult to determine as it depends strongly on the size of generated wear particles [95]. Therefore, the above linear relationship should be strictly limited to special test conditions with the same dominating wear mechanism. A more complex relationship was established by Fouvry et al [105], which integrated both debris formation and debris ejection mechanisms. The wear volume extension was expressed by:

$$w_v = \frac{\delta_g}{\delta_{g\_ref}} \sum E_d \alpha w_{v\_ref} \tag{1.6}$$

in which δ_g is sliding amplitude, δ_{g_ref} is sliding amplitude associated to a reference fretting wear condition, $\sum E_d$ is accumulated dissipated energy, α is half width of the Hertzian contact and w_{v_ref} is wear volume loss defined for a reference fretting condition.

Although the above equations or models are helpful for estimating the wear behaviour of materials in certain special cases, wear is normally very complicated, involving many more parameters such as surface changes and interaction depending on contact temperature. This makes wear predictions extremely elusive, and simple functions cannot always cover all the prevailing mechanisms of wear. Therefore, a new mathematical approach, artificial neural networks (ANN), has recently been introduced in this field.

1.4.3 Application of Artificial Neural Network for Wear Prediction

1.4.3.1 General Remarks

Artificial neural networks (ANNs) are computational systems that simulate the microstructure (neurons) of a biological nerve system [106]. The most basic components of ANNs are modeled after the structure of the brain. Inspired by bio-

logical neurons, ANNs are composed of simple elements operating in parallel, i.e. ANNs are the simple clustering of primitive artificial neurons. This clustering occurs by creating layers, which are then connected to one another. Fig.1.6 illustrates schematically a multi-layer feed-forward ANN configuration, which is currently the mostly widely applied neural network. It can be seen that ANNs are conventionally constructed with three layers, i.e. input, out and hidden layers. As in nature, the network function is determined largely by the interconnections between neurons, which are not simple connections, but certain non-linear functions. Each input to a neuron has a weight factor of the function that determines the strength of the interconnection and thus the contribution of that interconnection to the following neurons. ANNs can be trained to perform a particular function by adjusting the values of these weight factors between the neurons, either by using information from outside the network or by the neurons themselves in response to the input. This is the key to the ability of ANNs to achieve learning and memory.

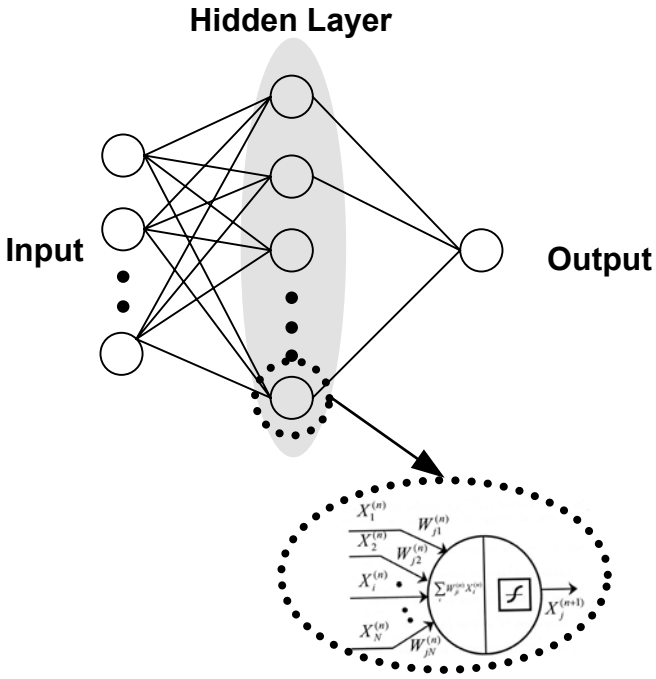

Figure 1.6: Artificial neural network configuration (upper part). The lower part gives a schematic description of the relationship between the input and output vectors of one neuron.

In order to evaluate the quality of ANNs, the coefficient of determination *B* (also called the R^2 coefficient in some publications) is frequently used,

$$B = 1 - \frac{\sum_{i=1}^{M} (O(p^{(i)}) - O^{(i)})^2}{\sum_{i=1}^{M} (O^{(i)} - O)^2} \tag{1.7}$$

where $O(p^{(i)})$ is the *i*th predicted property characteristic, $O^{(i)}$ is the ith measured value, O is the mean value of $O^{(i)}$, and M is the number of test data. The coefficient *B* describes the fit of the ANNs output variable approximation curve to the actual test data output variable curve. A higher *B* coefficient indicates an ANN with better output approximation capabilities.

The greatest advantage of ANNs is their ability to describe complex non-linear, multi-dimensional functional relationships without any prior assumptions about the nature of the relationships, in that the network is built directly from experimental data by the ANNs' self-organizing capabilities. Therefore, the most suitable applications for ANNs have the following characteristics [107]:

- A large database is available;
- It is difficult to find an accurate solution to the problem by existing mathematical approaches;
- The dataset is incomplete, noisy or complex.

Some properties of polymer composites, i.e. fatigue, creep and wear, have all these charactersitics and are therefore examples of material behavior that are suitable for netural network analysis [108,109]. In the following, however, only the application of this approach to the wear prediction on polymer composites is briefly reviewed.

1.4.3.2 ANN Applied to the Wear of Polymer Composites

Until now, the applications of ANNs in wear prediction have been mostly concentrated on metals. Jones et al [110] carried out a preliminary investigation of neural network techniques to predict tribological properties. Three different test rigs, a rub

shoe rig, a pin-on-disk rig, and a four-bar rig, were considered in this study. Load, speed, viscosity of lubricants, sliding distance, frictional coefficient, and temperature were applied as the ANN input variables, for predicting the wear rate as the output parameter. Relatively small datasets were used to train and test the neural network. Nevertheless, a satisfactory predictive quality was obtained, evaluated by the R^2-coefficient of determination. Contribution strengths were applied to describe the influence of the input variables on the output wear rate was, by analyzing the weight factors between the input layer and the hidden layers. Hutchings et al [111] successfully employed a simple ANN configuration to predict the abrasive wear performance of TiN/NbN multi-layers. An *8-[3]$_1$-1* ANN was chosen for predicting wear resistance, and an *8-[6]$_1$-1* ANN for hardness, based on an initial database of 42 coating systems. It was found that the ANN approach was helpful in quantifying the role of some of the key deposition parameters. Myshkin et al [112], classified wear debris by applying an ANN approach for lubricated wear testing of steel against steel. Similar work has been carried out in the field of the wear of polymers, but traditional statistical methods. For example, Zhang et al [113] have made some attempts to correlate the fractal dimensions of wear debris to wear mechanisms of polymers such as PEEK. The advantage of the ANN is its potential for condition monitoring as an on-line system [114].

More systemic studies of use of the ANN concept for the prediction of the wear properties of polymer composites have been performed by Friedrich and Zhang et al. [114-116]. Velten, Reinicke and Friedrich [114] were among the pioneers in exploring this approach in polymer composites, using an ANN to predict the wear volume of short-fibre/particle reinforced thermoplastics. A total dataset of 72 independent wear measurements was used to train and test the neural network. The dataset came from fretting tests with various material compositions (polyamide 4,6 matrix composites reinforced with short carbon/glass fibres, PTFE, and/or graphite) at different wear measuring conditions. The inputs were mechanical properties and measuring conditions, i.e. compressive strength, compression modulus, tensile strength, strain to failure, impact strength, environmental testing temperature, starting load, average load and average velocity. An automated “Bayesian” regularization of a backpropagation

algorithm was selected, which had the capability of automatically identifying the optimal size of the hidden layers of the ANN. Some successes have been achieved wtih this first attempt of property analysis using an ANN to deal with wear problems of polymer composites, although the predictive quality still needs to be improved. Zhang, Friedrich and Velten [115] developed further improvements based on an enlarged dataset of 103 independent measurements. The database contained (a) the material composition (volume fractions of the matrix, short glass fibres, pitch based carbon fibres, PAN carbon fibres, and PTFE and Graphite fillers), (b) mechanical properties of the composites studied (compression modulus and strength, impact strength, etc, all tested at related testing temperatures), and (c) testing conditions (temperature, normal force and sliding speed) as the input parameters. Wear characteristics such as specific wear rate or frictional coefficient were chosen as the output data. Again, the Bayesian algorithm was applied. It was found that the predictive quality was clearly improved when compared to reference [114]. Therefore, once a well-trained ANN has been obtained, new data can be predicted without performing too many, long experiments, so that an ANN can significantly reduce the time for designing new polymer composites for special purposes. It is clear that the predictive quality could be further improved by enlarging the datasets, employing material compositions as input data, and optimizing the ANN configuration.

Recently, Zhang et al [117] also applied this approach for dealing with the erosive wear data of three polymeric materials. As an example, an epoxy modified by hygrothermally decomposed polyurethane (EP-PUR) was studied. The impact angle for solid particle erosion and some characteristic properties (material composition for the case of EP-PUR as well) were selected as ANN input variables for predicting the erosive wear rate. It seems that the ranking of the importance of characteristic properties to the erosive wear rate could provide information about which property has a stronger relationship to the wear of polymers, which is of considerable assistance to a deep understanding of the wear mechanisms involved.

It is evident that the relatively new ANN approach, based on a limited amount of datasets, can be used for (i) predicting the wear rate and frictional coefficient of new

compositions of a composite system that has not been previously tested experimentally, (ii) parameter studies with regard to external testing conditions, and (iii) estimations about which input-parameters are of more or less importance for the output-parameter “wear rate”. A well-trained ANN is expected to be very helpful not only for the design of composite materials but also for understanding the importance of various parameters on wear properties.

1.5 Summary

Over the past few decades, interest has grown rapidly polymers and polymer composites for technical applications, in which low friction and low wear are essential. Nevertheless, new developments are still under way to explore other fields of application for these materials and to further enhance their properties for more extreme loading and environmental conditions. Nano-scale inorganic particles have recently come under consideration, which strongly suggests that this method promises new routes for the design of wear-resistant materials even at very low filler content. For example, the combinative effect of nanoparticles with short carbon fibres has exhibited a clear improvement in the wear resistance of both thermosetting and thermoplastic composites. In addition, this concept allows the use of these materials under more extreme wear conditions, i.e. higher normal pressures and higher sliding velocities. However, further study is required to investigate the reasons that very reduced size of fillers yields such a significant improvement in wear properties.

A new tool in the form of ANNs is now available for prediction of the wear properties of these materials as a function of composition and testing conditions. This method also facilities systematic parameter studies by computer for optimization of materials. Although an ANN cannot construct a mathematic equation directly, studies of the relationship between wear properties and mechanical properties under certain testing conditions, are expected to be of great assistance in developing an improved understanding of wear mechanisms.

2 Objectives of the Study

Over the past few decades, interest has grown rapidly in polymers and polymer composites for technical applications, in which low friction and low wear are essential. New investigations are still being undertaken to explore other fields of application for these materials and to further enhance their properties for more extreme loading and environmental conditions. Nano-scale inorganic particles have recently come under consideration, with indications that this method is promising for new routes of wear-resistant materials even at very low filler content (reviewed in detail in Chapter 1). With this background, the aims of the present work is to design novel polymeric composites with high load carrying capacity by using inorganic nanoparticles together with conventional fillers (including short carbon fibre and solid lubricants, e.g. PTFE powders and graphite flakes). The study is divided into three units. The main concerns and aims for each part are summarized in following paragraphs.

Thermosetting Composites

As detailed in Chapter 1, the integration of various functional fillers is a traditional route to achieve high wear-resistant polymer composites. In the selection of multi fillers, it is of great importance to harness synergistic reactions and avoid negative ones. Nevertheless, until now, few attempts have been made to develop such composites by integrating inorganic nanoparticles with conventional fillers. To obtain more knowledge in this field, a series of epoxy-based composites were designed with various content of short carbon fibres (SCF) and solid lubricants, as well as nano-TiO_2 (300nm). The mixture of the epoxy matrix with different fillers could be easily achieved by using a laboratory mixing device. Tribological performance of selected compositions was systematically investigated under different sliding conditions. The two targets of this part of the work were:

- To design high wear-resistant thermosetting composites with optimized filler content.
- To understand the role of various fillers in modifying the wear behaviour of polymer composites.

Thermoplastic Composites

To further advance the effort made in the first part of work, the optimized filler contents were subsequently applied to thermoplastic polymers, which are now widely used in injection moulded components with the strong commercial advantage of lower manufacturing cost. The commonly used polyamide 66 (PA 66) and high temperature-resistant polyetherimide (PEI) were selected as the matrix materials. The main aims of this part of the work were:

- To significantly enhance the tribological performance of thermoplastic polymers with optimized filler (including nanoparticles) content.
- To further investigate the possible synergy effect between nanoparticle and conventional fillers in different matrix systems under various sliding conditions.

Wear Modelling

It is a vital and persistent purpose in tribological studies to model the wear behaviour of contact materials, i.e. to establish the formulation to analyse and predict the wear behaviours of materials with all the parameters in the tribo-system. In view of the fact that tribological properties are generally not real material parameters but depend on the system in which these materials have to function, an energy-based procedure was developed to characterize the processes of friction and wear as an energetic process from a general system point of view. Moreover, an artificial neural network (ANN) approach was introduced in order to achieve a calculable solution for the wear problem. Most attention was paid to:

- Improved interpretation of the different wear performances of distinct systems using the energetic process
- Prediction of wear by a well-trained ANN (using existing experimental results)

3 Experimental Procedures

3.1 Materials

3.1.1 PolymerMatrices

In this study, two distinct polymeric systems, thermosetting and thermoplastic composites, were considered. A commercially available epoxy resin (Dow DER 331) cured by a polyamine hardener (Dow HY 2954) was used as the thermosetting matrix material. For thermoplastic polymers the commonly used PA 66 (Zytel 101L) and high temperature-resistant PEI (Ultem 1000) were selected.

3.1.2 Reinforcements

Pitch-based short carbon fibres (Kureha M-2007S), PTFE powders (Dyneon 9207) and graphite flakes (Superior 9039) were considered as conventional reinforcements.

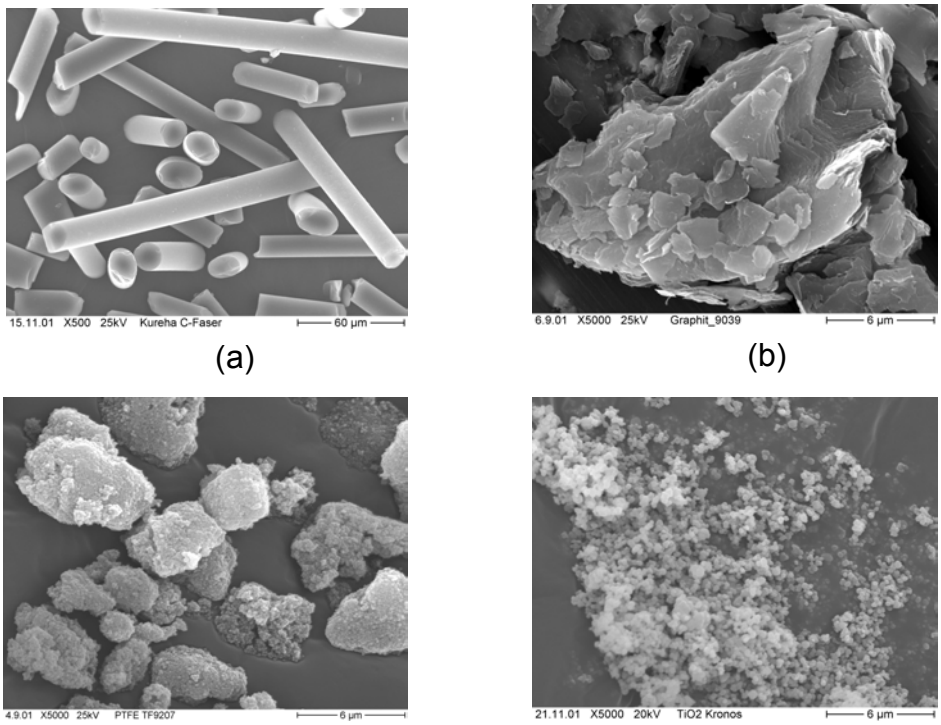

Figure 3.1: SEM configuration of fillers: (a) short carbon fibre, (b) graphite, (c) PTFE and (d) nano-TiO_2

The short carbon fibre had an average diameter of approximately 14.5μm and an average fibre length of about 90μm. The particle size of PTFE was about 4μm, and around 20μm for graphite flakes. TiO_2 (Kronos 2310) with an average diameter of 300 nm was also applied as an additional reinforcement. No surface treatments were applied to the fillers. Fig. 3.1 shows the photographs of the filler configurations obtained by scanning electron microscopy (SEM).

3.2 Sample Preparation

3.2.1 Thermosetting Composites

The epoxy resin was dried at 70°C for at least 4 hours prior to compounding. Thereafter, in a sequence of less to greater influence on the viscosity of the mixture, graphite, SCF, and PTFE were mixed in order using a laboratory mixing device. The mixture was cooled to 60°C with water, and the hardener was then added and stirred for more than 5 minutes. The composite was pre-cured at 70°C for 8 hours and finally cured at 122°C for 16 hours.

3.2.2 Thermoplastic Composites

The mixture of thermoplastic matrix with different fillers was achieved by a twin-screw-extruder with well-designed screw configurations. The screw temperature was set to 292°C for PA 66 and 385°C for PEI. There were three feeders along the screw for adding fillers. Nanoparticles were firstly added into the matrix for the longest mixing time in order to achieve better dispersion. The last addition was SCF, to avoid its being broken.

The extrudate was then moulded to a rectangular plate (80mm×80mm) with thickness of ~4mm using an Arburg Allrounder injection moulding. The mould temperatures for PA 66 and PEI were 70°C and 340°C respectively. Wear specimens were finally cut from the moulded plates with a size of $4\times4\times12mm^3$.

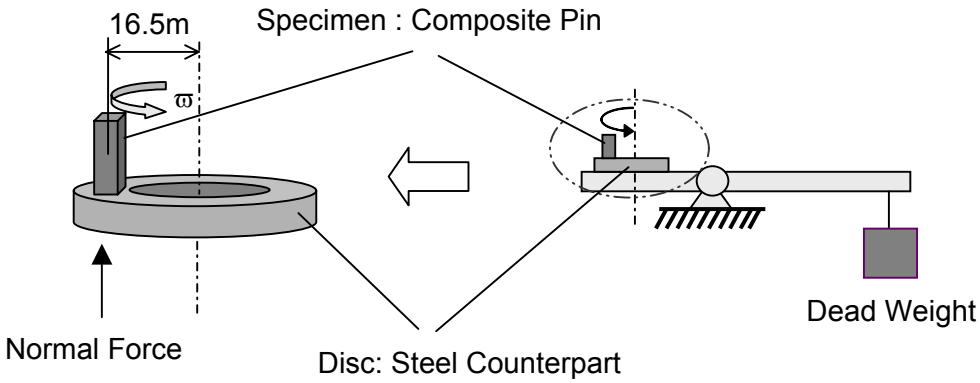

Figure 3.2: A schematic diagram of the pin-on-disc test apparatus.

3.3 Wear Test

The wear test was performed on a Wazau pin-on-disc (P-o-D) apparatus according to ASTM D3702. As shown in Fig. 3.2, the specimen pin was rotated on a flat steel disc with a radius of 16.5 mm. The initial surface roughness of the counterpart was about 0.23 μm. All tests involved in this study were conducted for 20 hours under dry condition at room temperature. Reduction of specimen's height was observed by a displacement sensor. The temperature of the disc was monitored by an iron-constantan thermocouple positioned on the edge of the disc, and was recorded as contact temperature [118]. The frictional coefficient was recorded and calculated by the ratio between the tangential force and normal load. After the test, the mass loss of the specimen was measured in order to calculate the specific wear rate (cf. equation 1.1 in Chapter 1).

3.4 Surface Observation

3.4.1 Scanning Electron Microscopy

After the wear testing, the worn surfaces were observed by scanning electron microscopy (SEM, JEOL-5400). To obtain stable images, the surfaces were firstly sputter coated by a sputtering device (SCD-050) with a Pt/Pd alloy for at least 120 seconds. In addition, SEM (JSM-T330A), equipped with wavelength dispersive X-ray (WDX) spectrometry, was used to characterize the titanium elements (TiO_2) on the steel counterfaces.

3.4.2 Atomic Force Microscopy

For more exact and detailed information, an atomic force microscope (AFM) (Digital Instruments) was employed to study highly localized damage and/or topographical changes. In particular, single fibres in the worn surface were examined by AFM, of which the lateral and vertical resolutions were 2 and 0.2 nm, respectively.

3.4.3 Laserprofilometry

In order to obtain the roughness profiles of the transfer films under different sliding conditions, the surface morphology of steel disks covered with polymer transfer film was investigated with laserprofilometry (UBM Messtechnik) using the definition of 10nm. The image analysis was carried out according to Din 4768.

3.5 Mechanical Characterization

3.5.1 Flexural Test

The flexural properties of the series of epoxy-based composites were measured by the three-point bending test (Din178) on a Zwick 1485 universal testing machine. The size of specimens was $4\times10\times80mm^3$. The load applied was 10kN with a crosshead speed of 1mm/min.

3.5.2 Fracture Test

The fracture behavior of the materials was investigated with a charpy impact tester (AFS-MKs fractorscope of Ceast, Torino, Italy). According to the standard of ISO179-1, unnotched specimens were cut with a dimensions of $4\times10\times80mm^3$. The energy of the striker was 4J and the speed was 2.9m/s. During the test, impact force was recorded as a function of deflection (F vs. s), by computer. The ‘deflection’ used here referred to the position of the impact striker.

3.5.3 Micro-Hardness Measurement

In order to determine the mechanical characteristics of the thin transfer film layers, micro-hardness was measured by a Vickers indenter of a Shimadzu micro-hardness tester. The tests were conducted at room temperature under controlled loading conditions. More specifically, when hardness-depth results are considered, the transfer film on a steel substrate shows typical layer behaviour according to its thickness. Therefore, the thicknesses of transfer films developed with different lubricants were further calculated and compared.

4 Enhancement of Wear Resistance of Epoxy-Based Composites by Nano-TiO_2 Particles

Epoxy resins form a very important class of thermosetting polymers, often exhibiting high tensile strength and modulus, excellent corrosion resistance and good stability of dimensions. Owing to their outstanding performance, epoxy resins with appropriate curing agents are used in protective coatings, adhesives, structural components, etc. In most of these applications the materials are subjected to different kinds of mechanical stresses and corrosive environments. Additional problems can arise from friction and wear conditions. In this case, it is the mechanical load-carrying capacity and the wear life of the components that determine their acceptability in industrial applications [4]. In order to improve the wear resistance of polymers, fibre reinforcements and solid lubricants are frequently used. It has been found that short fibre reinforcements, e.g. carbon, glass and steel fibres, can generally improve the mechanical properties of the composites and result in an enhanced wear resistance [4,23]. Solid lubricants, e.g. graphite and polytetrafluoroethylene (PTFE), have been shown to be helpful in developing a transfer film between the two counterparts and normally can drastically reduce the wear rate of the composites [7,26]. Recently, nanoparticles have come under consideration because of indications that they might effectively improve the wear resistance of polymer composites [11], even though the dominant mechanisms involved have not yet been fully explored.

In the present work, an inorganic nanoparticle TiO_2 was employed to further improve the wear resistance of the epoxy composites reinforced by traditional fillers such as short carbon fibres and solid lubricants. The tribological performance of a series of epoxy-based composites was systematically investigated under different sliding conditions. Based on experimental observations, the role of various fillers in modifying the wear behaviours of the composites was studied.

4.1 Wear Results

4.1.1 Standard Wear Condition: 1MPa and 1m/s

Table 4.1 summarizes the wear results under a standard sliding condition of 1MPa and 1m/s, each result being an average value of at least three experimental data. Both the frictional coefficient and the contact temperature given in the table are mean values during the steady state of the wear process. For convenience, in this chapter the materials are symbolized as [nano-TiO_2/PTFE/graphite/SCF] in volume content of each filler.

Table 4.1: Composition and wear properties of epoxy composites under 1MPa and 1m/s

Symbols of Composition	Matrix [vol.%]	Nano-TiO_2 [vol.%]	Graphite [vol.%]	SCF [vol.%]	PTFE [vol.%]	Density [g/mm³]	Frictional Coefficient	Specific Wear Rate [10^{-6}mm^3/Nm]
Neat matrix	100	0	0	0	0	1.13	1.18	5.63
5/0/0/0	95	5	0	0	0	1.28	1.02	17.56
5/0/0/15	80	5	0	15	0	1.3	0.43	3.95
0/0/10/0	90	0	10	0	0	1.14	0.59	7.07
0/0/0/10	90	0	0	10	0	1.23	0.59	4.6
0/0/10/0	90	0	0	0	10	1.58	0.54	1.02
0/10/10/10	70	0	10	10	10	1.18	0.59	0.75
0/5/5/5	85	0	5	5	5	1.2	0.59	0.94
0/5/5/15	75	0	5	15	5	1.28	0.59	0.81
0/5/10/15	70	0	10	15	5	1.27	0.72	0.88
5/0/5/5	85	5	5	5	0	1.35	0.41	0.55
5/0/5/15	75	5	5	15	0	1.39	0.34	0.45
5/0/10/15	70	5	10	15	0	1.42	0.38	0.64
5/10/0/15	70	5	0	15	10	1.31	0.5	0.86
5/5/5/15	70	5	5	15	5	1.44	0.49	0.89
5/0/15/15	65	5	15	15	0	1.48	0.41	0.47
2/0/15/15	68	2	15	15	0	1.4	0.37	0.53
6/0/15/15	64	6	15	15	0	1.58	0.38	0.57
10/0/15/15	60	10	15	15	0	1.61	0.35	0.52
10/0/5/5	80	10	5	5	0	1.5	0.43	0.67

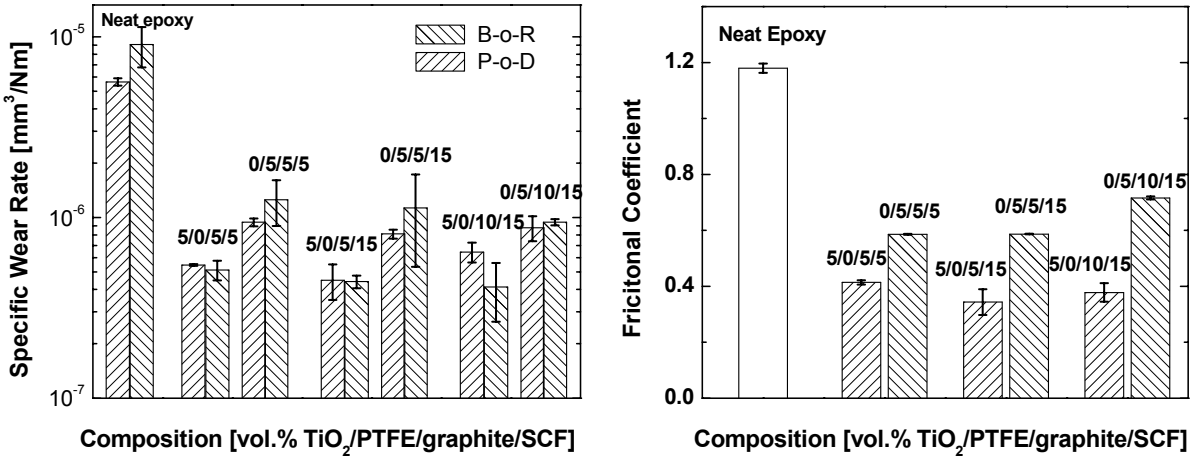

Figure 4.1: Comparisons of the wear performance of various groups of epoxy composites with 5vol.% of nano TiO_2 instead of the same amount of PTFE under a standard wear condition, i.e. 1MPa and 1m/s: (a) the specific wear rate measured with both a pin-on-disc (P-o-D) and a block-on-ring (B-o-R) apparatus and (b) the frictional coefficient measured with a pin-

As given in Table 4.1, the frictional coefficient of epoxy composites filled with short carbon fibres (SCF), graphite and/or PTFE could be further reduced by the addition of nano-TiO_2. Consequently, the wear resistance of the nanocomposites was also improved. In the present case, a composition of [5/0/5/15] demonstrated both the lowest frictional coefficient and highest wear resistance under 1MPa and 1 m/s.

To compare with our previous measurements conducted on a block-on-ring (B-o-R) apparatus [72], Fig. 4.1a summarizes the specific wear rate as a function of material composition filled with or without nanoparticles and tested on both apparatuses. It was found that the wear rates measured by the two apparatuses were comparable, and improved wear resistance was achieved for nanocomposites in both cases. As shown in Fig. 4.1b, a parallel tendency in reduction of the frictional coefficient was also observed. It is interesting to note in Fig. 4.1a that the specific wear rates of all three nanocomposites measured by the pin-on-disk (P-o-D) were a little lower than that measured by the B-o-R, which is quite the opposite for the composites without nanoparticles. To consider the configurations of the two test apparatuses, the contact surface between the composite pin and counterpart remains unchanged during sliding in the P-o-D, whereas the contact situation changes from a linear contact to an arc surface contact for the B-o-R. Therefore, extremely high contact pressure occurs

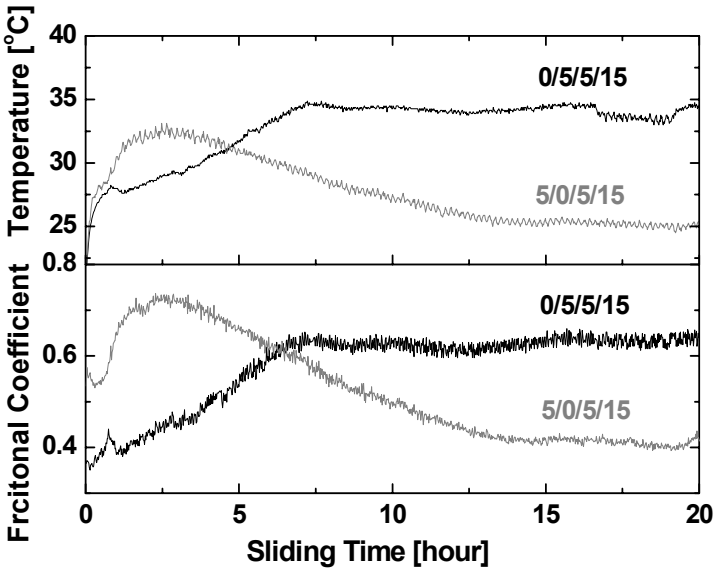

Figure 4.2: Comparison of the frictional processes i.e. the frictional coefficient and the contact temperature of the compositions [0/5/515] and [5/0/5/15] in a standard wear condition: 1MPa and 1m/s.

the case of the B-o-R. The wear resistance of the materials measured by the B-o-R was not only determined by the wear performance under a constant sliding condition but also influenced by the load-carrying capacity. It is clear that the lower wear rate result from the B-o-R could be attributed to the good mechanical load-carrying capacity of the nanocomposites, in comparison with the composites without nanoparticles.

Fig. 4.2 compares the typical variations in the frictional coefficient against sliding time for compositions [0/5/5/15] without and [5/0/5/15] with nanoparticles. For both composites, increased frictional coefficients were observed in the initial wear stages, which were mainly due to the increased real contact areas during the initial wear process. After about 5 h, the frictional coefficient of [0/5/5/15] became steady with a mean value of about 0.6. However, a significant decrease in the frictional coefficient was observed for the composition [5/0/5/15] with nanoparticles after the initial wear stage, and a peak value at about 2.5 h was reached. Finally, the frictional coefficient decreased to a stable value of 0.4. During sliding wear, frictional energy is a dominant cause of heat generation, which determines contact temperature. On the other hand, contact temperature can greatly affect the mechanical properties of polymer composite and consequently influence wear performance. Fig. 4.2 shows the curves

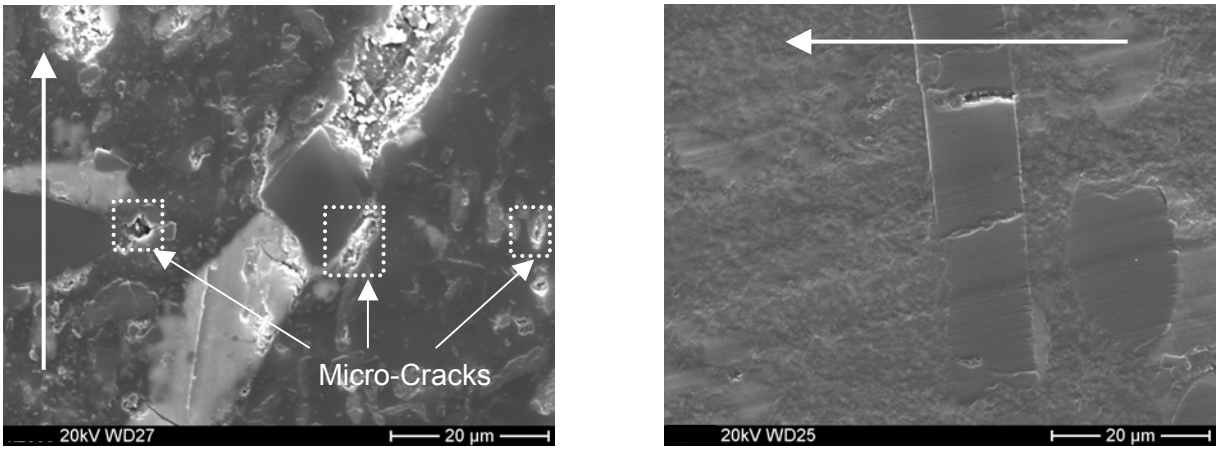

(a) (b)

Figure 4.3: SEM micrographs of the worn surfaces of (a) [0/5/5/15] and (b) [5/0/5/15] at 1MPa, 1m/s

of temperature during whole test durations of the two composites considered. It is clear that the tendencies of contact temperature and frictional coefficient coincided well with each other. The reduced frictional coefficient with nanoparticles led to a lower contact temperature for [5/0/5/15] in steady state wear. Therefore, the specific wear rate was accordingly reduced.

Fig. 4.3 depicts the worn surfaces of [0/5/5/15] and [5/0/5/15] tested at 1MPa, 1m/s. Arrow lines indicate the sliding directions. As shown in the figure, the surfaces of both composites appear relatively smooth and clearly show features characterizing the wear process of fibre-reinforced composites (cf. Fig. 1.2 in Chapter 1) [4] i.e. i), wear thinning of the fibre reinforcement; ii) subsequent breakdown of the fibre and iii) peeling off of fibre from matrix. For the composition [0/5/5/15] without nanoparticles, it was noticed that micro-cracking occurred on the brittle epoxy matrix particularly at the interfacial region between fibre and matrix, due to the concentration of stress. Finally, some slight furrows were left after fibre removal. However, with the addition of nanoparticles, the worn surface of [5/0/5/15] is much smoother and the fibre peeling-off is greatly limited [Fig. 4.3b]. As a result, the wear resistance of the material is evidently enhanced.

Table 4.2: Wear results of the composites under various contact pressures and sliding velocities

Composition	*pv* factors	Contact Temperature [°C]	Frictional Coefficient	Specific Wear Rate [10^{-6}mm^3/Nm]
0/5/5/15	1MPa, 1m/s	34.07	0.59	0.81
	2MPa, 1m/s	67.98	0.78	2.08
	4MPa, 1m/s	82.78	0.63	4.28
	1MPa, 0.5m/s	25.95	0.47	0.55
	1MPa, 2m/s	62.27	1.08	3.14
5/0/5/15	1MPa, 1m/s	26.06	0.33	0.45
	2MPa, 1m/s	32.09	0.28	0.72
	4MPa, 1m/s	41.67	0.22	0.83
	8MPa, 1m/s	50.36	0.14	1.49
	1MPa, 0.5m/s	24.56	0.32	0.51
	1MPa, 2m/s	30.35	0.40	0.69
	4MPa, 2m/s	46.41	0.17	1.72
5/0/10/15	1MPa, 1m/s	29.00	0.38	0.64
	4MPa, 1m/s	38.84	0.21	0.82
	8MPa, 1m/s	44.12	0.13	1.54
	12MPa, 1m/s	43.14	0.09	0.96
	4MPa, 2m/s	40.91	0.15	1.54
	4MPa, 3m/s	55.77	0.16	2.64
5/10/0/15	1MPa, 1m/s	29.41	0.50	0.86
	4MPa, 1m/s	52.33	0.33	1.12
	8MPa, 1m/s	69.12	0.26	1.71
	12MPa, 1m/s	74.92	0.18	1.26
	4MPa, 2m/s	71.45	0.30	2.64
	4MPa, 3m/s	78.57	0.23	2.31
5/5/5/15	1MPa, 1m/s	29.74	0.49	0.89
	4MPa, 1m/s	50.99	0.33	0.98
	8MPa, 1m/s	57.24	0.21	1.22
	12MPa, 1m/s	60.65	0.14	0.95
	4MPa, 2m/s	54.90	0.21	1.09
	4MPa, 3m/s	67.20	0.20	1.40

4.1.2 Under High *pv* Conditions

In order to evaluate load-carrying capacity, selected compositions were tested in a wide range of *pv* factors, e.g. nominal pressure in a range from 0.5 to 12 MPa and sliding velocity from 0.5 to 3 m/s. Results are given in Table 4.2.

Fig. 4.4 presents the typical friction process of the composition [5/0/5/15] with nanoparticles in comparison with that of [0/5/5/15] without nanoparticles, under a high *pv* condition, i.e. 4MPa, 1m/s. In comparison with Fig. 4.2, the duration of the running stage of both composites was apparently reduced. This reduction was caused by the more rapid formation of transfer films due to the accelerated generation of wear debris. After the running-in stage, the frictional coefficient of the composite without nano-TiO_2 became stable. However, for nanocomposite, the frictional coefficient subsequently decreased, and resulted in an observed reduction of friction. Accordingly, the contact temperature for the nanocomposite was much lower.

Fig. 4.5a shows the worn surfaces of composition [0/5/5/15] without nanoparticles tested at 4MPa, 1m/s. Due to the friction force and consequently the contact temperature being greatly increased at a higher pressure, the breakage of the matrix was seriously exacerbated, especially in the interfacial region. As a result surface damage

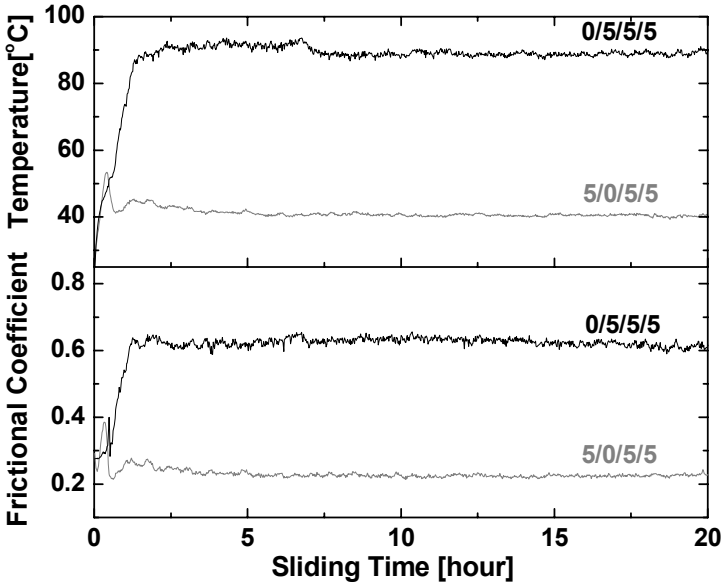

Figure 4.4: Comparison of the frictional process of the compositions [0/5/515] and [5/0/5/15] at high *pv* conditions i.e. 4MPa, 1m/s and 1MPa, 2m/s.

was remarkably increased with serious fibre peeling-off (Fig. 4.5a). Accordingly, almost the entire fibre debris was observed on the counter surface (Fig. 4.5b). In this case, fibres were removed in larger patches and underwent little wear process [120,121]. Moreover, the large fibre debris could further decrease the wear resistance of the composite owing to a three-body abrasive wear effect [14], whereas the smaller ones are believed to be helpful to the formation of transfer film and lead to a reduced frictional coefficient [119]. Therefore, the wear rate of the composites without nanoparticles was progressively increased at increased pv factors.

Fig. 4.5c shows the worn surface of the nanocomposite tested at 4MPa, 1m/s. In comparison with Fig. 4.5a, it is clear that the worn surfaces are much smoother under

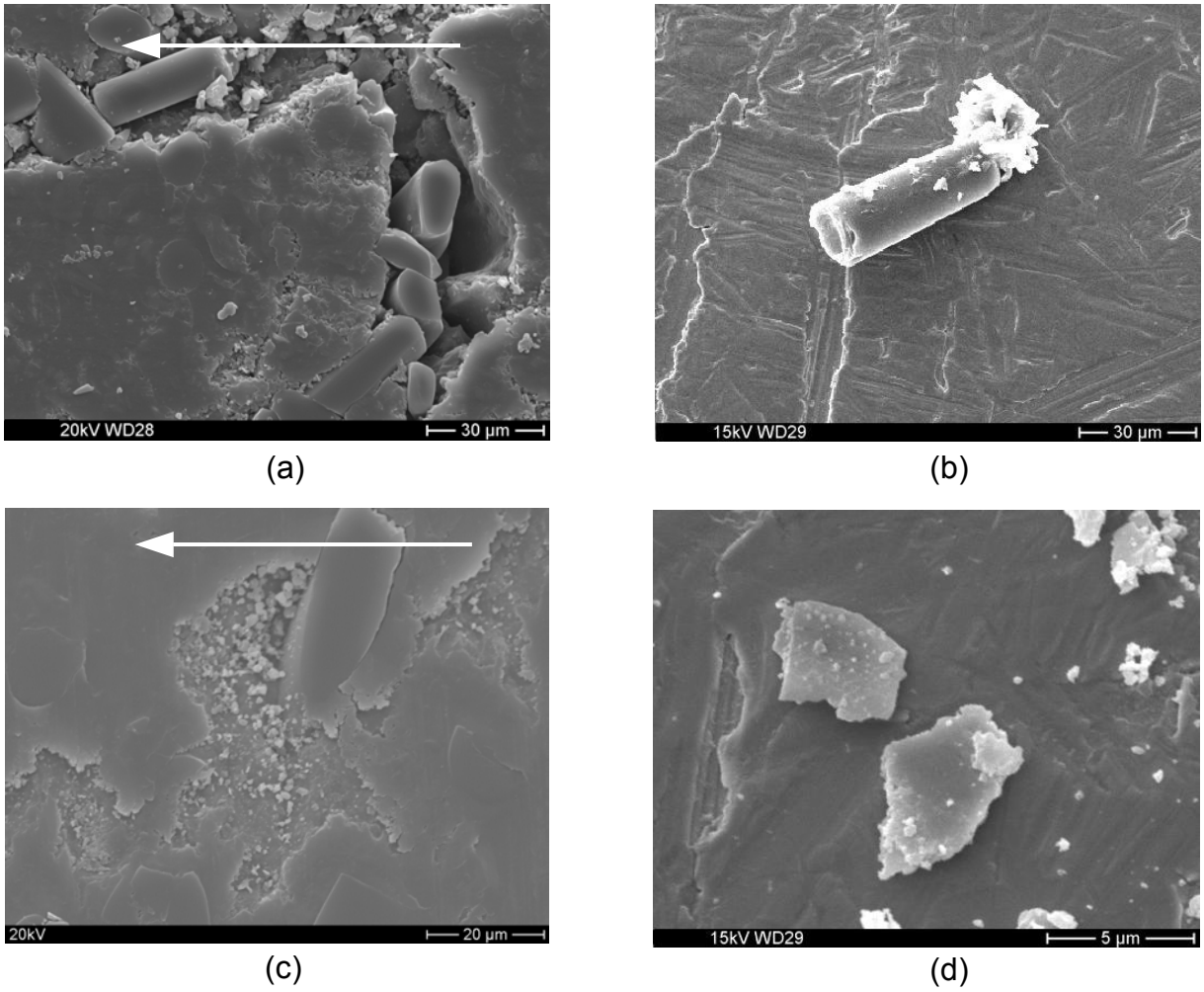

Figure 4.5: SEM micrographs of (a) the worn surface of [0/5/5/15] and (b) the fibre debris on the counterface and (c) the worn surface of [5/0/5/15] and (b) the fibre debris on the counterface at 4MPa, 1m/s

the same sliding conditions and the SCF peeling-off is greatly limited with the addition of nano-TiO2. As shown in Fig. 4.5c, even under relatively high contact pressure the worn surface performed relatively smoothly and is characterized by micro surface damage caused by fatigue wear, which normally occurs at high temperatures and removes the surface layer by micro-cracks [14]. Accordingly, the fibre debris generated from the nanocomposite (cf. Fig. 4.5d) is much thinner and smaller than that of [0/5/5/15] under the same sliding condition. Therefore, with the addition of nanoparticles, the fibres are maintained in the matrix with a very gradual wear process even at high *pv* conditions, leading to an enhanced load-carrying capacity of the nanocomposites. This enhancement also supports the explanation of the lower wear rate resulting from the B-o-R compared to that from the P-o-D, discussed in section 4.1.1.

It was noticed that the features of the worn surfaces of both nanocomposites [5/0/5/15] and [5/5/5/15] were very similar at relatively lower *pv* conditions. However, with both graphite and PTFE, the composition of [5/5/5/15] showed more stable wear performance under extremely high *pv* conditions, e.g. 12MPa m/s. It seems that although additional lubricants contribute to stable development of transfer film even under extreme sliding conditions, the wear mechanisms of nanocomposites are mostly determined by a combinative effective of short carbon fibre and nanoparticles. To understand the dominant wear mechanisms, the highly localized characterization of fibres in worn surfaces was examined by AFM on a nanoscale, as further discussed in section 4.2.1.1.

4.1.3 Time-Related Depth Wear Rate

The time-related depth wear rate calculated by equation 1.2 was evaluated as a function of the *pv* factor (see Fig. 4.6), in order to comprehensively understand the wear behaviour of epoxy composites with and without nano-TiO2. To avoid measurement error with regard to height reduction which may be caused by elastic deformation under high contact pressure, the finial mass loss was applied to calculate the depth wear rate. It is evident that the basic wear factor k* of the nanocomposite was lower

(cf. equation 1.2 in Chapter 1). Furthermore, for the composition [0/5/5/15] without nanoparticles, the change of the depth wear rate curve from linear to nonlinear occurred between 2 and 4MPa m/s, whereas for the nanocomposite [5/0/5/15] it occurred between 4 and 8MPa m/s. It is clear that the "*pv* limiting" for the latter was certainly enhanced.

On the basis of further investigation of the epoxy nanocomposites with lubricants in different proportions and combinations, it was found that at an extreme high *pv* factor, e.g. 12MPa·m/s, the composite with a combination of two lubricants, i.e. a composition of [5/5/5/15], produced the best wear resistance, as shown in Table 4.2. Nevertheless, different compositions should still be considered in practice according to various wear conditions. The contribution of various fillers to enhance the wear performances of the composites is further discussed in the following sections.

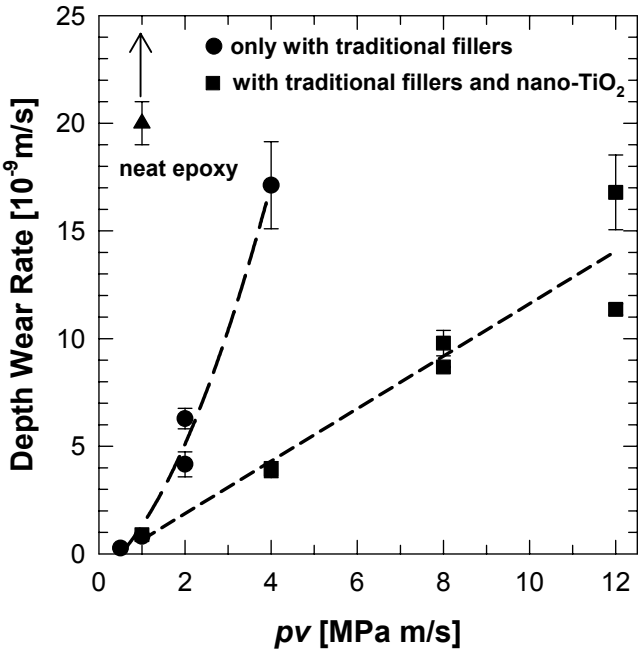

Figure 4.6: Comparison of the time-related depth wear rate of epoxy composites with and without nano-TiO_2 as a function of *pv* factor.

4.2 Contribution of Various Fillers

4.2.1 A Combinative Effect of Short Carbon Fibre with Nano-TiO_2

4.2.1.1 AFM Observations

In order to further understand the dominant wear mechanisms, highly localized characteristics of fibres in worn surfaces, were examined by AFM on a nanoscale. Fig. 4.7a shows an AFM image of a nearly normal directional carbon fibre of the composition [0/5/5/15] without nanoparticles tested at 1MPa and 1m/s. Cross-sectional measurement was performed (as shown in Fig. 4.7b) and the results are summarized in Table 4.3. It can be seen that the fibre surface is quite smooth, but tilted to the worn surface. Interfacial damage between SCF and matrix has occurred behind the sliding direction. The height of the exposed fibre, i.e. the difference in height between 'A' and 'B' (0.31μm), is close to the initial roughness of the counterpart surface (about 0.22μm). Therefore, during friction, the exposed fibre sustained most of the load and was tilted due to the impact of the asperities of the counterpart.

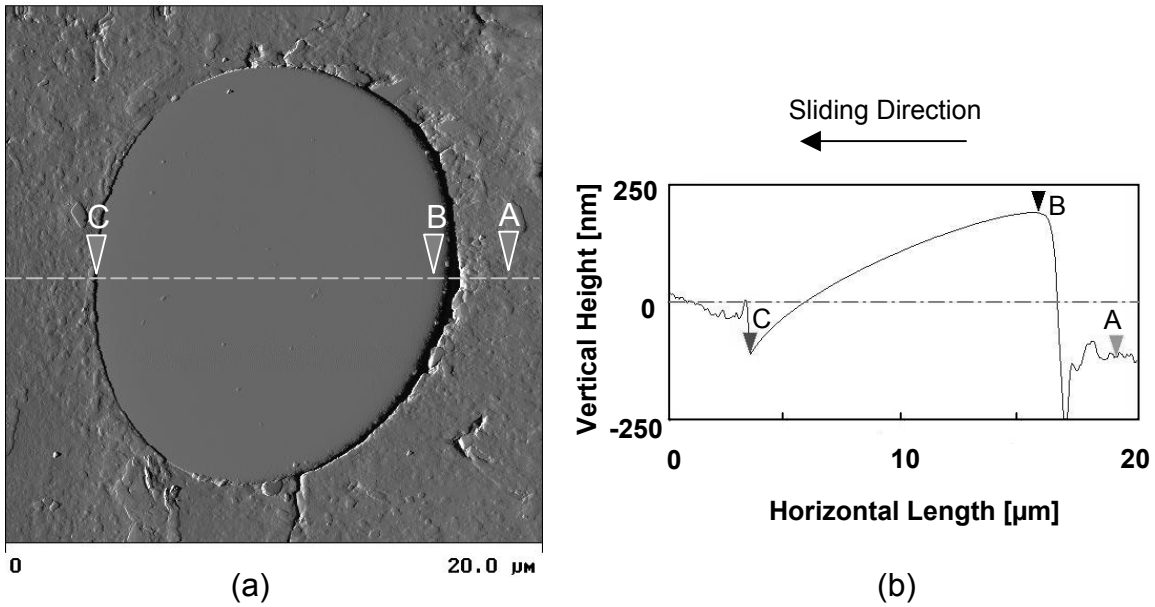

Figure 4.7: (a) AFM image of fibre in the worn surface of [0/5/5/15] without nanoparticles at 1MPa and 1m/s, and (b) a cross-sectional measurement. The arrows represent the sliding directions.

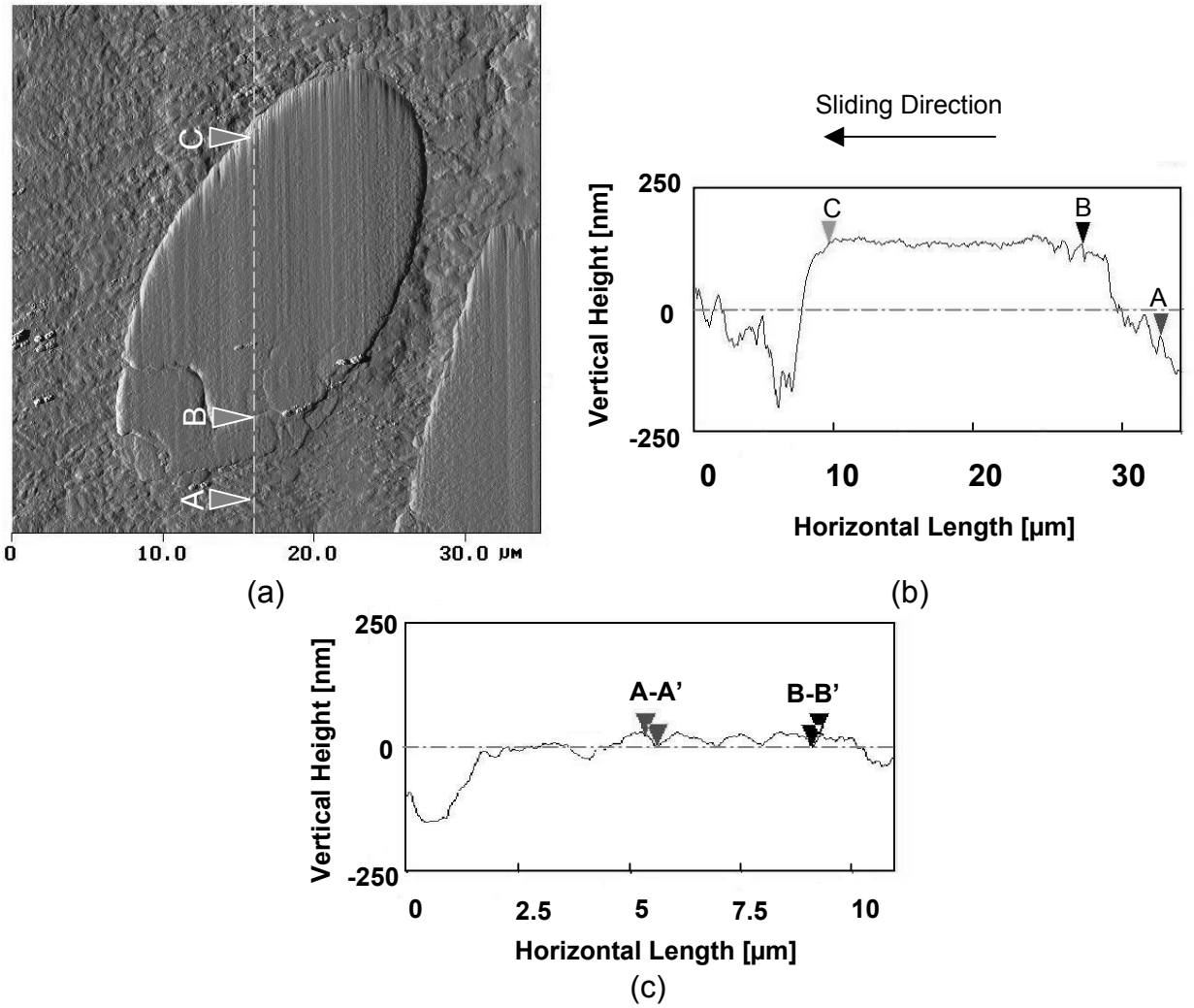

Figure 4.8: (a) AFM image of fibre in the worn surface of [5/0/5/15] at 1MPa and 1m/s, (b) a cross-sectional measurement, and (c) AFM sectional measurement of the nanoscale grooves.

Table 4.3: Summary of cross-sectional measurement results by AFM.

	Fig. 4.9b [0/5/5/15]		Fig. 4.10b [5/0/5/15]		Fig. 4.10c [5/0/5/15] (nanoscale grooves)	
	A-B	B-C	A-B	B-C	A-A'	B-B'
Surface-distance[1] [µm]	3.610	12.310	5.647	18.272	0.266	0.178
Horizontal-distance[2] [µm]	3.320	12.305	5.605	18.252	0.264	0.176
Vertical-distance[3] [nm]	307.570	310.880	178.60	2.089	22.955	23.551
Angle[4] [degree]	5.292	1.405	1.917	0.007	4.976	7.631

[1]The 'surface-distance' refers to the surface trace between two points.

[2]The 'horizontal-distance' refers to the linear length in the horizontal direction.

[3]The 'vertical-distance' is the linear height in the vertical direction.

[4]The 'angle' indicates that of the horizontal direction and the line determined by the two measured points.

Fig. 4.8a provides an AFM image of a carbon fibre nearly in the normal direction of nanocomposite [5/0/5/15] tested at 1MPa and 1m/s. A cross-sectional measurement is presented in Fig. 4.8b and the results are summarized in Table 4.3. In comparison to Fig. 4.7 the fibre surface is relatively rough with tiny nanoscale grooves (Fig. 4.8a) which are parallel to the sliding direction. In this case, parts of the fibre behind the sliding direction were broken. The height of the exposed fibre was about 0.18μm, which coincides with the roughness of the counter surface (0.22μm). However, the fibre surface is parallel to the worn surface, whereas it was tilted for the composite without nanoparticles (Fig. 4.7). It is clear that the performance of short carbon fibres during sliding was very different for the composites with and without nanoparticles.

As shown in Fig. 4.8a, obvious nanoscale grooves were observed on the fibre surfaces of the nanocomposite. Fig. 4.8c shows a perpendicular sectional measurement of nanoscale grooves and the results are given in Table 4.3. The width of the grooves is in a range of 300~500nm, which is in the same order as the nanoparticle size (300nm). However, the depth of the grooves is only around 20~30nm. It is therefore considered that some of the individual hard nanoparticles were possibly embedded in the counter surface, whilst they scratched the fibres slightly as third bodies [16-19]. The very shallow grooves suggest that the size of the nanoparticles is close to the gap between two counterparts. In this case, it is reasonable to hypothesize that for hard nanoparticles, the sliding/grooving and rolling/indentation wear occurred simultaneously. The latter protected the short fibre from the impact of counterface asperities. This hypothesis is further confirmed by observation of the tracks on fibre surfaces caused by the nanoparticles at high *pv* conditions.

Fig. 4.9 shows the worn surfaces of the nanocomposite [5/5/5/15] tested at 12MPa, 1m/s and 4MPa, 3m/s respectively. Discontinuous nano-indentations were observed (Fig. 4.9a), suggesting that indentation/rolling wear prevailed on the rubbing surface [20], that is, nanoparticles tended to roll rather than slide when traversing the wear specimens. However, at 4MPa and 3m/s, the wear tracks were clearly combined with continuous grooves and interrupted dents (Fig. 4.9b). The change of particle behaviour could be explained by the remarkably increased flash temperature at the real contact area under extreme sliding conditions, which can be much higher than the

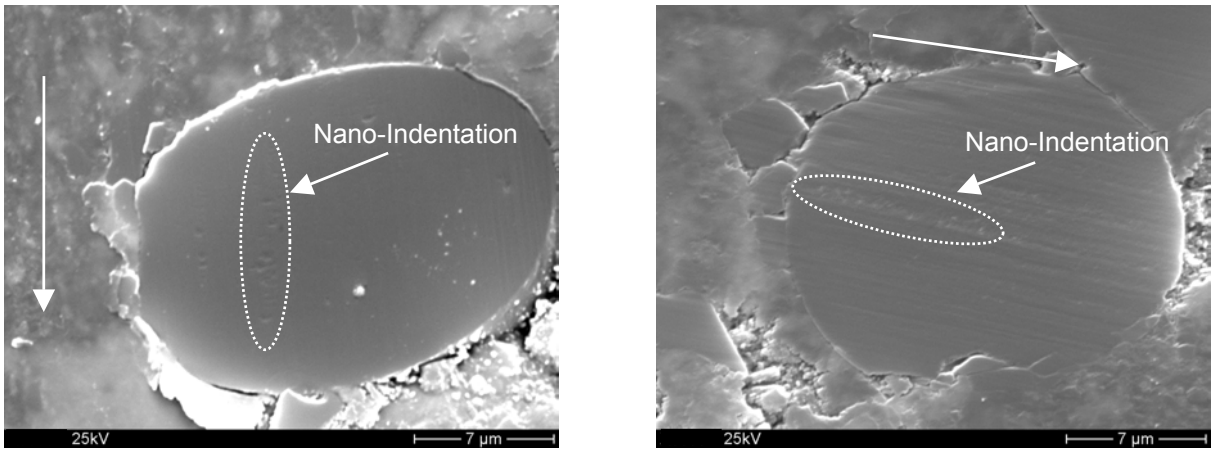

(a) (b)

Figure 4.9: Nanoscale grooves of the nanocomposite [5/5/5/15] at higher *pv* factors: (a) 12MPa and 1m/s and (b) 4MPa and 3m/s. The arrows represent sliding directions.

bulk contact temperature [21]. In this case, the viscosity of the transfer film, which was mainly composed of epoxy wear debris, was evidently increased during friction. Therefore, the nanoparticles were relatively free to roll/indent during the process rather than slide/plough. This could also explain the observed reduction of frictional coefficient of the nanocomposite under higher *pv* conditions (Table 4.2).

4.2.1.2 Mechanical Models of Short Fibre Peeling off

Over the last decades, remarkable developments have been made to understanding the micro-abrasion mechanisms of materials caused by the addition of hard particles in rubbed components, which normally results in a three-body abrasive wear. It has been noticed that the wear rate of three-body abrasion was sometimes 10 times lower than that of two-body abrasion [13]. Most analyses have assumed that the apparently reduced wear rate resulting from three-body abrasion is caused by a rolling effect of the particles, which depends strongly on their size and shape, as well as the hardness and sliding conditions of the pairs of materials [16,18–20]. The benefit of the rolling effect is mainly attributed to the following two factors: (i) the remarkable reduction of the frictional coefficient, and (ii) the spontaneous restriction of the grooving/cutting wear by hard particles. In our case, for the short carbon fibre reinforced composites, a special advantage achieved by the rolling effect of nanoparticles is protecting carbon fibres from serious peeling off. Schematic illustrations of the above

mentioned mechanisms are presented in Figs. 4.10 and 4.11, respectively. For composites without nanoparticles, the following three stages are involved (cf. Fig. 4.10):

a) Matrix worn off, fibre exposed, and fibre thinned. The fibre is tilted by shear force and then interfacial damage occurs [22].

b) Marked damage to the brittle matrix in the interfacial region, and severe fibre/matrix debonding.

c) The exposed fibres are peeled off from the matrix.

The following characteristics are proposed for nanocomposites (cf. Fig. 4.11):

a) Nanoparticles are considered as third body abrasive particles.

b) During sliding, a rolling effect of nanoparticles, especially at the edge of SCF, can reduce the shear stress and accordingly the frictional coefficient.

c) Matrix damage in the interfacial region is reduced by this rolling effect. This rolling effect protects the SCF remaining in the epoxy matrix, which finally is cut in very thin pieces (as shown in Fig. 4.5d). This process probably plays a key role in the enhanced wear resistance.

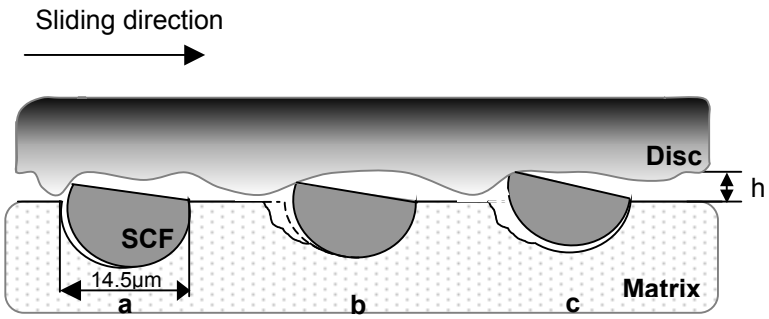

$h \approx R_{a\_disc} = 220nm$

Figure 4.10: Schematic outline of a process model of fibre removal for the composite without nanoparticles: (a) interfacial debonding and rotation of fibre, (b) breakage of the matrix at interfacial regions, and (c) the peeling-off of entirely exposed fibres.

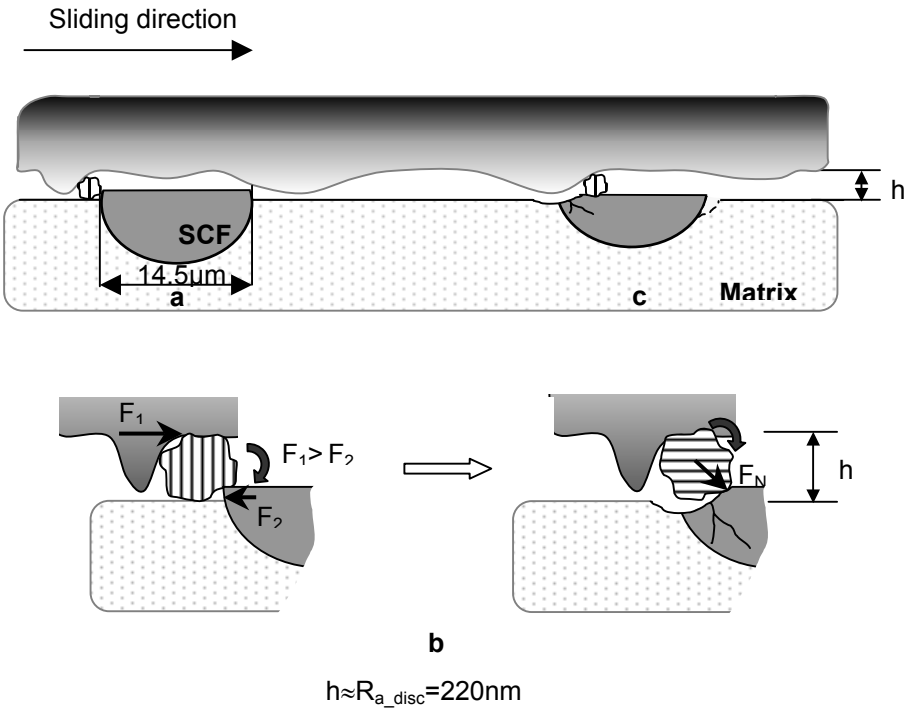

Figure 4.11: Schematic outline of a process model of fibre removal for the composite with nanoparticles: (a) three-body contact of nano-TiO_2, (b) rolling effect of nano-TiO_2, and (c) damage of fibre.

For the model of this positive rolling effect, it is evident that particle dimension should be consistent with the gap between rubbing surfaces, which is mostly determined by the roughness of the steel counterpart. To validate the proposed rolling mechanism, the wear properties of the composites were further investigated against a finely polished smoother disk with *R*a of 0.03μm, which is markedly smaller than the nanoparticles. The results are presented in the following section.

4.2.1.3 Influence of Surface Roughness of the Counterface

Fig. 4.12 compares the typical friction processes of two composites with and without nanoparticles against the normal (rougher) steel disk (Ra=0.23μm) and the finely polished (smoother) steel disk (Ra=0.03μm) at 2MPa, 1m/s. Here, the insert shows the value of the specific wear rate and the frictional coefficient, which is a mean value during the steady state of the friction process. Each result is an average value of at least three experimental data, with scatter in data being within ±10%.

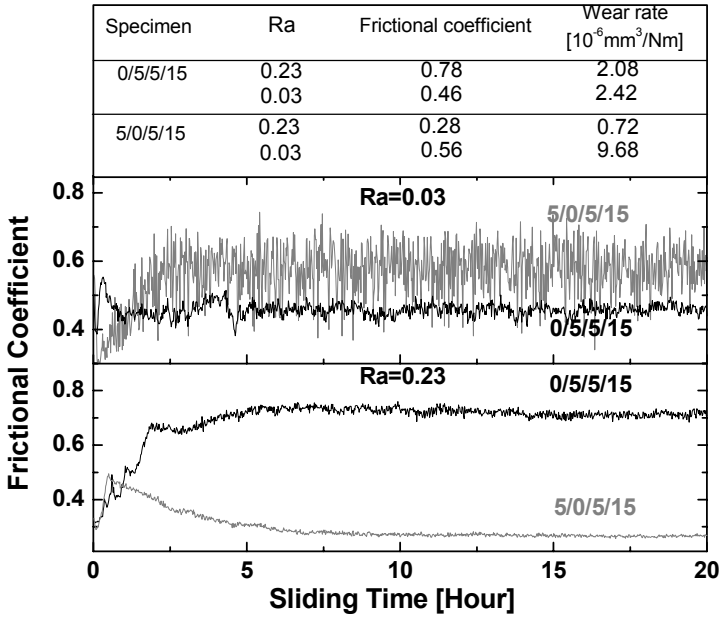

Figure 4.12: Typical frictional processes of the compositions [0/5/515] and [5/0/5/15] against unpolished (0.23μm Ra) and polished (0.03μm Ra) disks at 2MPa, 1m/s.

As shown in the figure, the frictional coefficient of nanocomposite was apparently reduced after the running-in stage when sliding against the rougher disk. Accordingly, the wear resistance of the composite was remarkably improved by additional nanoparticles, which is consistent with our earlier observations. However, the frictional coefficient of the composite without nanoparticles was reduced from 0.78 to 0.46 when running against the smother disk. This reduction may be caused by a decrease in the impact of asperities of the polished counterface. However, the wear rate of the composite [0/5/5/15] was slightly increased, probably as a result of more severe adhesive wear due to the larger real contact area. For nanocomposite [5/0/5/15], it was interesting to note that no friction reduction was observed after the running-in stage when sliding against the smoother disk. On the contrary, the frictional coefficient of [5/0/5/15] was slightly higher than that of [0/5/5/15]. Simultaneously, the wear rate of the nanocomposite increased markedly.

Fig. 4.13 shows the features of the worn surfaces of the two composites tested against the polished counterfaces. For both composites, the patterns of the two worn surfaces are very similar and much small wear debris is clearly observed, which was produced by micro-cracks at the surface or sub-surface due to a strong adhesive

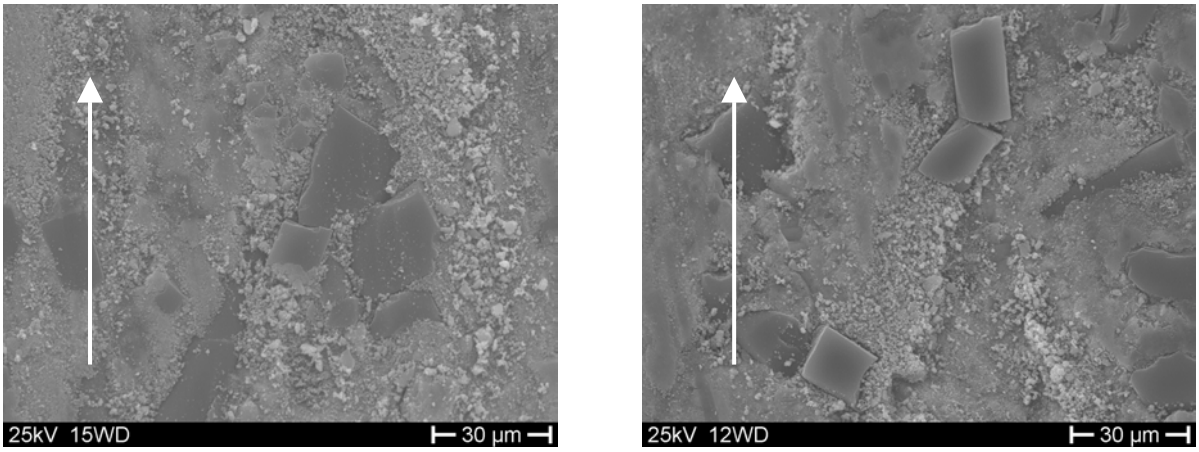

(a) (b)

Figure 4.13: SEM micrographs of the worn surfaces of compositions (a) [0/5/515] and (b) [5/0/5/15] against a polished disk (0.03µm Ra) at 2MPa and 1m/s.

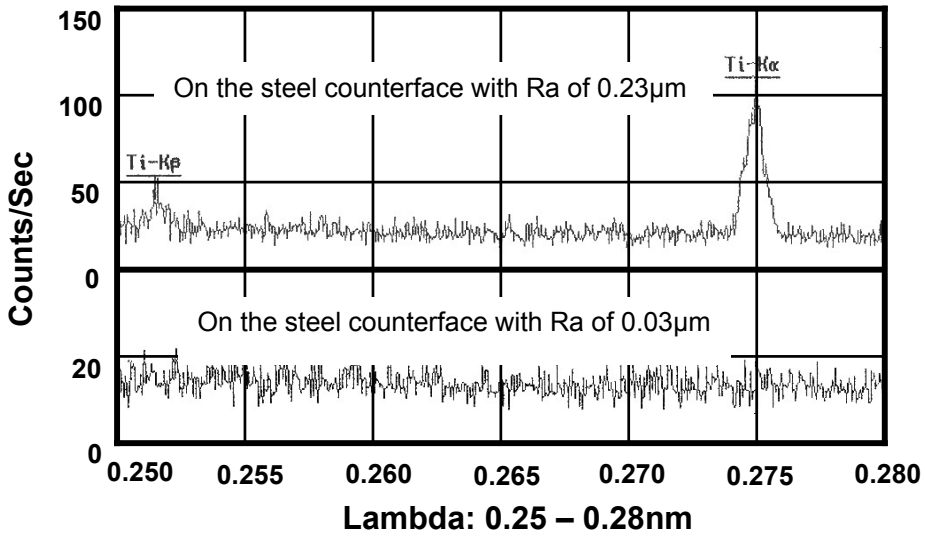

Figure 4.14: WDX analysis of Ti-K_α and Ti-K_β on both unpolished (0.23µm Ra) and polished (0.03µm Ra) steel counterfaces

wear mechanism. The much higher wear rate of the nanocomposite may be the result of two negative effects caused by the addition of nanoparticles: (i) deterioration of the mechanical properties of the composite owing to weak interfacial bonding, and (ii) introduction of the third body abrasive wear mechanism.

To characterize nano-TiO_2 particles, spectral analysis of WDX was carried out on the wear regions within an area of 100µm×100µm for both normal (rougher) and finely polished (smoother) counterfaces against nanocomposite [5/0/5/15]. As shown in Fig.

4.14, obvious peaks of Titanium elements (representing nano-TiO_2) are observed on the rougher counterface but not on the smoother one. Therefore, when the nanocomposite slid against the rougher disk, nano-TiO2 was embedded on the counterface and resulted in sliding and/or rolling wear mechanisms. As a result, slight grooves and/or nano-indentations were correspondingly produced on the fibres (cf. Fig. 4.9). However, when the nanocomposite slid against a smoother disk, if fibre and/or graphite and/or matrix pieces were detached, their dimensions were much greater than those of the nanoparticles (cf. Fig. 4.13b) due to strong adhesive wear. As a result, the nanoparticles could not provide the expected rolling effect. Accordingly, reduction in the frictional coefficient was not observed. The experimental results confirmed, albeit indirectly, the hypothesis of the positive effect of nanoparticles on the reduction of the frictional coefficient.

4.2.2 Comparison of Two Solid Lubricants: Graphite and PTFE

As already mentioned, PTFE and graphite are widely used as internal lubricants to reduce the frictional coefficient and additionally the wear rate of polymeric composites [5]. The crystalline structure of the two lubricants is shown in Fig. 4.15. As shown in the figure, the lubricating effect of PTFE is provided by its unique molecular structure, which consists of crystalline slices with a thickness of 20~50 nm [13]. The individual slices can easily slip and transfer as small lumps with an average diameter of 1 μm. Because of a strong adhesion between PTFE and metallic surfaces, a third-body transfer film can be developed, resulting in reduction of the frictional coefficient. Graphite also has a layer structure, in which the atoms are arranged in a hexagonal pattern with a layer space of 3.35Å [23]. These hexagonal carbon sheets are held together by weak van der Waals interactions, which may be easily broken under applied stress. Especially within the carbon layer, graphite is quite stiff, and therefore its transfer film also exhibits stiff behaviour compared to that of PTFE. In order to evaluate the different tribological effects of the two lubricants on nanocomposites, the surface morphology and mechanical properties of the transfer films developed with each of the lubricants were investigated. In order to study and compare the contributions of of two solid lubricants, four compositions were involved: (1) [5vol.%nano-TiO_2+15vol.%SCF], (2) [5vol.%nano-TiO_2+10vol.%graphite+ 15vol.%SCF], (3)

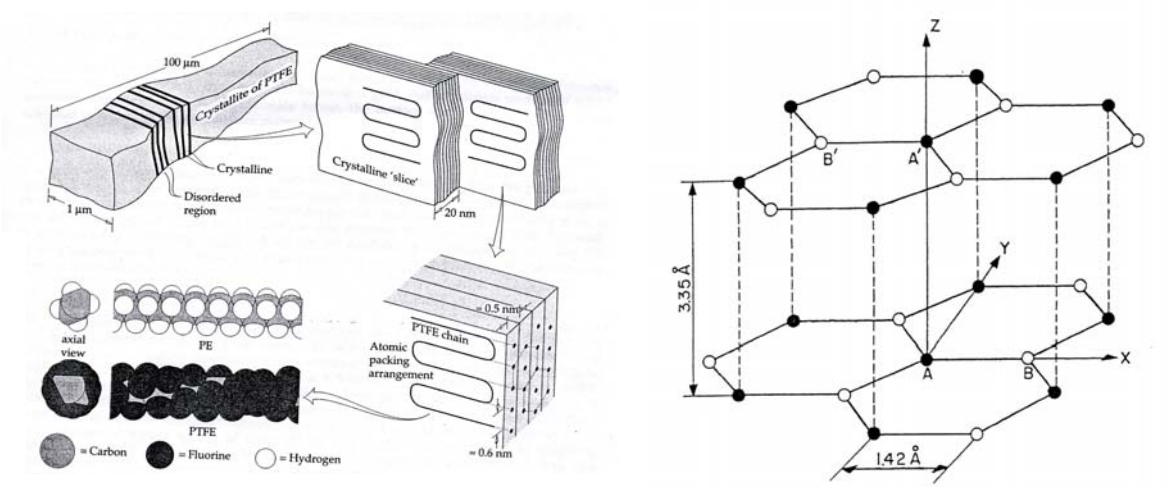

(a) (b)

Figure 4.15: Crystalline structure of (a) PTFE [14], (b) graphite [124]

[5vol.%nano-TiO_2+10vol.%PTFE+5vol.%SCF], and (4) [5vol.%nano-TiO_2+5vol.%graphite+5vol.%PTFE+5vol.%SCF]. For convenience, the materials are described as composites 'without lubricants', 'with graphite', 'with PTFE' and 'with both PTFE and graphite', respectively.

4.2.2.1 Under Standard Wear Condition: 1MPa and 1m/s

Fig. 4.16 compares the typical variations of the frictional coefficient against the sliding time for the composite without lubricant and the other two compositions filled with only one kind of lubricant. It was clear that both the lubricants effectively reduced the duration of the running-in stage, and accordingly the final wear rate (Table 4.1). The composite with PTFE achieved the lowest peak value of frictional coefficient and the shortest duration of running-in stage, which was attributable to the special transfer mechanism of PTFE, so-called 'lumpy transfer'. In comparison to the atom layer transfer formed by graphite flakes, the 'lumpy transfer' of PTFE has the advantage of quicker formation of a stable transfer film due to its larger size and lower combination between crystalline slices. However, it can be also observed in Fig. 4.16 that graphite flakes contributed to a lower stable frictional coefficient (0.38 in comparison to 0.5 of only with PTFE) and thus a lower average wear rate in general ($6.4\times10^{-7}mm^3/Nm$ in comparison to $8.6\times10^{-7}mm^3/Nm$ of only with PTFE).

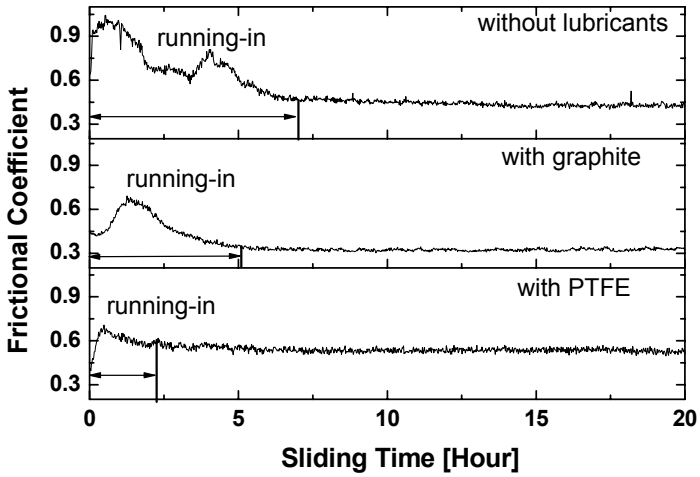

Figure 4.16: Typical variations of the frictional coefficient against sliding time of the composite without lubricant and the composites with graphite and with PTFE

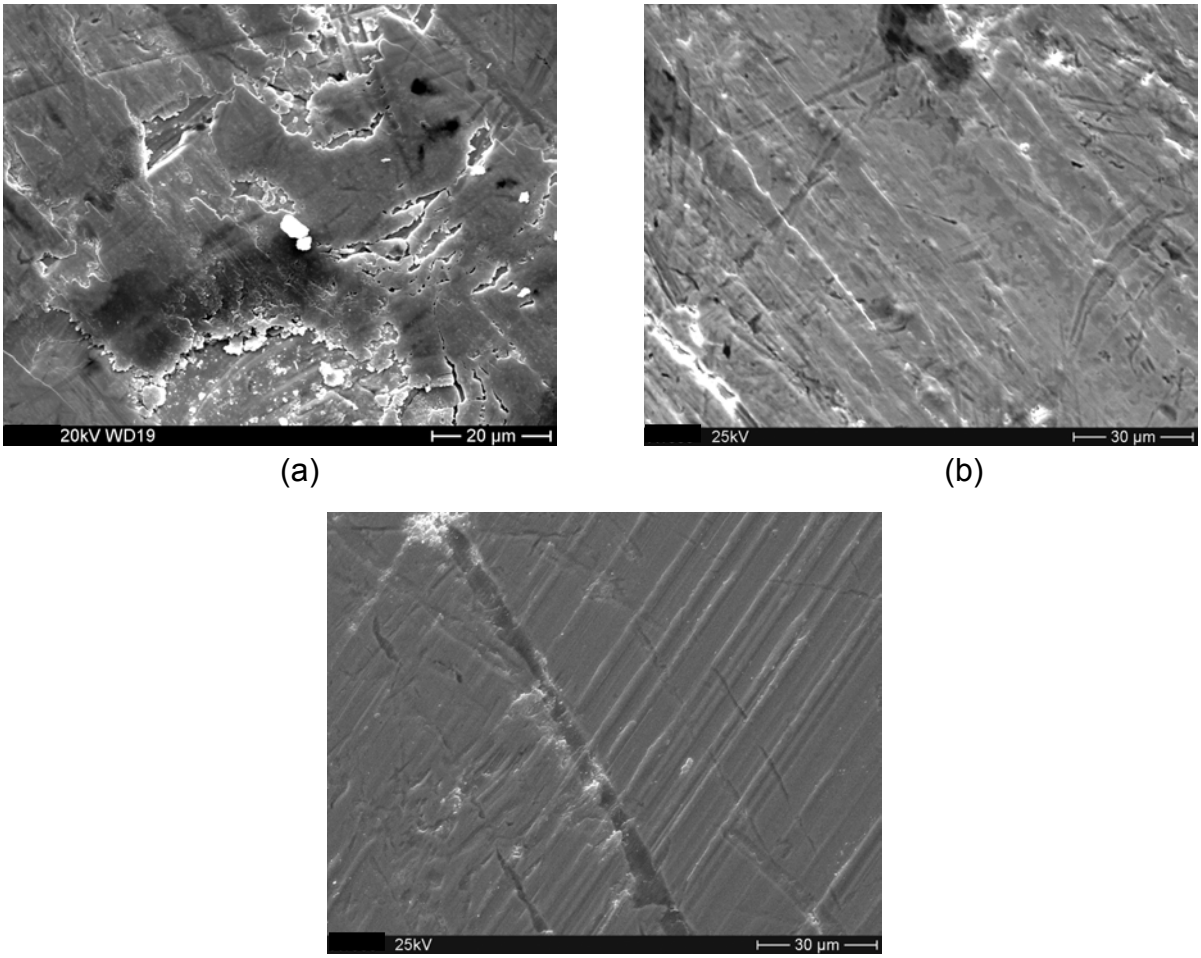

(a) (b)

(c)

Figure 4.17: SEM micrographs of the transfer film developed on counterface by (a) the composite without lubricants, (b) the composite with graphite and (c) the composite with PTFE.

Fig. 4.17 shows the micro-morphologies of the transfer films on the metallic counterpart surfaces formed by three nanocomposites. Transfer films were evident in in the sliding regions for all three compositions. With the magnified view, it can be observed that the transfer film developed slightly discontinuously for the composition without lubricants. The transfer film for the composition with graphite seemed to be more compact and smooth with slighter fibre scratches, generating a relatively lower stable frictional coefficient (cf. Fig. 4.16).

4.2.2.2 Under Extreme High *pv* Conditions

Fig. 4.18 shows the sliding processes for the two lubricated composites under extreme high *pv* conditions i.e. 12MPa, 1m/s and 4MPa, 3m/s. In comparison with low *pv* factors, it is clear that the duration of the running-in stages was greatly reduced in both cases, which corresponds to the accelerative effect of the formation of stable transfer films. However, at 12MPa, 1m/s, due to the more noticeable effect on the atom layer transfer for graphite under the very high pressure, the composite with graphite showed even lower frictional work and therefore a lower contact temperature during the running-in stage. At the same time, the stable frictional coefficient of both nanocomposites was greatly decreased. Nevertheless, the composite with graphite achieved a lower stable frictional coefficient and average wear rate as a whole (Table 4.1).

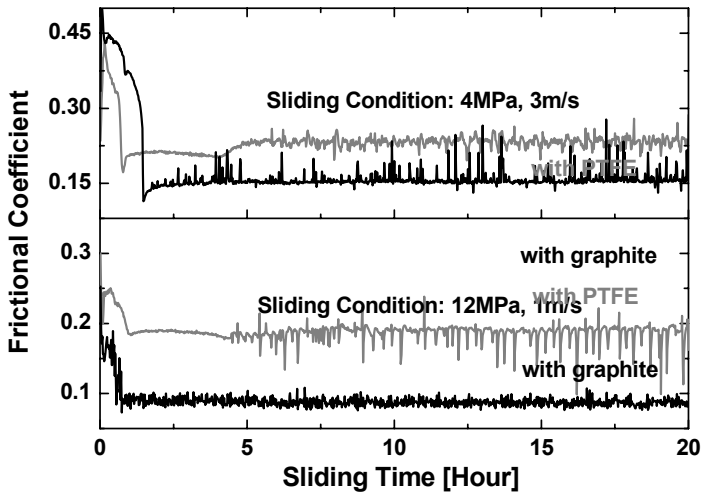

Figure 4.18: Comparisons of the friction processes of the compositions with graphite and with PTFE at high *pv* factors, i.e. 12MPa, 1m/s and 4MPa, 3m/s.

At 4MPa, 3m/s, the frictional work for the composite with graphite in the running-in stage was much higher, although the stable frictional coefficient was still low. Consequently, a very high peak value of surface temperature of 153°C occurred at about half an hour. This value was even close to the T_g of the epoxy matrix, which was near 160°C determined by the peak value of $tan\delta$ measured by a dynamic-mechanical-thermoanalyzer (DMTA, GABO Qualimeter Tesanlagen, GmbH). With a strong softening effect in the glassy region, the wear rate of this material could be relatively high [125]. As a result, the average wear rate of the composite with graphite was slightly higher than that with PTFE, even with lower stable frictional coefficient (Table 4.1).

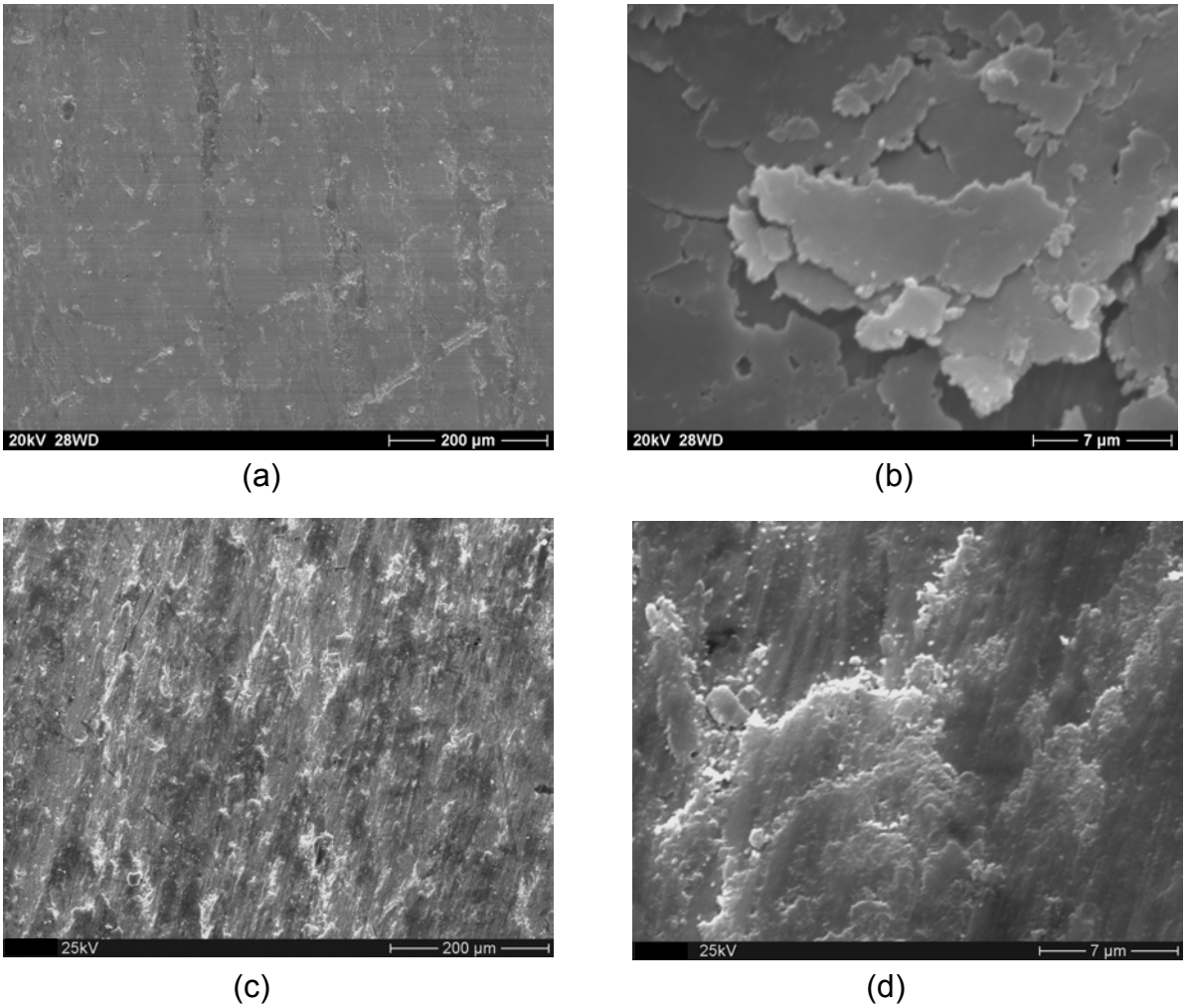

Figure. 4.19: SEM micrographs of (a) the transfer film formed by the composite with graphite, and (b) a magnified view and (c) SEM micrographs of the transfer film formed by the composite with PTFE and (d) a magnified view. Sliding condition: 4MPa and 3m/s.

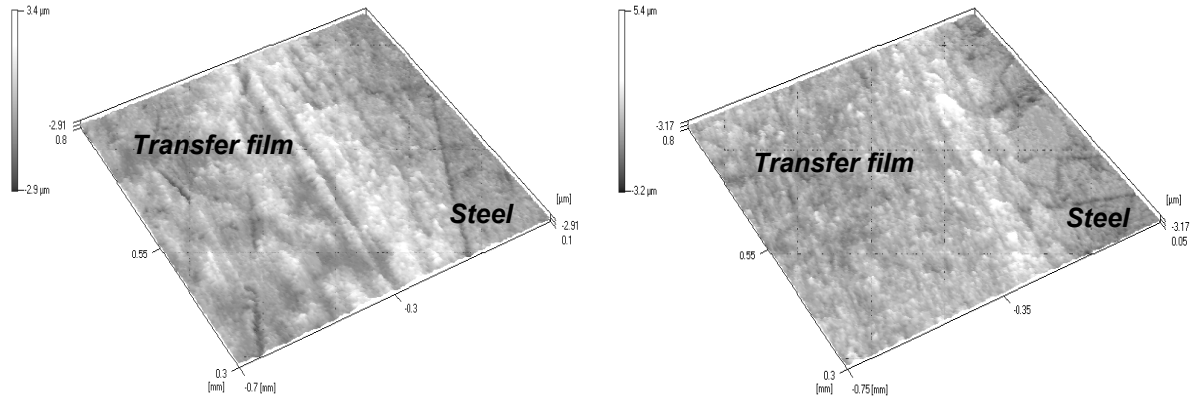

(a) (b)

Figure 4.20: Surface profiles of transfer film on the counter surfaces formed of the composition (a) with graphite, and (b) with PTFE. Sliding condition: 4MPa, 3m/s.

Fig. 4.19 shows the SEM micrographs of transfer films formed with the two lubricants at 4MPa and 3m/s. The transfer film formed with graphite appears rather compact and smooth while that formed with PTFE is more uniform and continuous, suggesting stronger adhesion to the metallic counterpart surface. With magnified views, the transferred material from the composite with graphite is found to be formed by many thin sheets (Fig. 4.19b), whereas with PTFE it is formed of tiny clumps (Fig. 4.19d). Thus, due to the different molecular structures and transfer formation of these two lubricants, the transfer films developed with different features and resulted in different friction processes. However, the role of transfer films in the sliding process is very complex because it involves a number of factors and the interactions among them, e.g. the thickness and hardness of the transfer film, the frictional coefficient, surface temperate etc. Fig. 4.20 presents scanning pictures by the laser profilometer of counterpart surfaces covered by transfer films. According to the different grey scales, the transfer film formed with PTFE appears more uniform and thicker, which is consistent with the SEM observations.

4.2.2.3 Hardness of Transfer Films

Micro-hardness tests were performed to characterize the mechanical properties of the transfer film layers. It was reported by K. Friedrich et al [41] that, when hardness-depth results were considered, the transfer film on a steel substrate showed typical

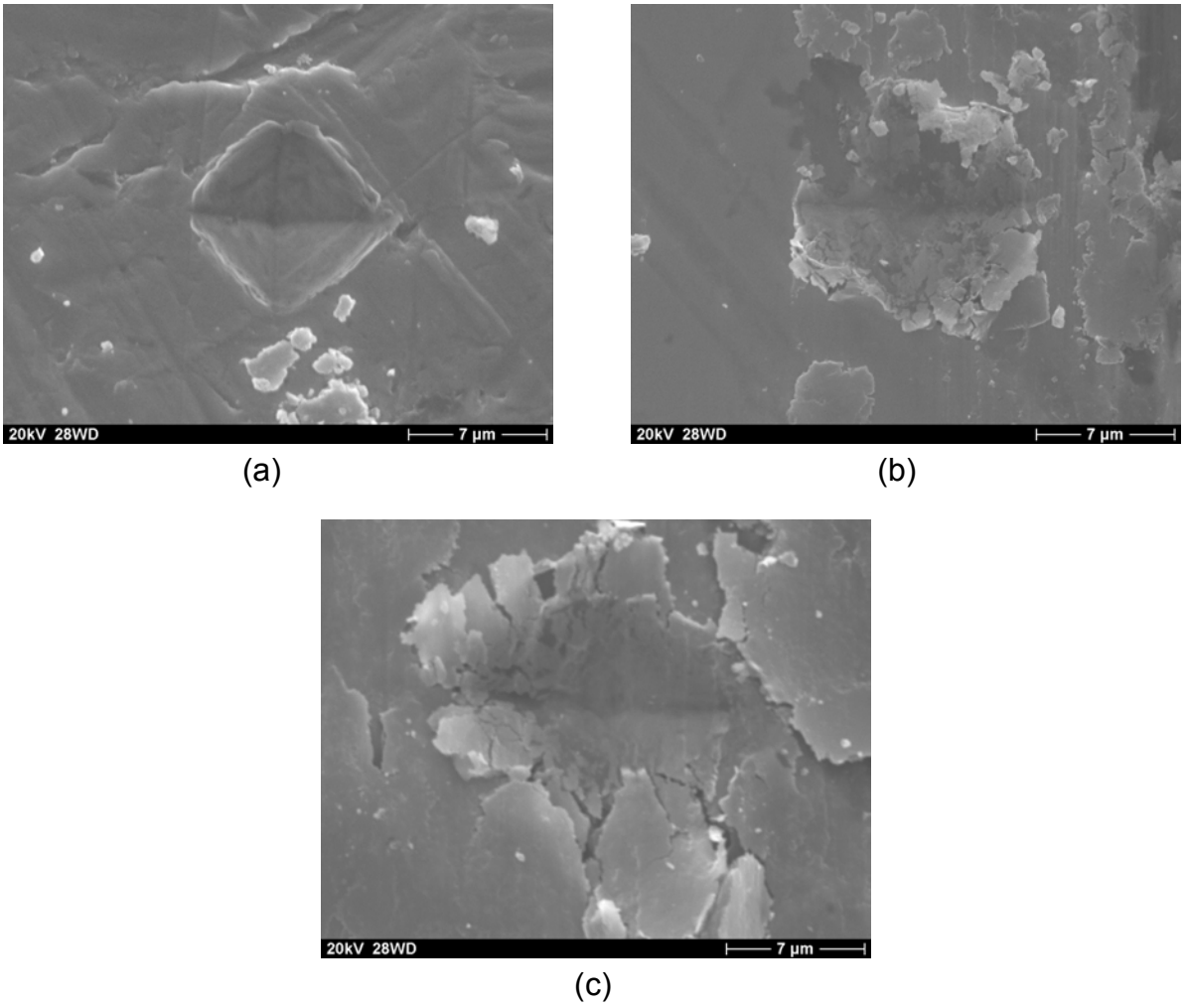

Figure 4.21: SEM pictures of micro-indentations on (a) the metallic counter surface, (b) the transfer film on the steel substrate formed by the composite with graphite, and (c) the transfer film formed by the composite with PTFE. Sliding condition: 4MPa and 3m/s.

layer behaviour according to its thickness. Two corresponding stages can be recognized during the indention process on the transfer film, which can also be indicated by the SEM pictures of micro-indention sites as shown in Fig. 4.21. The first stage is deformation of the transfer film, and the second stage is indention of steel substrate.

Fig. 4.22a shows the loading-unloading curves of micro-hardness tests carried out under 50mN with a load speed of 6.62mN/s. The hardness measures of the steel, the film with graphite and that with PTFE were 14.02, 5.89 and 2.58 GPa, respectively. As shown in the figure, although the full depths of the materials are very different, the

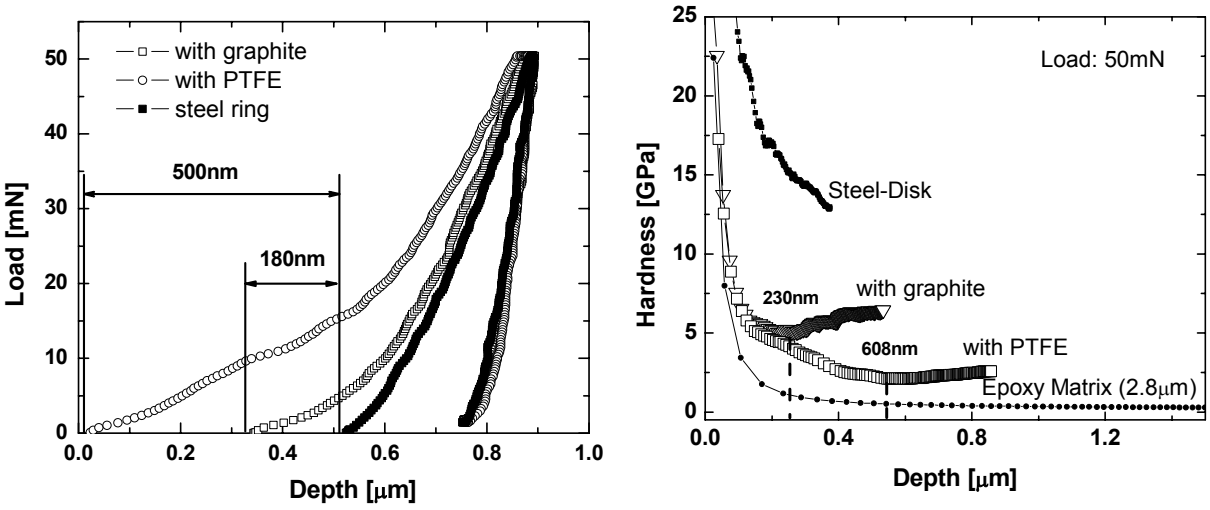

(a) (b)

Figure 4.22: (a) Measured load-depth curves for the steel disc without and with the transfer films, and (b) the hardness-depth curves. Sliding condition: 4MPa and 3m/s.

unloading characteristics of three curves agree well with each other. Based on the model of the two indention phases mentioned above, the same unloading processes can be inferred for the same indentions occurring on the steel substrate. This is reasonable since the hardness of the transfer films was much lower than that of steel. Therefore, the full depth differences between the discs with and without film could be used to estimate the thickness of the transfer film. As shown in the figure, the thickness of the transfer film formed with PTFE is about 500 nm, compared with 180 nm with graphite.

According to the standard [126], universal hardness is calculated as in the case of Vickers indenter,

$$HU = \frac{F}{26.43h^2} \tag{4.1}$$

where F is the applied test force and h is the indentation depth. The dependence of hardness on depth is shown in Fig. 4.22b. For comparison, the results for the steel disc and the neat epoxy (with a hardness of 212 MPa) are also presented in the figure. Regarding the two phases during the indention process, two regions were observed in the hardness curves of the transfer films. Firstly, the hardness characteristic was close to that of neat epoxy, representing mainly the indention of the film.

Then, increasing hardness occurred at higher indentation depths, due to the metallic steel substrate. Consequently, the tangent of the curves changed, which was determined by the thickness of film. As shown in the figure, the thickness of the film with PTFE was 608 nm determined by the lowest point, whereas it was 230 nm for the film with graphite. This coincided well with the estimation made with full depth differences and the observation of surface profiles (Fig. 4.20).

Considering the load transmission and wear process, two competing effects of the thickness of transfer films correlated with the final wear resistance of the polymer composites. On the one hand, contact temperature would be higher with a thicker film because of the lower thermal conductivity of the transfer film. As a result, the adhesion between contact bodies tends to increase because of the rise of temperature and thus there is a higher frictional coefficient and wear rate. On the other hand, the thicker film could decrease the wear rate due to the lower hardness of the counter surface. Therefore, an optimised thickness of transfer film is expected.

4.2.2.4 A Combined Composition with Both Lubricants

In order to integrate the positive features of the two lubricants, PTFE powders and graphite flakes, a composition with 5vol.% of each was evaluated. Fig. 4.23a shows the sliding process of this combined composition at the extremely high *pv* factors of 12MPa·m/s. In comparison with Fig. 4.18, it was clear that the peak values of the frictional coefficient was much lower and the duration of running-in period was shorter, although the value of either the stable frictional coefficient or the contact temperature was between that of the two composites filled with only one lubricant [cf. Table 4.2]. Fig. 4.23b compares the volume loss against sliding time for these three nanocomposites measured at 4MPa and 3m/s. Here, the volume loss was calculated by the loss of height multiplied by the surface area of specimen. It can be seen that the composition with both two lubricants achieved the lowest wear rate in both the running-in stage and the steady sliding period. Meanwhile, the composite with graphite presented the highest volume loss during running-in stage due to having the highest frictional coefficient peak and the longest duration in this stage. However, the wear

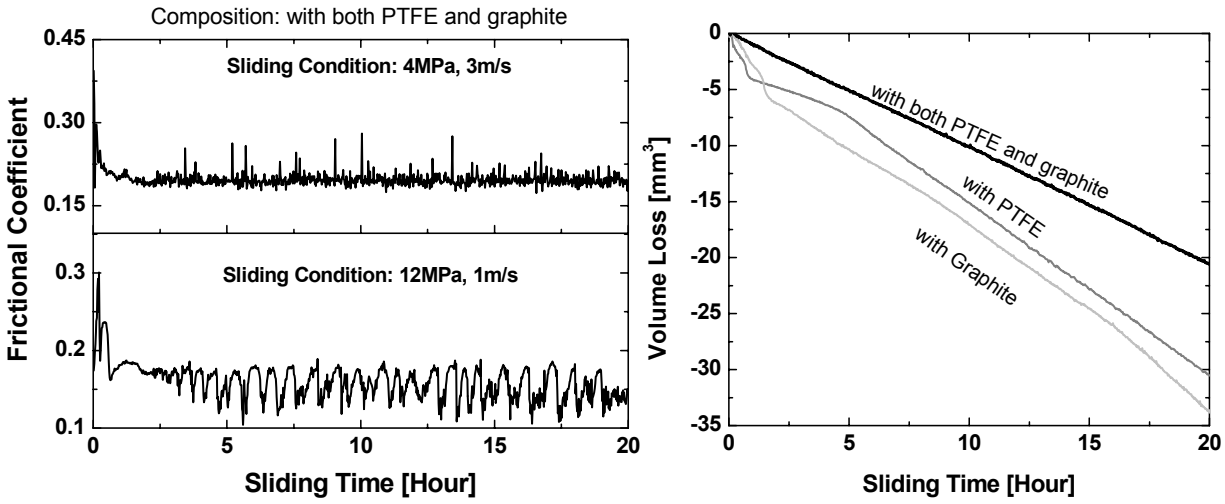

(a) (b)

Figure 4.23: (a) Typical curves of frictional coefficient and contact temperature against sliding time for the compositions with both PTFE and graphite, and (b) the variations of volume loss of the composites with PTFE, with graphite and with both PTFE and graphite at 4MPa and 3m/s.

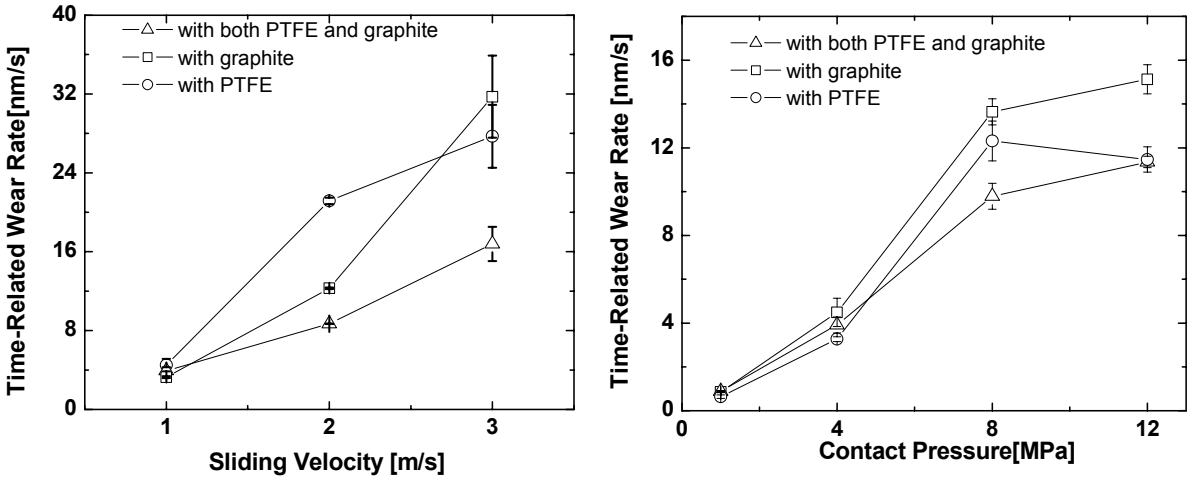

(a) (b)

Figure 4.24: Comparisons of the time-related depth wear rate of three compositions under sliding conditions: (a) at different sliding velocities under a constant pressure of 4MPa, (b) under different loads with a constant velocity of 1m/s.

rates of the two composites with a single lubricant were very close during the steady wear process, even though the stable frictional coefficient of the composite with graphite was much lower.

Fig. 4.24 summarizes the time-related depth wear rate of the three nanocomposites under different sliding conditions. It can be seen the lowest wear rate was obtained with both PTFE and graphite, especially in higher *pv* situations, whereas the lowest stable frictional coefficient was achieved by the composition with graphite (Table 4.2).

Fig. 4.25 shows a schematic presentation of the effect of PTFE powders and TiO_2 nanoparticles on changes in frictional coefficient and contact temperature as functions of time [11]. PTFE is effective in keeping the frictional coefficient relatively low within the initial period, whereas nano-TiO_2 become quite effective in the longer range. It is clear that the combination of SCF and solid lubricants (PTFE and/or graphite) together with TiO_2 nanoparticles can achieve an optimum effect during both the running-in and the steady state sliding stage.

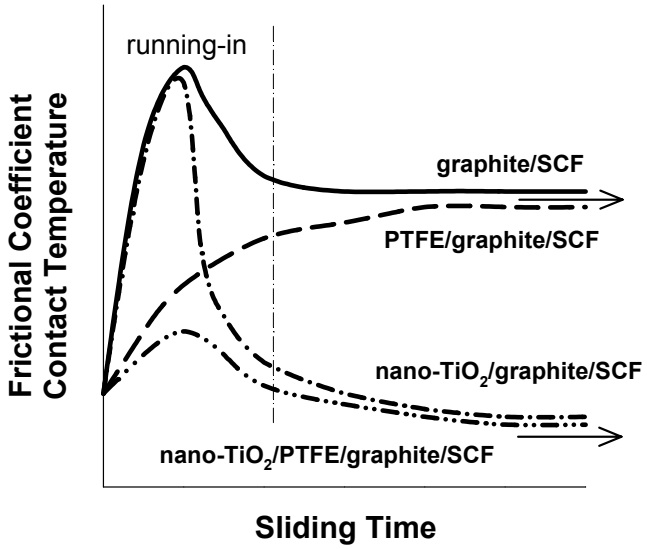

Figure 4.25: A schematic presentation of the effects of PTFE powders and TiO_2-nanoparticles on changes of frictional coefficient and contact temperature of graphite and short-carbon-fibre filled polymer composites.

5 Enhancement of Wear Resistance of Thermoplastic Composites by Nano-TiO_2 Particles

5.1 Polyamide 66 Based Composites

Over the past decades, polymer composites have been increasingly used as structural materials in the aerospace, automotive and chemical industries, providing lower weight alternatives to traditional metallic materials. Numerous such applications are concentrated on tribological components, such as gears, cams, bearings and seals, where the self-lubrication of polymers and polymer composites is of special advantage. The feature that makes polymer composites so promising in industrial applications is the opportunity to tailor their properties with special fillers. Although most polymers with special fillers can provide a low frictional coefficient and low specific wear rate, their applications are generally limited to relatively lower contact temperatures and consequently lower *pv* (the product of *p* and *v*) conditions [14]. For instance, as shown in Fig. 5.1 measured by a Dynamic Mechanical Thermal Analyser (DMTA), the glass transition temperature of polyamide 66 (PA66) is around 75°C. PA66 becomes soft when the service temperature reaches about 50°C, which could occur in dry sliding wear under higher *pv* conditions. The wear rate of the material with its consequent degraded mechanical properties would be seriously increased [5].

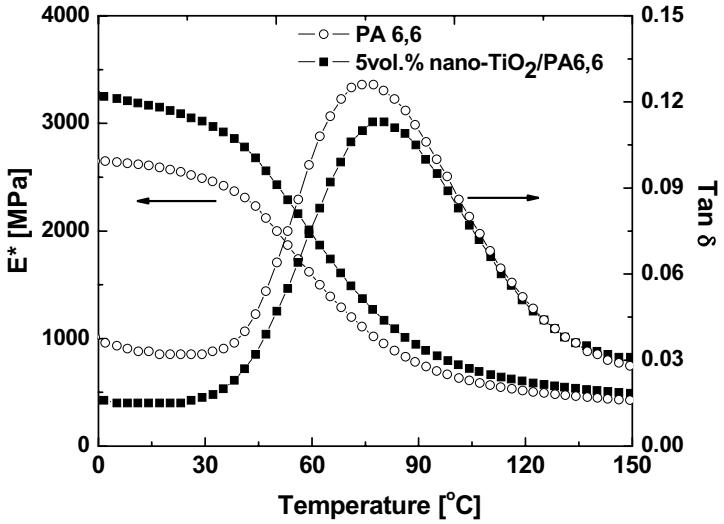

Figure 5.1: Dynamic mechanical properties of the neat PA66 and PA66-based nanocomposite with 5vol.% nano-TiO_2 for the temperature range -110 to 230°C.

In our previous study (Chapter 1), the wear behaviour of epoxy-based nanocomposites was investigated under different normal pressures and sliding velocities. It was found that the addition of nano-TiO_2 reduced both the frictional coefficient and the wear rate, especially under high *pv* conditions. To further exploit this effort, the current study focuses on the thermoplastic PA66 matrix composites. PA66 is selected as an important thermoplastic, which is widely used in injection moulded components [127-130], with the strong commercial advantage of lower manufacturing cost. The tribological properties of the addition of naon-TiO_2 particles, containing short carbon fibre (SCF) and graphite flakes, were examined under various sliding conditions. It is expected that this study will promote a better understanding of the role of nano-TiO_2 in reducing of wear rate of the polymer composites.

5.1.1 Wear Results

All the test results of PA 66, based composites are summarised in Table 5.1. Both the frictional coefficient and the contact temperature given in this table are mean values during the steady state of the sliding process. The characteristics of friction and wear under various sliding conditions are further discussed in subsequent sections.

Table 5.1: Tribological properties of PA66 and PA66 matrix composites under various wear conditions

Composition	*pv* factors	Frictional Coefficient	Contact Temperature [°C]	Specific Wear Rate [$10^{-6}mm^3/Nm$]
neat PA66	1MPa, 1m/s	1.16	45.09	6.70
graphite +SCF/PA66	1MPa, 1m/s	0.60	30.57	0.53
	2MPa, 1m/s	0.57	46.07	0.80
	4MPa, 1m/s	0.69	94.98	2.92
	8MPa, 1m/s	0.35	97.37	16.93
	2MPa, 2m/s	0.78	97.67	4.87
	2MPa, 3m/s	0.62	115.80	5.73
nano-TiO_2+graphite +SCF/PA66	1MPa, 1m/s	0.44	26.66	0.50
	2MPa, 1m/s	0.34	33.21	0.72
	4MPa, 1m/s	0.26	45.55	0.80
	8MPa, 1m/s	0.22	64.69	3.26
	2MPa, 2m/s	0.34	45.94	0.63
	2MPa, 3m/s	0.38	62.36	3.35

5.1.1.1 Standard Wear Condition - 1MPa and 1m/s

Fig. 5.2 shows typical variations of the frictional coefficient and contact temperature against sliding time of neat PA66 in comparison with the other two compositions under 1MPa and 1m/s. It is evident that the two parameters are closely correlated and their tendencies coincided well, as has also been reported in a previous study [73]. The frictional coefficient of neat PA66 clearly increased during the initial wear stage. This was probably caused by the increase in the real contact area and contact temperature owing to frictional heating [127,128,131]. Thereafter, the frictional coefficient

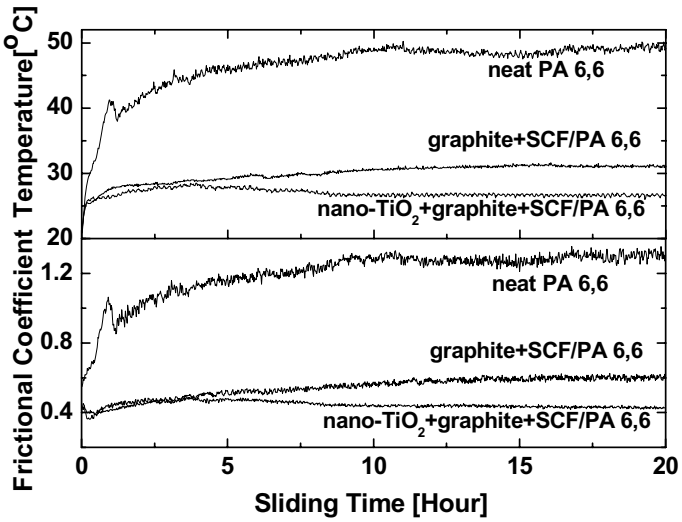

Figure 5.2: The typical sliding process curves of frictional coefficient and contact temperature against sliding time of neat PA66 and without and with nano-TiO_2 under a standard wear condition of 1MPa and 1m/s.

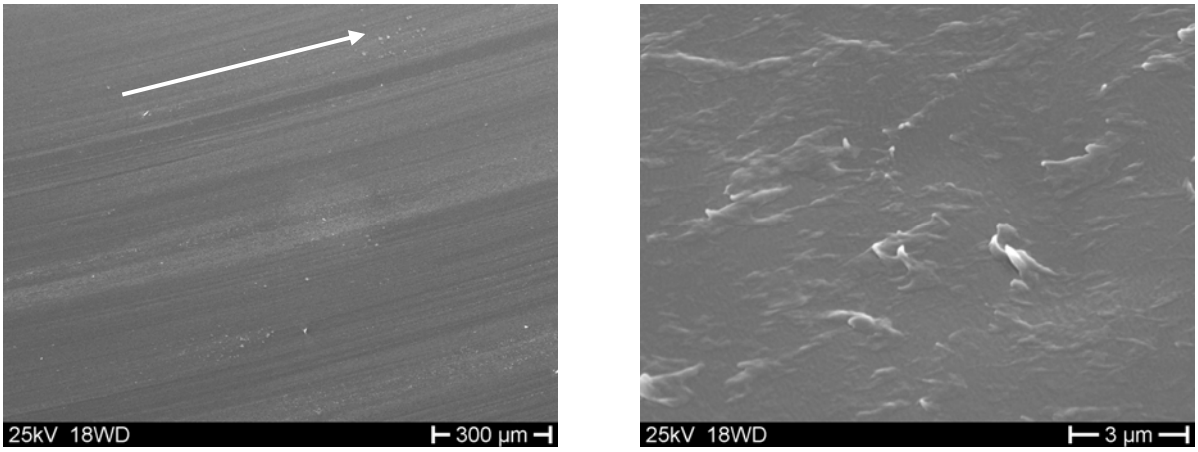

(a) (b)

Figure 5.3: (a) SEM micrographs of the worn surfaces of neat PA66 measured at 1MPa and 1m/s, and (b) the magnified view of viscous flow.

stabilised at a value higher than 1.0. This resulted in a rather high specific wear rate. When only combined SCF and graphite was used as filler, the frictional coefficient and the contact temperature were remarkably reduced. With the further addition of nano-TiO_2, the stable frictional coefficient was reduced to a mean value of about 0.4 after the initial wear stage (cf. Fig. 5.2). Thus, the wear rates of the two composites were remarkably reduced, to a level more than ten times lower than that of neat PA66 (cf. Table 5.1).

The worn surface of neat PA66 is shown in Fig. 5.3. Grooves paralleling to the sliding direction are clearly observed, suggesting that the wear process is governed by abrasive wear mechanism. In this case, the polymer generally exhibits a high wear rate, depending on the original roughness of the harder counterpart and the contact pressure [128,132]. With a magnified view, viscous flow of PA is observed in a micron scale due to the high flash temperature occurring at the real contact area. Owing to its low load carrying capacity, the softened PA66 was rapidly removed by the hard asperities of the metallic counterpart surface.

Figs. 5.4 and 5.5 present the worn surfaces of the two composites without and with nano-TiO_2, respectively. It is clear that the surfaces of both composites are quite smooth as a resulted of adhesive wear. With a magnified view, local matrix micro-

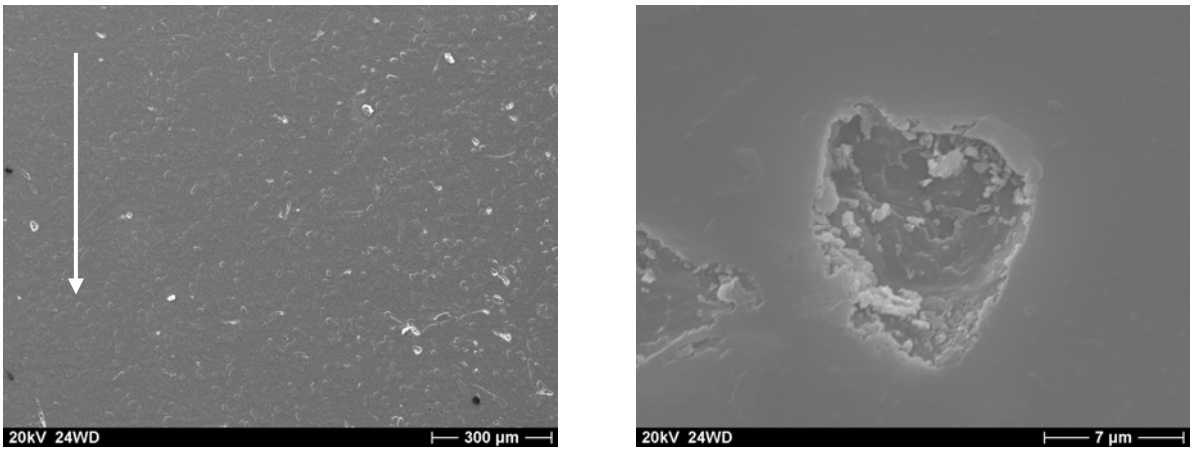

(a) (b)

Figure 5.4: (a) SEM micrographs of the worn surfaces of the composition without nanoparticles at 1MPa and 1m/s, and (b) the magnified view of matrix ploughing damage.

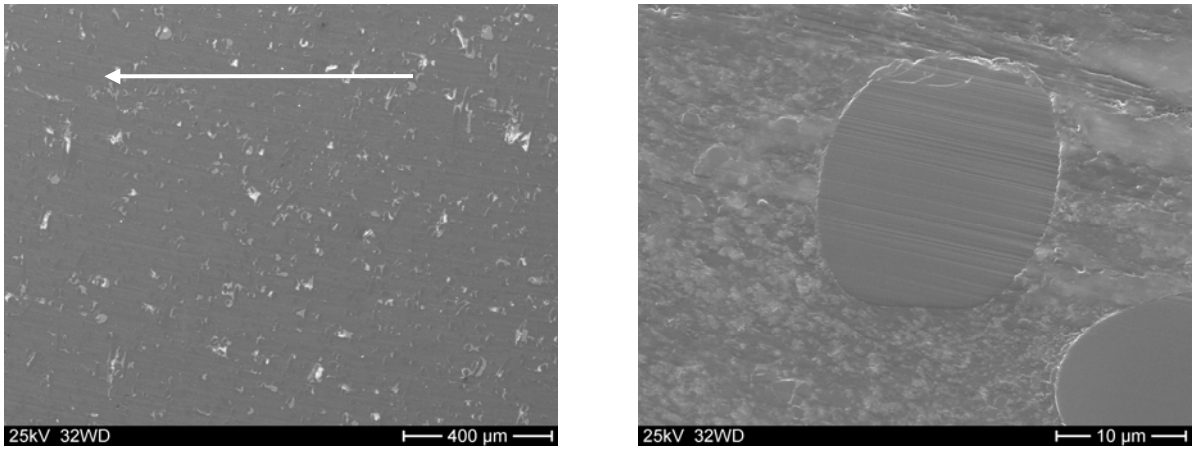

(a) (b)

Figure 5.5: (a) SEM micrographs of the worn surfaces of the composite nano-TiO_2+graphite +SCF/PA66 with nanoparticles at 1MPa and 1m/s, and (b) the magnified view of nano-grooves on the fibre.

cracks may occur (Fig. 5.4b), probably caused by the "fatigue wear" of adhesive contact [14]. A polymer layer may transfer onto the metallic counterpart surface during the running-in stage, resulting in this adhesive wear mechanism. For the nanocomposite, slight nano-grooves were observed on the carbon fibres, which are parallel to the sliding direction (Fig. 5.5b).

5.1.1.2 High *pv* Factor

With the improved load-carrying capacity engendered by the fillers, the composites could be subjected in much higher *pv* conditions than neat PA66. Fig. 5.6 illustrates the sliding processes of the two composites under 4MPa and 1m/s. In comparison to Fig. 5.2, it can be seen that the duration of the running-in stages of both composites was apparently reduced. This reduction was caused by the more rapid formation of stable transfer films, due to the accelerated generation of wear debris and easier formation of transfer film under high compaction pressure. After the running-in stage the frictional coefficient of the composite without nano-TiO_2 became stable and obtained a high contact temperature. However, for the nanocomposite, the frictional coefficient then sharply decreased and achieved a much lower value. As a result, the wear resistance of the nanocomposite was remarkably enhanced.

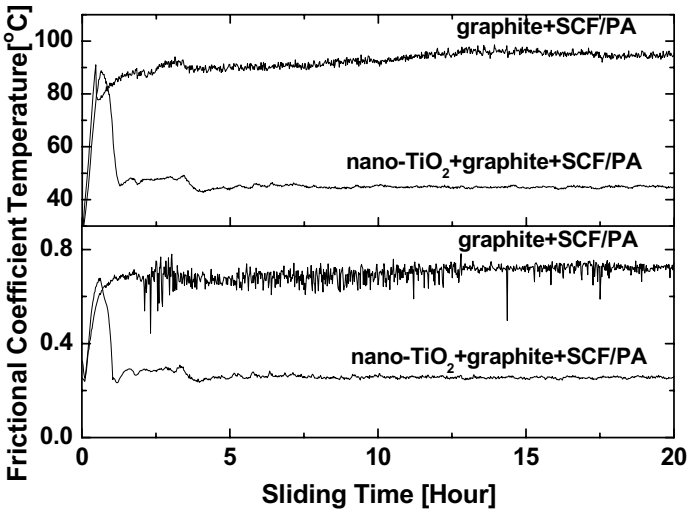

Figure 5.6: Comparison of typical sliding process curves against sliding time of the composites without and with nano-TiO_2 at a high sliding velocity of 3m/s and a contact pressure of 2MPa.

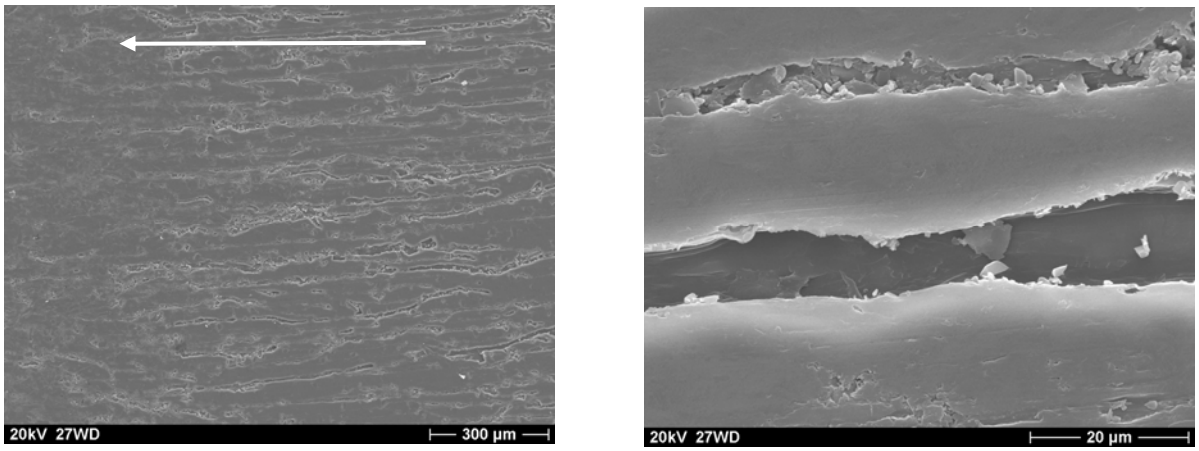

(a) (b)

Figure 5.7: (a) SEM micrographs of the worn surfaces of the composition without nanoparticles at 4MPa and 1m/s, and (b) magnified view of fibre removal.

Fig. 5.7 shows SEM micrographics of the worn surface of the composition without nano-TiO_2 at 4MPa and 1m/s. Due to the high contact temperature during sliding, the PA66 matrix was markedly softened. Associated with the increase of friction force, fibre removal aggravated seriously, since the softened polymer matrix could not effectively protect the SCF from peeling off (Fig 5.7b). In comparison to the breakage of brittle epoxy composite (cf. Fig.4.7 in Chapter 4.), it was noticed that the breakage in interfacial region of SCF/PA66 was more limited because of the ductility of the polyamide, which deformed through elongation rather than breakage, thus the debris

evinced a roll formation [129]. Additionally, Fig. 5.8 shows typical roll debris on the counterpart surface formed by the composite.

The worn surface of the nanocomposite is shown in Fig. 5.9. Because of the reduction of friction and contact temperature, the fibres could effectively withstand the load and were gradually removed within a normal process, i.e. fibre thinning, fibre fracture, and finally fibre peeling-off [74]. Fig. 5.9b shows the patterns of the fibre fracture of nanocomposite with good interfacial bonding even under high pressure.

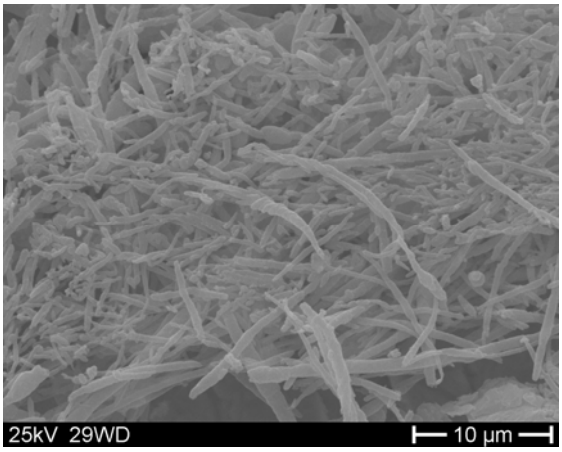

Figure 5.8: SEM micrographs of roll debris on the metallic counterpart surface.

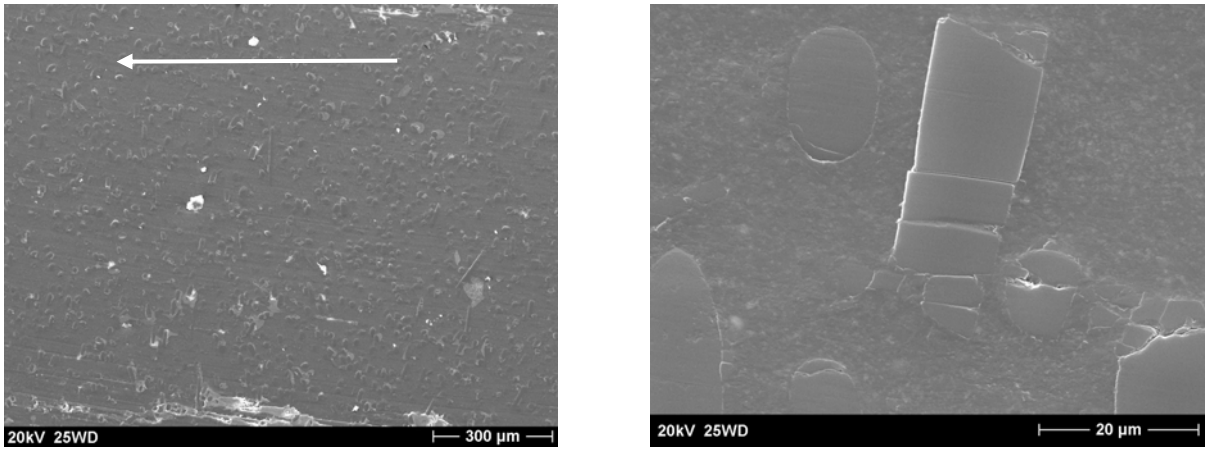

(a) (b)

Figure 5.9: (a) SEM micrographs of the worn surfaces of the composition with nanoparticles at 4MPa and 1m/s, and (b) the magnified view of fibre fracture.

5.1.1.3 Time-Related Depth Wear Rate

The time-related depth wear rate calculated by equation 1.2 is given in Fig. 5.10 as a function of the *pv* factor. It is clear that the basic wear factors, *k**, of the two composites were very similar to each other under low *pv* conditions, e.g. lower than 2MPa·m/s. However, for the composition without nanoparticles, the slope change occurred between 2 and 4 MPa·m/s, whereas for the nanocomposite it occurred between 4 and 6 MPa·m/s. A huge wear rate of the composite without nanoparticles as occurred at 8MPa·m/s, i.e. 135nm/s of depth wear rate, which is almost 5 times of that of the nanocomposite under the same condition. This means that the "*pv* limiting" for the nanocomposite is clearly enhanced. It was noticed that for both composites, the slope change occurred when the contact temperature was above 50°C (Table 5.1), which was in the glassy region of the PA66 matrix (Fig. 5.1). However, the composite with nanoparticles achieved this value under a higher *pv* condition than that without nanoparticles due to the reduction in the frictional coefficient. Therefore, although the addition of nanoparticles has little effect on the value of the T_g of PA66 (Fig. 5.1), the nanocomposite could be used for higher duties with lower heat generation because of the remarkable reduction of the frictional coefficient. It can be concluded that the enhancement of the wear resistance of the PA66 nanocomposite was mostly caused by the reduction in contact temperature, thus abating the degradation of the mechanical properties of thermoplastic matrix. However, for thermosetting ma-

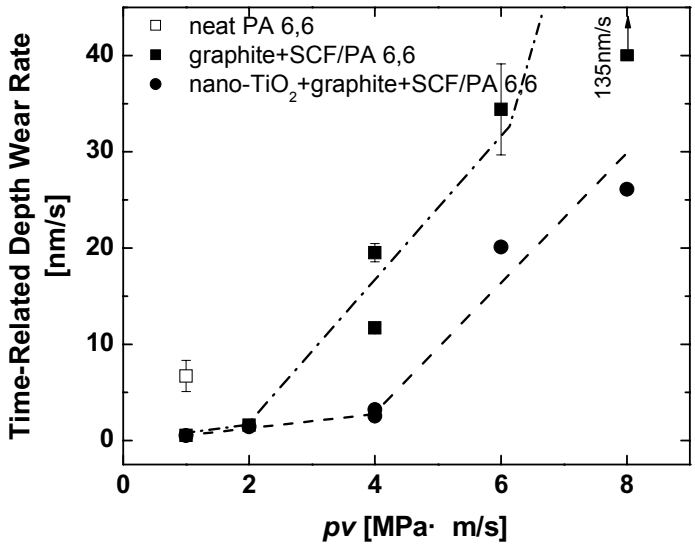

Figure 5.10: Time-related depth wear rate as a function of *pv* factor of the composites filled with and without nano-TiO_2.

terial such as epoxy based nanocomposite, the addition of nanoparticles effectively improves the wear performance of material mostly by protection of the matrix material in the interfacial region, consequently protecting the SCF from serious wear [74].

5.1.2 Mechanism Considerations Based on AFM Observations

In order to understand the role of nanoparticles in improving the wear performance of polymer composites, AFM was employed to investigate the worn surfaces, especially focusing on single carbon fibres with and without nanoparticles. Fig. 5.11a shows an AFM image of an almost normal directional carbon fibre of the composition without nanoparticles tested at 1MPa and 1m/s. A cross-sectional measurement was performed in Fig. 5.11a (as shown in Fig. 5.11b) and the results are summarized in Table 5.2. The height of the exposed fibre, i.e. the difference between 'A' and 'B' (0.26μm), is close to the initial roughness of the counterpart surface (about 0.22μm). It can be seen that the fibre surface is relatively smooth, but apparently tilted to the worn surface. Therefore, during the friction process, the exposed fibre underwent most of the load and was impacted by the asperities of the counterpart. In comparison with that of epoxy-based composite (cf. Fig. 4.9 in Chapter 4), interfacial damage did not occur between the SCF and matrix due to the better interfacial bonding of thermoplastic matrix and carbon fibre. As a result, the worn surface of the material was quite smooth and no serious fibre removal was observed (cf. Fig. 5.4).

Fig. 5.12a shows an AFM image of a carbon fibre of the nanocomposite in the normal direction tested at 1MPa and 1m/s. A cross-sectional measurement is presented in Fig. 5.12b and the results are summarized in Table 5.2. The height of the exposed fibre is about 0.22μm, which again coincides with the roughness of the counterpart. However, the fibre surface is almost parallel to the worn surface, whereas it was tilted for the composite without nanoparticles (Fig. 5.11). This can be explained by a rolling effect of nanoparticles proposed in our early study of epoxy-matrix nanocomposites [74,75,94], which reduces the shear stress especially at edge of the SCF and protects the fibre from the impact of the asperities of the counterpart (cf. Fig. 4.13 in Chapter 4). In addition, Fig. 5.12c shows a perpendicular sectional measurement of

nano-grooves by AFM with a magnified view of the area marked in Fig. 5.12a. The width of the grooves is in a range of 150~200nm (Table 5.2), which is in the same order as the nanoparticle size (300nm). However, the depth of the grooves is only around 5nm. It is therefore considered that some individual hard nanoparticles were possibly embedded in the transfer film layer on the counterpart, slightly scratching the fibres. The very shallow grooves suggest that the friction produced by particle grooving or sliding is quite slight. In this case, the size of the nanoparticles is very close to the gap between the two counterparts. For hard particles, sliding and rolling commonly occur together.

Therefore, according to these phenomena, two competing effects of nanoparticles are proposed. On the one hand, nanoparticles tend to enhance the wear resistance of the composite by reducing friction through a proposed rolling effect. On the other hand, mild abrasive was simultaneously induced by the hard particles acting as third bodies, which counteracted the effect of the friction reduction in a certain extent. On the whole, the specific wear rates of the composites with and without nanoparticles were almost similar under low *pv* conditions, even though the frictional coefficient of

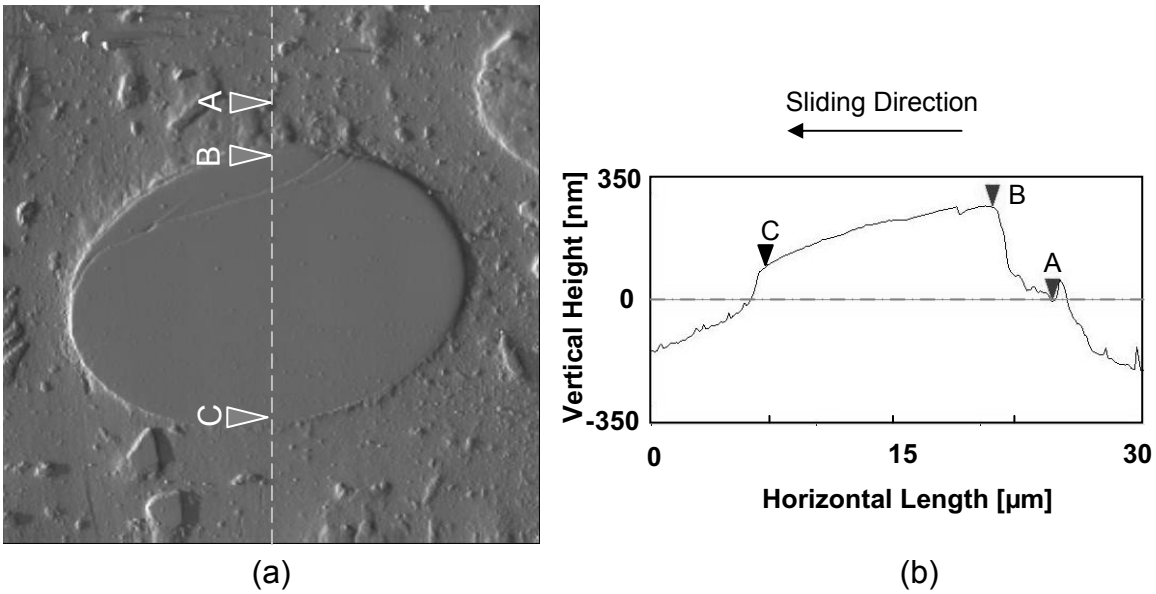

(a) (b)

Figure 5.11: (a) AFM image of fibre in the worn surface of the composite without nanoparticles at 1MPa and 1m/s, and (b) a cross-sectional measurement. The arrow represents the sliding direction.

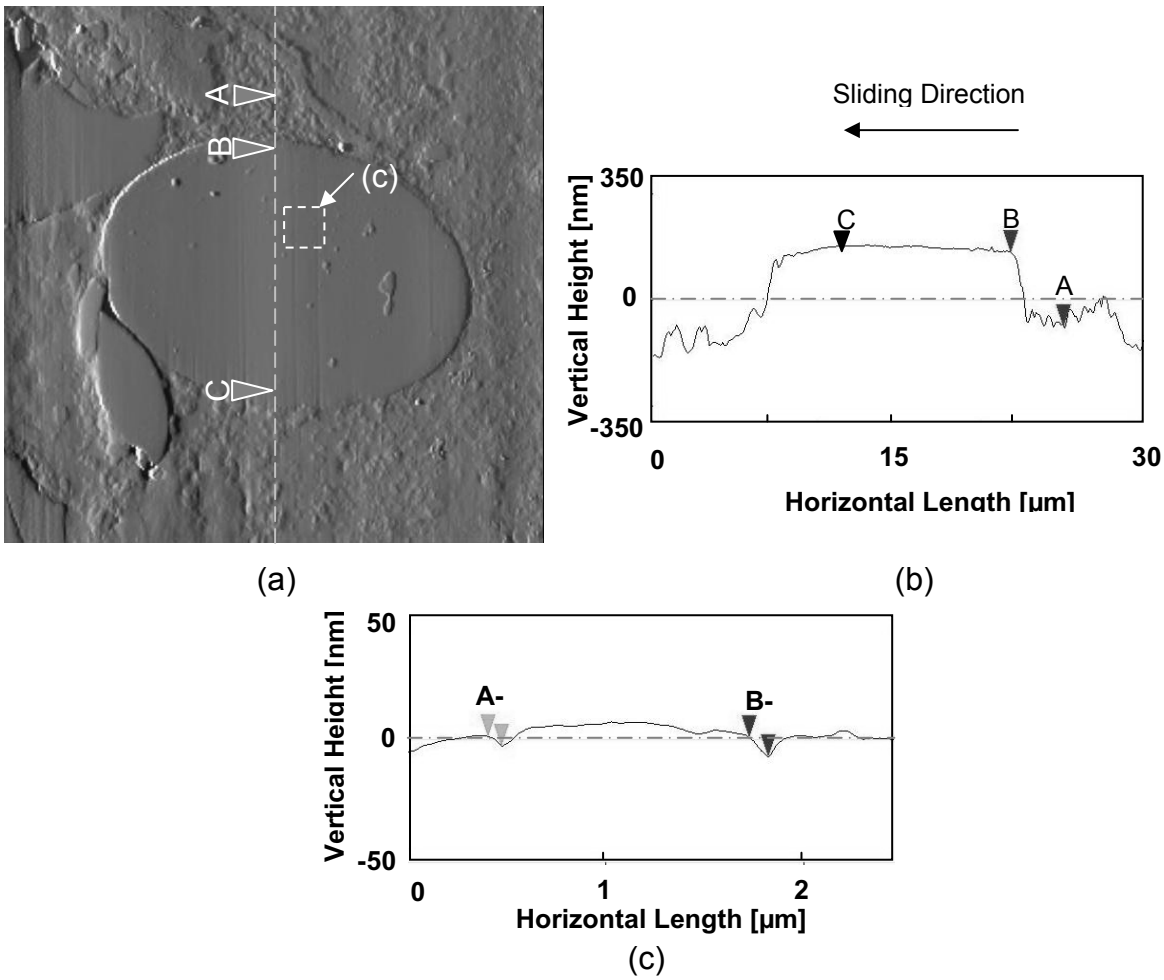

Figure 5.12: (a) AFM image of fibre in the worn surface of the composite with nanoparticles at 1MPa and 1m/s, (b) a cross-sectional measurement, and (c) AFM sectional measurement of the nanoscale grooves with a magnified view of the area marked in (a). The arrow represents the sliding direction.

Table 5.2: Summary of the cross-sectional measurement results by AFM.

	Fig. 5.11 (b)		Fig. 5.12 (b)		Fig. 5.12 (c) (nanoscale grooves)	
	A-B	B-C	A-B	B-C	A-A'	B-B'
Surface-distance[1] [nm]	3661	1430.2	3329	1359.6	67.427	96.465
Horizontal-distance[2] [nm]	3633	1429.7	328.1	1359.4	67.291	96.130
Vertical-distance[3] [nm]	263.8	193.51	215.87	6.555	3.994	7.816
Angle[4] [degree]	4.153	0.775	3.764	0.028	3.397	4.648

[1]The 'surface-distance' refers to the surface trace between two points.

[2]The 'horizontal-distance' refers to the linear length in the horizontal direction.

[3]The 'vertical-distance' is the linear height in the vertical direction.

[4]The 'angle' indicates that of the horizontal direction and the line determined by the measured two points.

the nanocomposite was always apparently lower. When the *pv* factor increased, for the composition without nanoparticles, the contact temperature was apparently increased due to higher frictional work. In this case, the wear resistance of the nanocomposite was remarkably improved.

5.1.3 Time Dependence of the Wear Behaviours

5.1.3.1 "Running-in" Stage

To further understand the contribution of nano-TiO_2 during friction process, the time dependence of the wear behaviour was further investigated. Firstly, the running-in stages of two composites were compared at various sliding durations, i.e. 10, 30, 60 and 120 minutes, respectively. Fig. 5.13 shows the dependence of the frictional coefficient and the contact temperature on sliding time. The correlated SEM worn surfaces are shown in Fig. 5.14.

As shown in the figures, the patterns of the surface damages were consistent with the performance of the frictional coefficient for both compositions. During the first 10 minutes, the two compositions displayed a similar frictional coefficients and contact

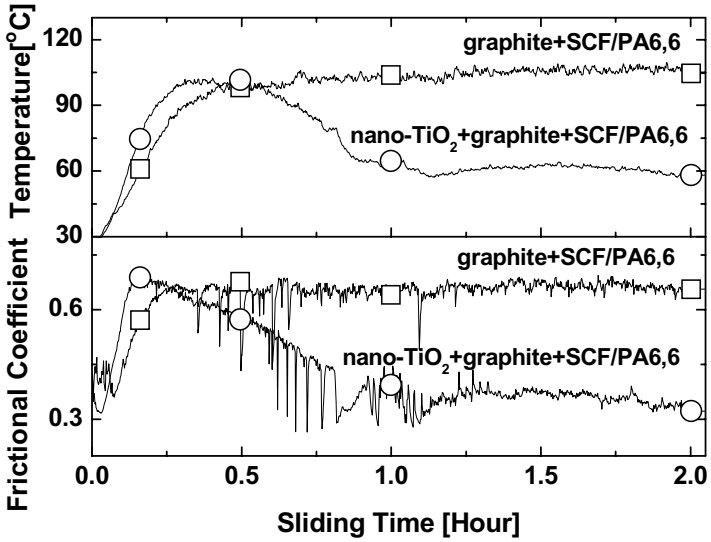

Figure 5.13: Comparisons of the sliding process of the two compositions, i.e. graphite+ SCF/PA66 and nano-TiO_2+graphite+SCF/PA66, with different durations, i.e. 10, 30, 60 and 120 minutes.

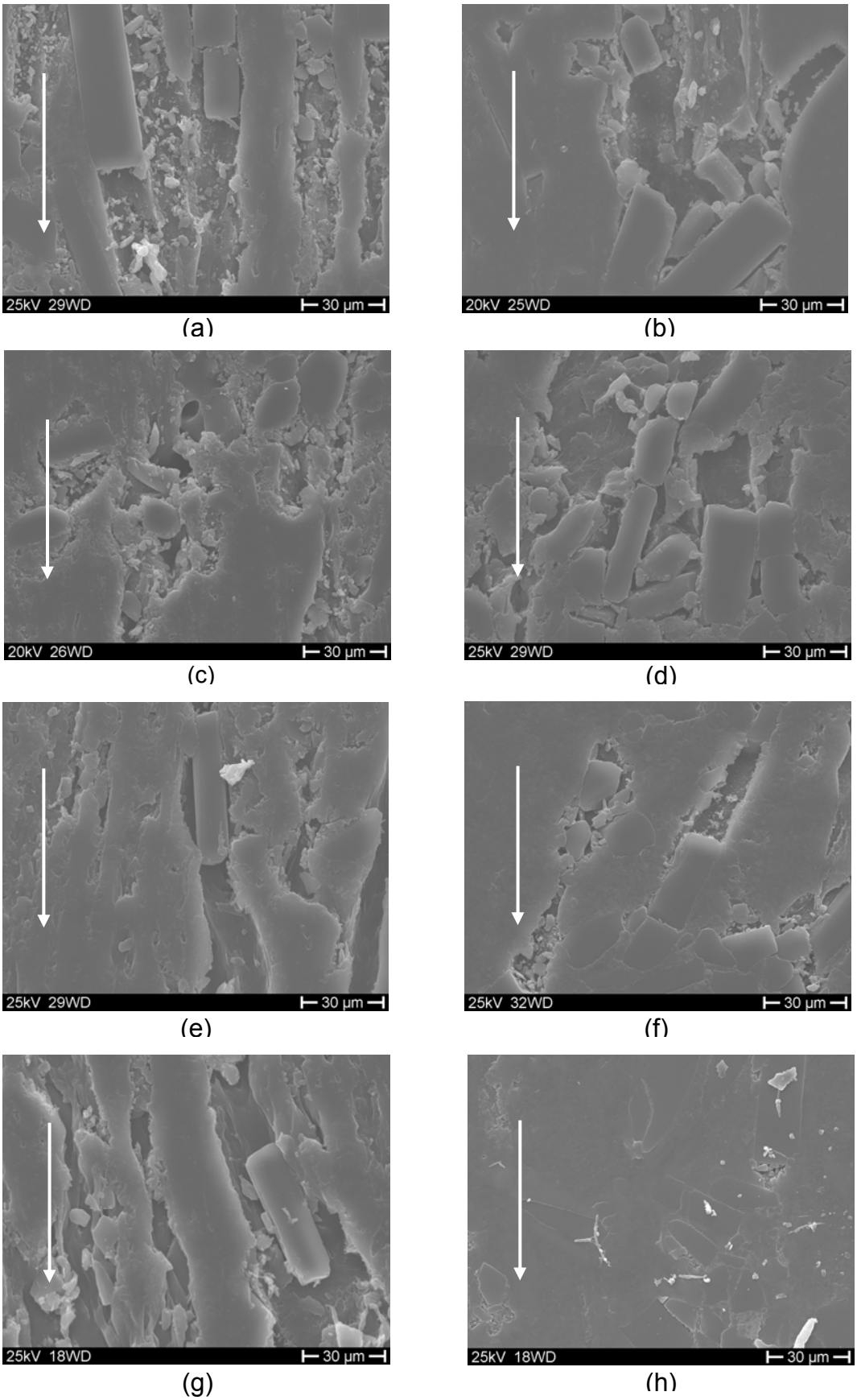

Figure 5.14: Comparisons of the worn surfaces of graphite+SCF/PA66 after (a) 10minutes (c) 30 minutes, (e) 60 minutes (g) 120 minutes, and that of nano-TiO_2+graphite+ SCF/PA66 after (b) 10minutes (d) 30 minutes (f) 60 minutes (h) 120 minutes.

temperatures. Accordingly the worn surfaces are also very similar (cf. Figs. 5.14a and 5.14b). After 30 minutes, both compositions reached almost the highest contact temperature and severe fibre removal was observed correspondingly (cf. Figs. 5.14c and 5.14d). Thereafter, the sliding process of the composition without nano-TiO_2 became stable and the severe fibre removal continued (cf. Figs.5.14e and 5.14g). However, for the composition with nanoparticles, the surface became much smoother with reduced fibre breakage and removal (cf. Figs. 5.14f and 5.14h) due to the reduction of the frictional coefficient and the contact temperature once the nanoparticles started to function.

In relation to the sliding processes of the two composites under various conditions (Figs.5.2, 5.6, and 5.13), it was noticed that the reduction of friction by nanoparticles occurs always occurs after the initial wear stages, during which the sliding processes for two compositions are very similar. This effect could be explained by that nanoparticles were collected and distributed on the counterpart surface, greatly reducing the friction by the means of the rolling effect. Because the transfer films generally developed during the running-in stage and produced an adhesive wear mechanism, another assumption was also proposed. With the addition of nanoparticles the real contact area was reduced by virtue of three-body contact instead of surface contact, and thus the adhesive force was lower. As a result, the frictional coefficient was effectively reduced by nano-TiO_2 in all test conditions and restricted the elevation of contact temperature, especially under very high *pv* conditions. This reduction consequently enhanced the load carrying capacity of the composite.

5.1.3.2 Steady Stage

During the steady stage, the wear performance of polymers is mostly determined by the transfer film developed on the metallic counterpart [7]. In fact, many researchers have assumed that the friction/wear reduction caused by various micro- or nanoparticle results from the improvement in the wear performance of the transfer films [7,40,47,48] that is these particles can improve bonding strength between transfer film and counterface due to some kinds of chemical and/or mechanical reactions. In

this case, the particles contribute to wear behaviour of materials mainly during the running-in stage, whereas the high-performance transfer film layers were responsible to the reduction of friction/wear in the steady stage. Therefore, in this section, the wear performance of transfer films during the steady stage is examined.

In the experiments, a special wear test was performed at 2MPa, 1m/s and separated into three periods. First, a normal sliding test was conducted for 10 hours, which is

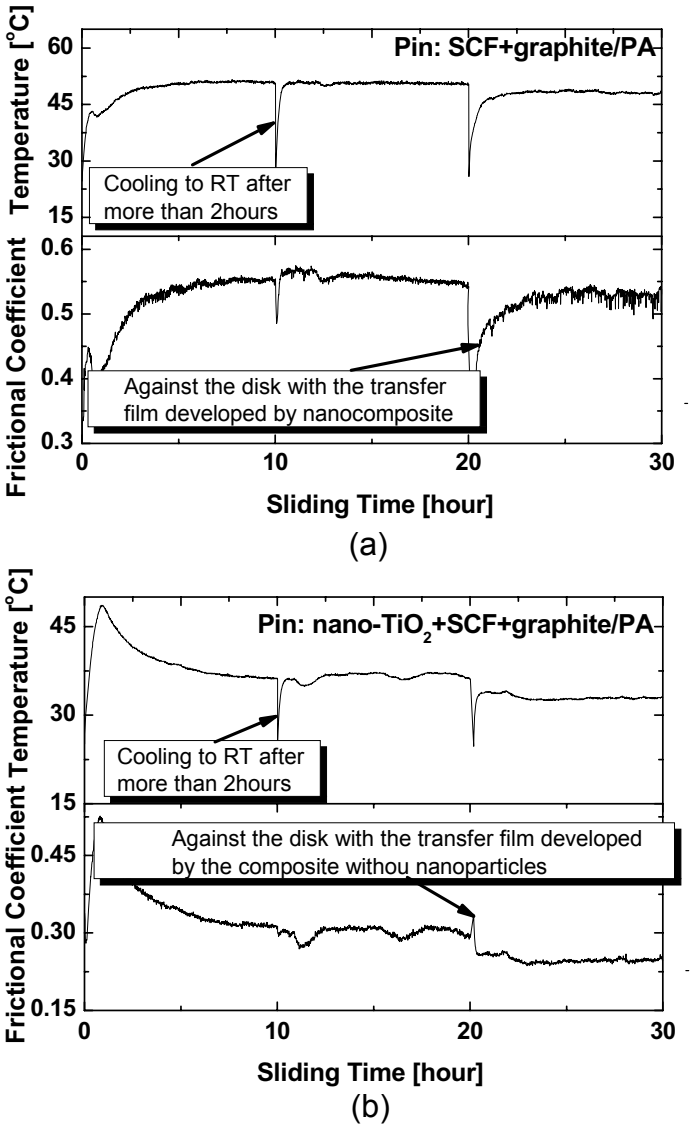

Figure 5.15: Comparison of the tribological performance of transfer films developed (a) without and (b) with nanoparticles during the steady stage.

long enough for the system to come enter the steady stage with the development of continuous transfer film. The test was then stopped and the material cooled to room temperature. Second, the test continued for another 10 hours. As shown in Fig. 5.15, for composites with and without nanoparticles, the duration of the running-in during the second period of the test was greatly reduced with the development of transfer film. However, the frictional coefficient and accordingly the contact temperature in the steady stage remained almost unchanged. Therefore, the steady stage was independent of the process occurring in “running-in”.

Finally, during the last 10 hours, the steel disks were exchanged in order to compare the tribological performance of the transfer film developed with and without nanoparticles. As shown in Fig. 5.15a, against the transfer film developed with nanoparticle, the value of the frictional coefficient of the composites without nanoparticles was almost unchanged in the steady stage. For the nanocomposite, there a small peak was observed in the initial friction process, while the value of the frictional coefficient was also unchanged in the steady stage (Fig.5.15b). For both composites, there were no such processes observed for the breakage of original transfer films and/or the development of the new ones. The changes in the frictional coefficient for the two composites during the initial wear processes can be explained as the effect of the removal or redistribution of nanoparticles between the rubbing surfaces. Therefore, at least in this case, nanoparticles did not contribute to the development of the high performance transfer film. The wear process for the nanocomposite in the steady stage was determined by the combination of the transfer film that has been developed and the embedded nanoparticles. Therefore, the reduction of the friction was caused by the rolling effects of nanoparticles occurring in both the running-in and steady stages.

5.1.4 Influence of Surface Roughness of the Counterface

5.1.4.1 Against Finely Polished Disk

Fig. 5.16a presents the typical friction processes of the two composites with and without nanoparticles against the normal (rougher) steel disk (Ra=0.23μm) at 2MPa and 1m/s. Here, the insert shows the value of the specific wear rate and frictional coeffi-

cient, which is a mean value during the steady state of the friction process. Each result is an average value of at least three experimental data, with the scatter in data being within ±10%. As shown in the figure, the frictional coefficient of the nanocomposite was apparently reduced after the "running-in" stage. Accordingly, the wear resistance of the composite was noticeably improved by the addition of nanoparticles, which is consistent with our earlier observations.

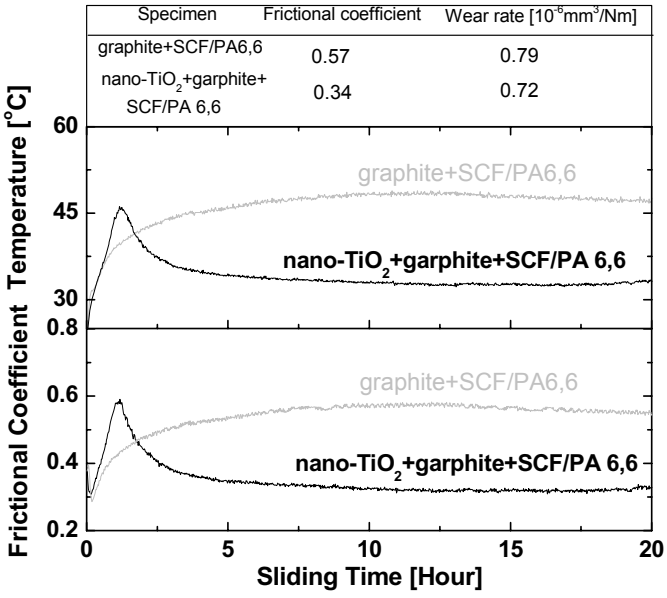

(a)

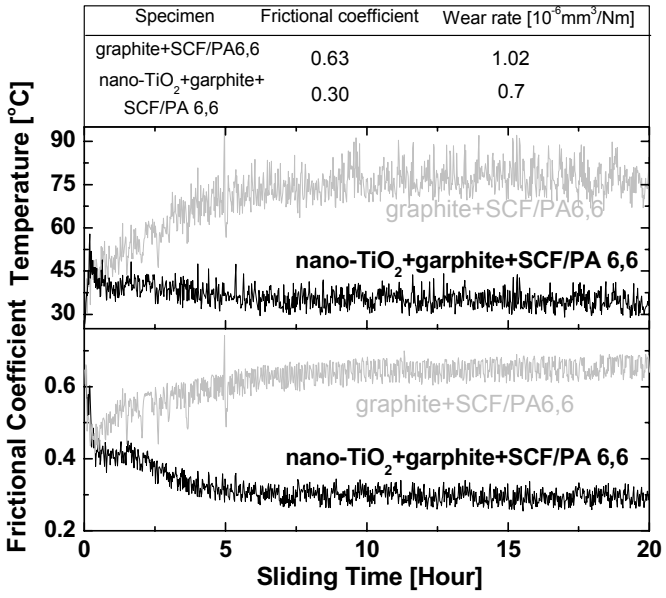

(b)

Figure 5.16: Typical frictional processes of the two compositions i.e. graphite+ SCF/PA66 and nano-TiO_2+graphite+SCF/PA66 against (a) rougher (0.23μm Ra) and (b) smoother (0.03μm Ra) disks and at 2MPa, 1m/s.

Fig. 5.16b shows typical sliding processes of the two composites against the finely polished (smoother) disk (Ra=0.03μm) at 2MPa and 1m/s. It is interesting that the reduction of friction and wear rate also occurred with the addition of nanoparticles. The features of the worn surfaces of the two composites against the smoother disk are shown in Figs. 5.17 and 5.18 respectively. Arrows indicate the sliding directions. As shown in the figures, the surfaces of both composites appear relatively smooth, which suggests an adhesive wear mechanism due to the formation of transfer film on the metallic counterfaces. With a magnified view, slight fibre removal was observed on the surface of the composite without nanoparticles (Fig. 5.17b). However, in keep-

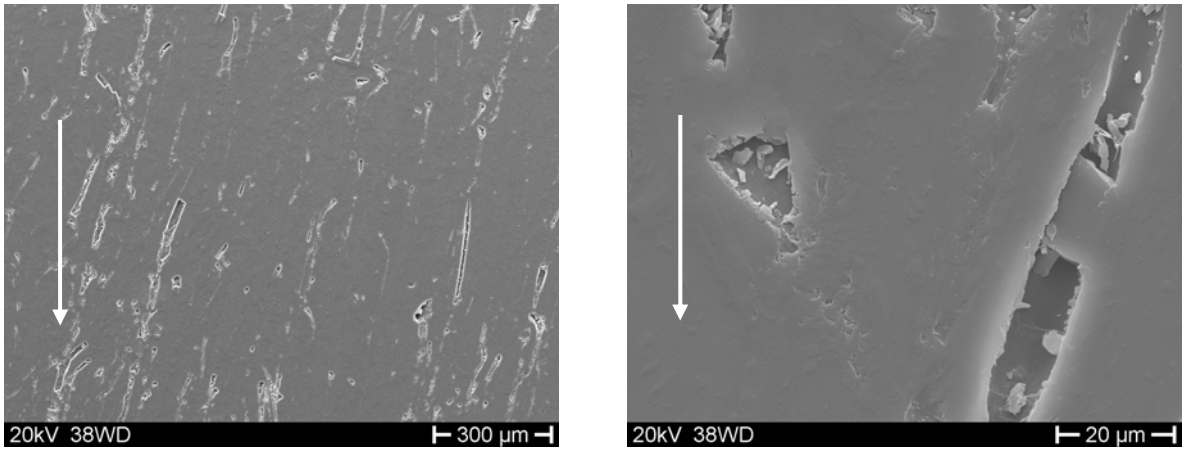

(a) (b)

Figure 5.17: (a) SEM micrographs of the worn surfaces of the composition without nanoparticles against smoother disk (0.03μm Ra) at 2MPa and 1m/s, and (b) magnified view of fibre removal.

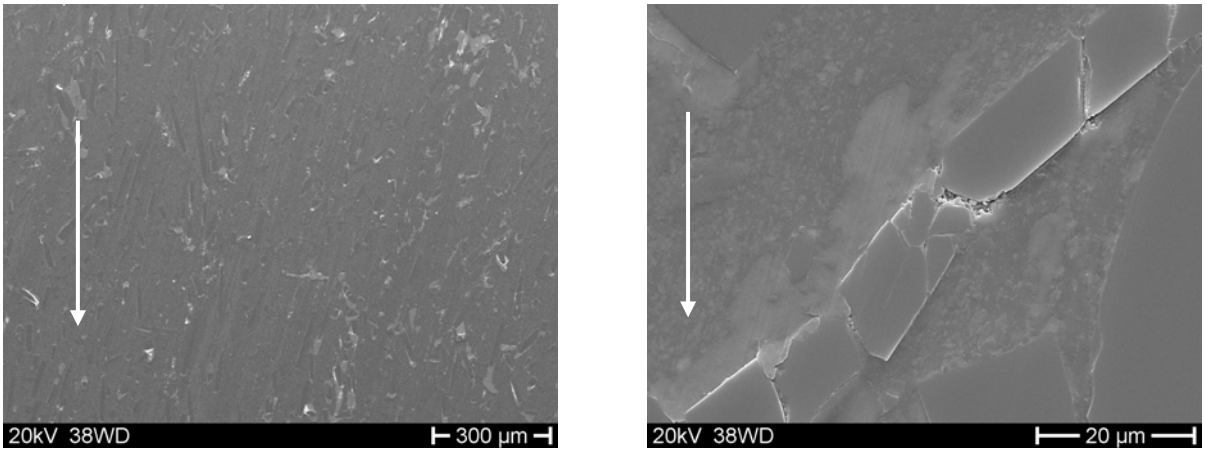

(a) (b)

Figure 5.18: (a) SEM micrographs of the worn surfaces of the composition with nanoparticles against smoother disk (0.03μm Ra) at 2MPa and 1m/s, and (b) magnified view of fibre fracture.

ing with the lower frictional coefficient, the worn surface of nanocomposite is smooth without obvious fibre removal.

To comprehensively understand the wear behaviour of the composites against the smoother disk, the wear tests were further carried out under different pressures with a constant sliding velocity of 1m/s. The results are summarized in Fig. 5.19. For comparison, the wear results of the materials against the rougher disk (Ra=0.23μm) were also given. It is obvious that the wear performance of the materials is almost independent of the surface roughness of the counterfaces. In both cases, the frictional coefficient and wear rate of the composites are reduced by the additional nanoparticles, especially at high *pv* factors. This is very different from what occurred for the epoxy based composites (cf. Fig. 4.14 in Chapter 4). As already mentioned, the wear behaviour of composites against metallic counterparts is mostly determined by the properties of the transfer films developed. To understand the dominant wear mechanisms, transfer film developed on smoother surfaces is further investigated in the following section. In particular, the wear behaviour of PA66 based composites against the smoother disk is compared with that of epoxy based on composites.

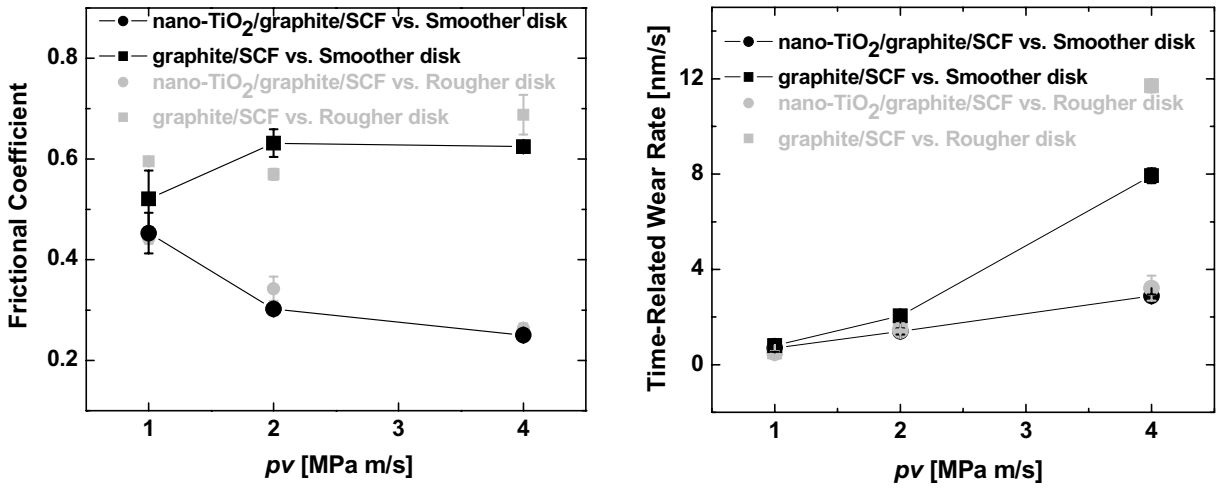

(a) (b)

Figure 5.19: Wear results of the two composites against the smoother disks in comparison with that against the rougher disks: (a) friction coefficient and (b) time-related depth wear rate as a function of contact pressure. Sliding velocity was kept constant at 1m/s.

5.1.4.2 Observation of Transfer Film on a Finely Polished Disk

Fig. 5.20 shows scanning pictures of smoother counterpart surfaces covered by transfer films. It is observed that for both the composites continuous thin films have developed on the metallic counterfaces, with greater surface roughness than that of the original disk. The similar transfer film layers result in the similar wear behaviour of the composites, even with counterparts with different original surface profiles. Moreover, for the nanocomposite, the soft transfer film makes it possible for nanoparticles to be embedded in the counterfaces. Thus there is a reduction of the frictional coefficient against the finely polished disk, although the value of the original surface roughness of the disk is much smaller than the size of nanoparticle.

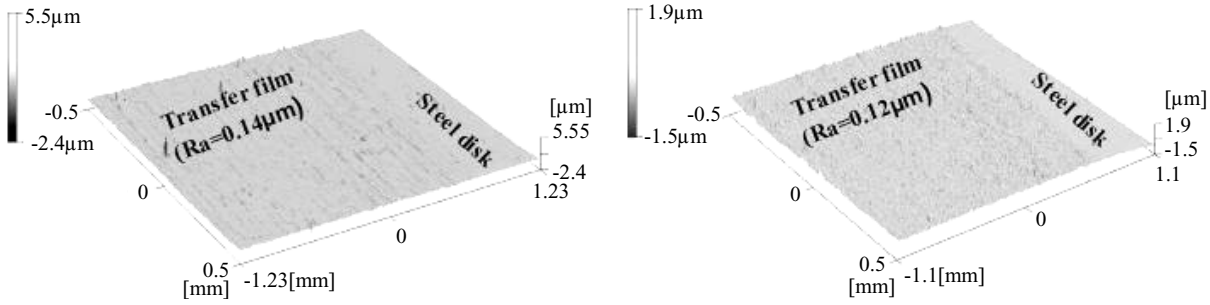

(a) (b)

Figure 5.20: Surface profiles of the transfer film on the counterfaces formed by the composites based PA 6,6 (a) without, and (b) with nanoparticles against a smoother disk at 2MPa and 1m/s.

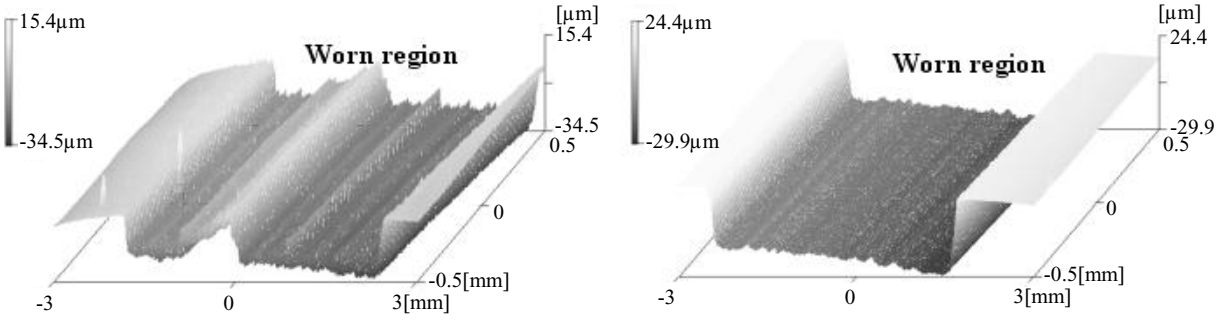

(a) (b)

Figure 5.21: Surface profiles of the worn regions on the counterfaces against epoxy composites (a) without and (b) with nanoparticles against a smoother disk at 2MPa and 1m/s.

For comparison, the surface profiles of the smoother disks (Ra=0.03μm) against epoxy-based composites are shown in Fig. 5.21. Serious wear occurs on the metallic counterpart, even resulting in an obvious scar in the worn region. This result cannot be explained by the mechanical reactions between the composite pin and steel disk, because even with much higher friction and contact temperature at 4MPa, 3m/s no obvious wear scar was observed on the rougher disk (Ra=0.23μm) against the same composite material (cf. Fig.4.22 in Chapter 4). Therefore, a chemical reaction, oxidation of the polished steel counterface, was proposed to account for these phenomena. For an epoxy-steel system, it has been assumed that metallic friction could occur with following sequence [118]: transfer of a steel fragment by adhesion to the counterface; oxidation of the transferred fragment; removal of the oxide in the form of loose wear particles. In the experiment, red wear debris was clearly observed on the worn surfaces of the epoxy composites, which further confirms the assumption. These hard metallic wear particles could result in serious abrasive wear for composite material with a relatively high wear rate.

To further understand the difference in wear behaviour between the composites with epoxy matrix and that with PA66, the sides of worn surfaces of the two nanocomposites are shown in Fig. 5.22 and 5.23 respectively. With a magnified view, the viscous flow of PA66 material can be clearly observed (Fig. 5.22b). This enables the material to develop a continuous transfer film even on a very smooth disk. The thin film may also protect the metallic disk from the atmosphere and thus from being oxidized dur-

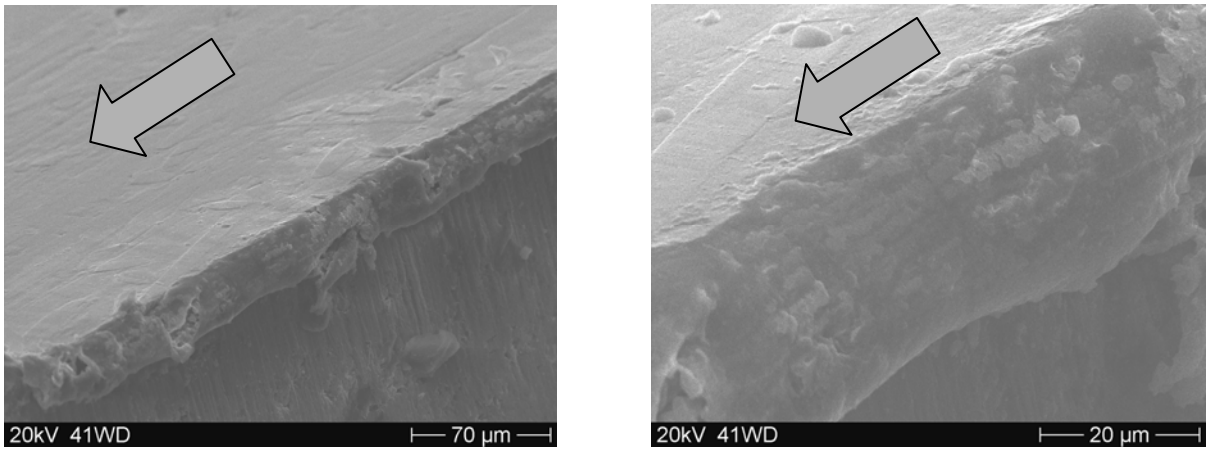

(a) (b)

Figure 5.22: (a) SEM micrographs of the side of worn surfaces of the PA66 based nanocomposite against smoother disks (0.03μm Ra) at 2MPa and 1m/s, and (b) magnified view of the viscous flow of the material.

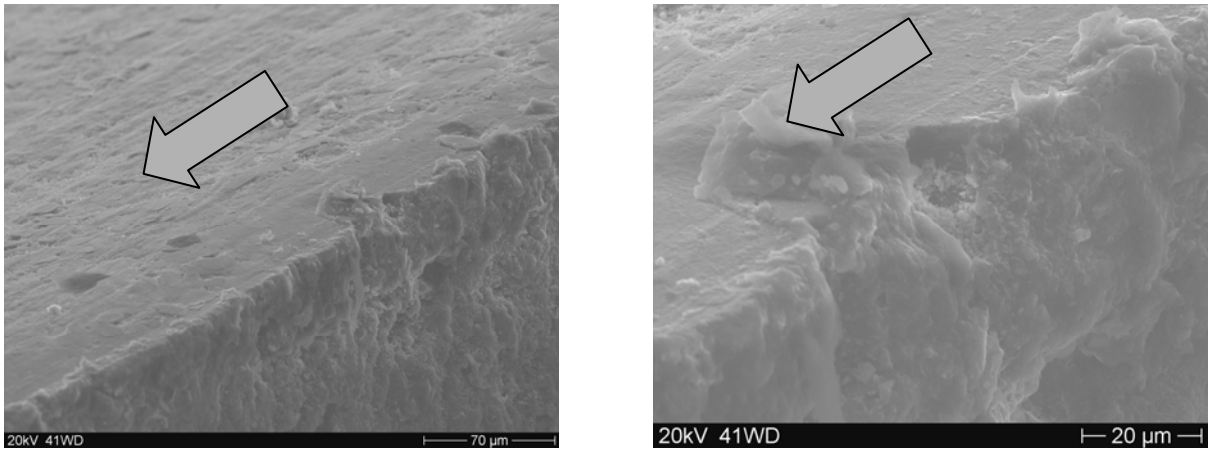

(a) (b)

Figure 5.23: (a) SEM micrographs of the side of worn surfaces of the epoxy based nanocomposite against smoother disks (0.03µm Ra) at 2MPa and 1m/s, and (b) magnified view of the brittle fracture the material.

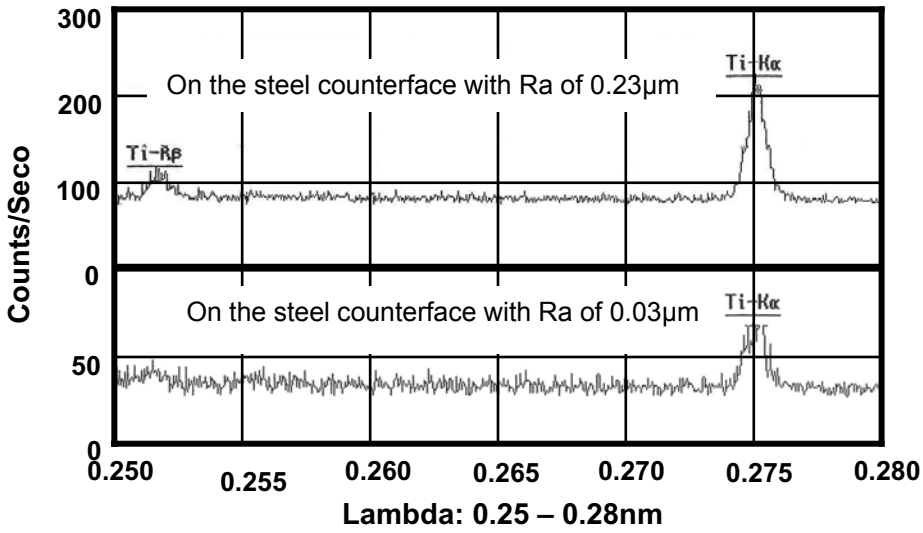

Figure 5.24: WDX analysis of Ti-K_α and Ti-K_β on both the smoother (0.03µm Ra) and rougher (0.23µm Ra) steel counterfaces.

ing the friction process. However, for epoxy-based composites, brittle cracks were observed. As shown in Fig. 5.23b, the size of the particulate wear debris was clearly greater than that of nano-TiO_2. As a result, the nanoparticles could not provide the positive rolling effect expected.

5.1.4.3 WDX Analysis

To characterize nano-TiO_2 particles, spectral analysis by WDX was carried out on wear regions within an area of $100 \times 100 \mu m^2$ for both normal (rougher) and finely pol-

ished (smoother) counterfaces against nanocomposite [5/0/5/15]. As shown in Fig. 5.24, peaks of Titanium elements (representing nano-TiO_2) are observed on both counterfaces. Therefore, with the development of transfer film on the disks, nano-TiO_2 can be embedded on the counterfaces and result in the reduction of frictional coefficient against both rougher and smoother counterfaces.

5.2 Polyetherimide Based Composites

As mentioned earlier, for sliding elements under tribological load, the industrial acceptability of thermoplastics is often limited by their thermal behaviours. The degradation of their mechanical properties at elevated temperature restricts the possibility to applying these materials under high sliding speed and loading conditions. For this reason, high temperature-resistant polymers are generally preferred for such tribological applications [10, 14]. PEI is an amorphous thermoplastic with excellent mechanical and thermal properties due to its relatively high glass transition temperature (T_g). However, neat PEI is not suitable as a tribo-material because of its very poor wear resistance even under low *pv* (the product of the normal pressure, *p*, and the sliding velocity, *v*) conditions. In order to overcome this weakness, different fillers, e.g. short glass fibres and PTFE, have been used to fill PEI materials subjected to various wear modes [133-136]. In the present study, the wear behaviour of PEI-based composites, reinforced by short carbon fibre (SCF) and internally lubricated with graphite flakes, was investigated under different *pv* conditions. In particular, the influence of the addition of inorganic nano-TiO_2 particles was systematically studied.

All the test results of PEI based composites are summarized in Table 5.3. Both the frictional coefficient and the contact temperature given in this table are mean values during the steady state of the sliding process. The characteristics of friction and wear processes under various sliding conditions are further discussed in following sections.

5.2.1 Wear under Standard Conditions: 1MPa and 1m/s

Fig. 5.25 shows the typical variations of the frictional coefficient and the contact temperature against sliding time for the neat PEI compared to the other two composites. It is obvious that the two parameters are strongly correlated. Similar tendencies have also been reported in an earlier study [73]. Besides a high frictional coefficient, the neat PEI also exhibited very poor wear resistance at 1MPa and 1m/s. The wear test had to be stopped only after 2.5 hours due to enormous wear loss. However, when the PEI was filled with conventional reinforcement fillers, i.e. SCF and graphite flakes, the wear resistance of the material was remarkably enhanced. It can be seen that the frictional coefficient of the composite without nanoparticles was initially increased due to the increase in the real contact area during the running-in stage. Thereafter it stabilized at a mean value of about 0.55 with a specific wear rate even less than $1\times10^{-6}mm^3/Nm$. With the addition of nano-TiO_2, the duration of the running-in stage and the stable frictional coefficient were further reduced and the lowest wear rate was achieved (Table 5.3).

Table 5.3: Tribological properties of neat PEI and PEI-based composites under various wear conditions (*pv*-factor).

Composition	*pv*-factor	Frictional Coefficient	Contact Temperature [°C]	Specific Wear Rate [$10^{-6}mm^3/Nm$]
neat PEI	1MPa, 1m/s	0.61	28.21	598.67
SCF+graphite/PEI	1MPa, 1m/s	0.56	30.81	0.77
	4MPa, 1m/s	0.35	52.58	1.14
	8MPa, 1m/s	0.22	58.96	0.73
	12MPa, 1m/s	0.25	98.80	1.34
	4MPa, 2m/s	0.30	73.95	2.17
	4MPa, 3m/s	0.35	126.26	39.14
nano-TiO_2+SCF+graphite/PEI	1MPa, 1m/s	0.36	25.87	0.30
	4MPa, 1m/s	0.27	44.79	2.99
	8MPa, 1m/s	0.15	47.79	1.62
	12MPa, 1m/s	0.09	43.61	1.28
	4MPa, 2m/s	0.16	43.49	1.12
	4MPa, 3m/s	0.14	43.75	0.68

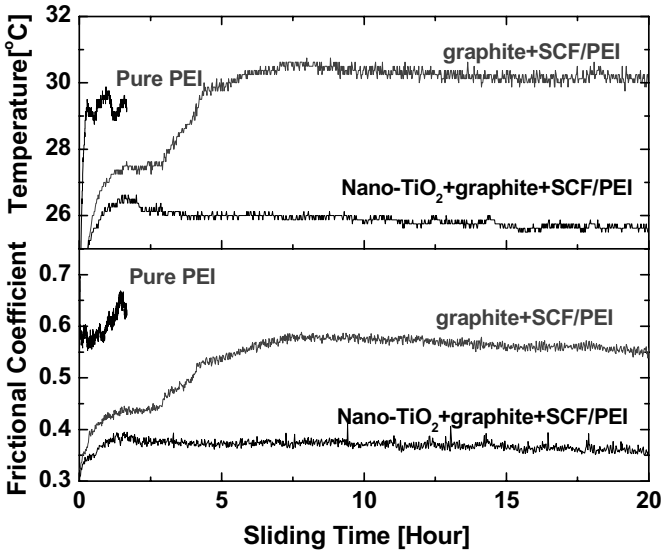

Figure 5.25: Typical sliding process curves of frictional coefficient and contact temperature against sliding time of neat PEI and PEI composites without and with nano-TiO_2 under a standard wear condition of 1MPa and 1m/s.

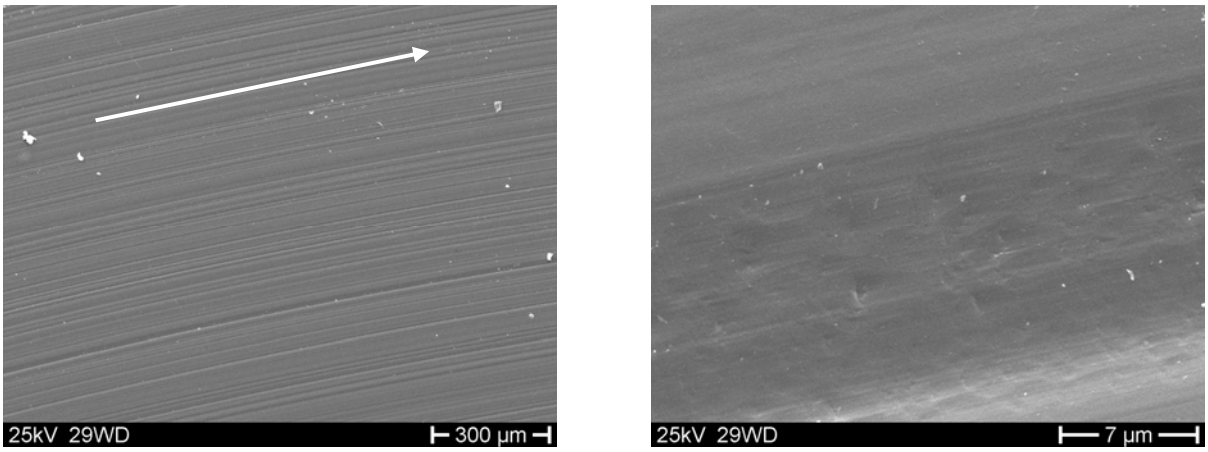

(a) (b)

Figure 5.26: (a) SEM micrographs of worn surfaces of neat PEI measured at 1MPa and 1m/s, and (b) magnified view. The Arrow represents the sliding direction.

A worn surface of the neat PEI is shown in Fig. 5.26. From the linear grooves it can be concluded that an abrasive mechanism dominated the wear process. In this case, the soft polymer was rapidly removed by the hard asperities of the metallic counterpart, resulting in high wear loss. The process is considered to be clearly dependant on the original roughness of the harder counterpart and the pressure applied [128, 130]. Fig. 5.27 presents a worn surface of the PEI composite without nanoparticles. For the PEI composite modified with SCF and graphite flakes, a polymer film layer is transferred to the steel counterpart, resulting in a new counter surface producing pri-

marily an adhesive wear mechanism. This mechanism is generally less dangerous for a polymer sliding surface than an abrasive one, resulting in a lower frictional coefficient and specific wear rate [11, 12]. As shown in this figure, the worn surface appears smooth i.e. without obvious grooves. However, micro-cracks occurred in the region of the fibre/matrix interface, caused by brittle fracture of the PEI matrix. With propagation of these interfacial cracks, fibres exposed to the asperities of the counterpart are finally removed, leaving voids on the worn surface (Fig.4.3b) [123].

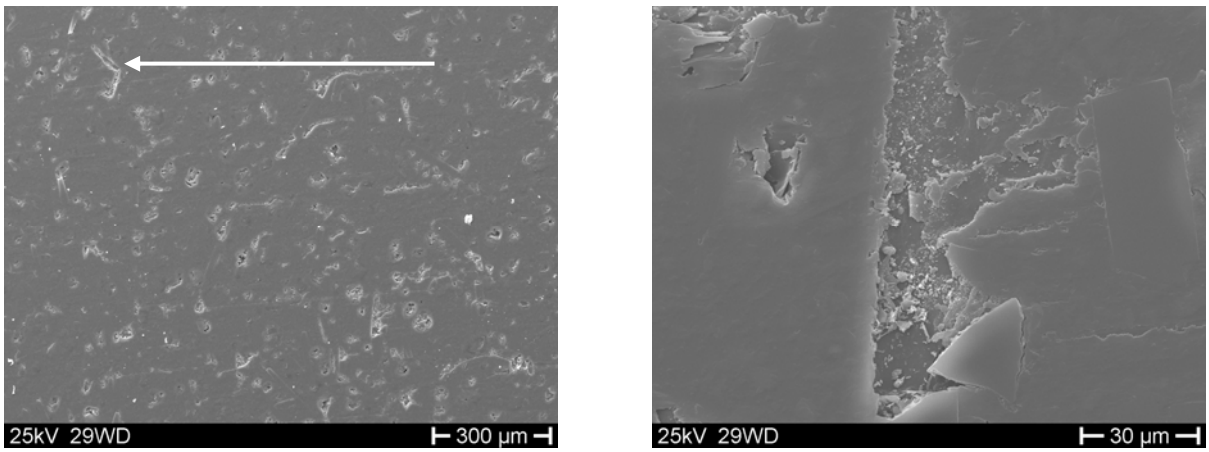

(a) (b)

Figure 5.27: (a) SEM micrographs of the worn surfaces of the composite graphite+ SCF/PEI without nanoparticles at 1MPa and 1m/s, and (b) the magnified view of micro-crack. Arrow line represents the sliding direction.

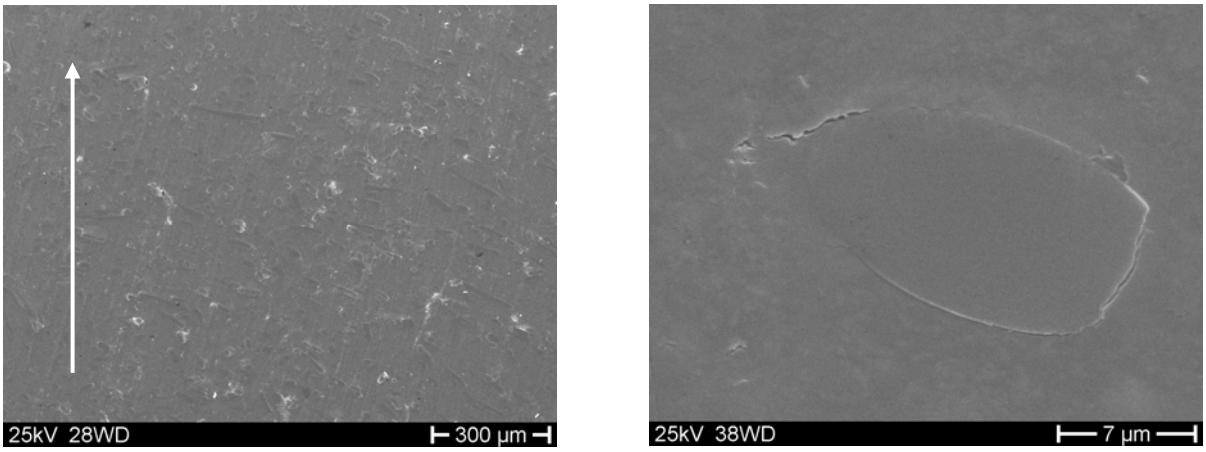

(a) (b)

Figure 5.28: (a) SEM micrographs of the worn surfaces of the composite nano-TiO_2+graphite +SCF/PEI at 1MPa and 1m/s, and (b) the magnified view of the worn fibres. Arrow line represents the sliding direction.

The worn surface of the PEI-based nanocomposite is presented in Fig. 5.28. It is obvious that the amount of fibre removal was greatly restricted, and the surface is much smoother in comparison to the samples without nanoparticles. A positive rolling effect of the nanoparticles between the material pairs during the sliding process, was proposed [11, 74]. Such a rolling effect was also reported by others for WS_2 nanoparticle systems under mixed lubrication [75, 76]. It is assumed that this effect reduces the frictional coefficient during sliding, as well as the shear stress and the contact temperature, especially in high sliding pressure and speed situations. Furthermore, this rolling effect seems also to protect the SCF from more severe wear mechanisms by restricting the micro-crack mechanism in the interfacial region between the fibres and matrix [74]. As a result, the SCF remains in the polymer matrix longer, providing high wear resistance of the composite.

5.2.2 Under Higher Contact Pressure

Fig. 5.29 summarizes the wear results of the two composites when the normal pressure was increased from 1 to 12 MPa while the sliding velocity was kept constant at 1m/s. The frictional coefficient of the composite without nano-TiO_2 decreased noticeably from 1 to 8 MPa, and increased slightly under 12 MPa. This was associated with a higher value in the contact temperature (cf. Table 5,3). Also, the depth wear

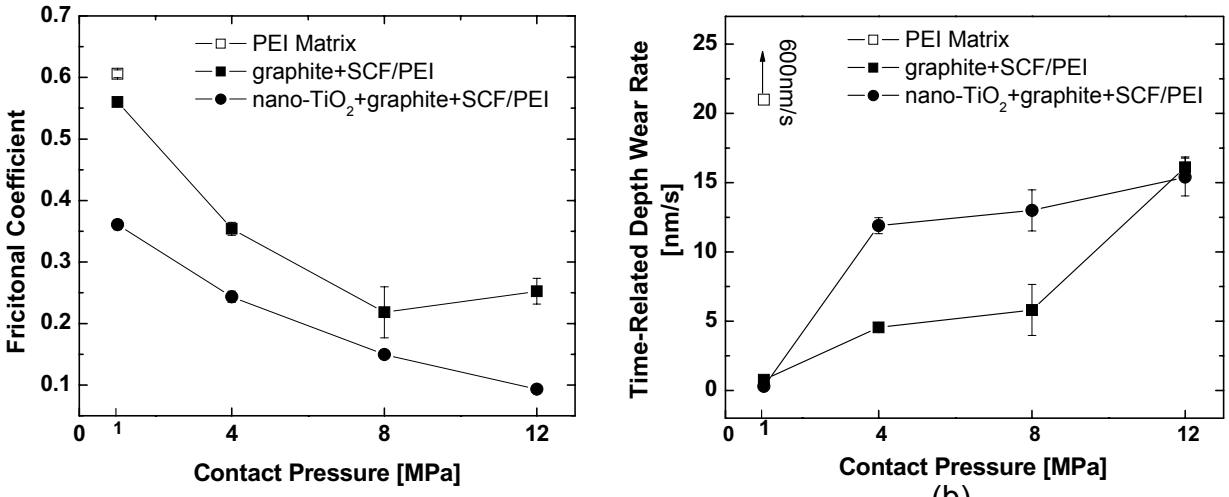

Figure 5.29: (a) Friction coefficient and (b) time-related depth wear rate as a function of contact pressure. Sliding velocity is kept constant of 1m/s.

rate of the material increased progressively. With the addition of nanoparticles, the frictional coefficient was further reduced under all test conditions and decreased steadily with an increase in contact pressure. However, it was noticed that the wear rate of the nanocomposite was not always lower than that without nano-TiO_2. As shown in Fig. 5.29b, the nanocomposite displayed a lower wear rate than the composite without nanoparticles under 1MPa and 12MPa, whereas higher wear rates occurred under 4MPa and 8MPa. Two competing effects of nano-TiO_2 on the wear resistance of these composites are probably the reason for this inconsistency. On the one hand, nanoparticles tend to reduce the wear rate of composite by a reduction of the frictional coefficient as a result of their rolling effect. On the other hand, a mild abrasive is simultaneously created by hard nanoparticles acting as third bodies, and this counteracts the former effect to a certain extent [77].

To understand the wear mechanisms involved, the surfaces of two composites worn under extremely high pressure were examined by SEM. Fig. 5.30 shows the surface of the composite without nanoparticles worn under 12MPa and 1m/s. In comparison to Fig.4.3, the surface here is apparently smoother and without micro-cracks. This can be explained by the increased ductility of PEI at elevated temperature. As reported by Kim et al [138], the yield stress of PEI is nearly two times reduced as temperature is increased from 25 to 130°C, whereas the fracture toughness remains al-

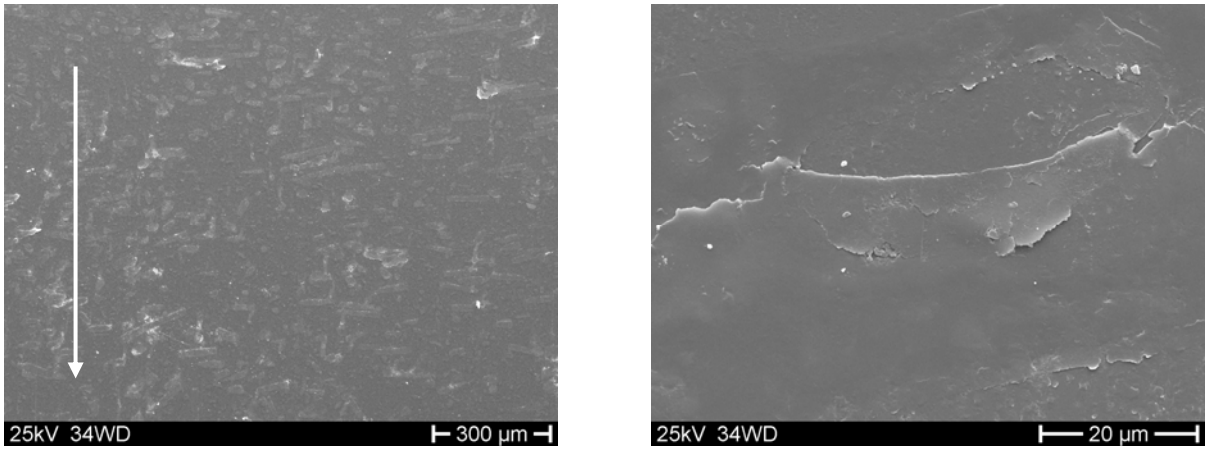

(a) (b)

Figure 5.30: (a) SEM micrographs of the worn surfaces of the composite graphite+ SCF/PEI without nanoparticles at 12MPa and 1m/s, and (b) the magnified view of adhesion. Arrow line represents the sliding direction.

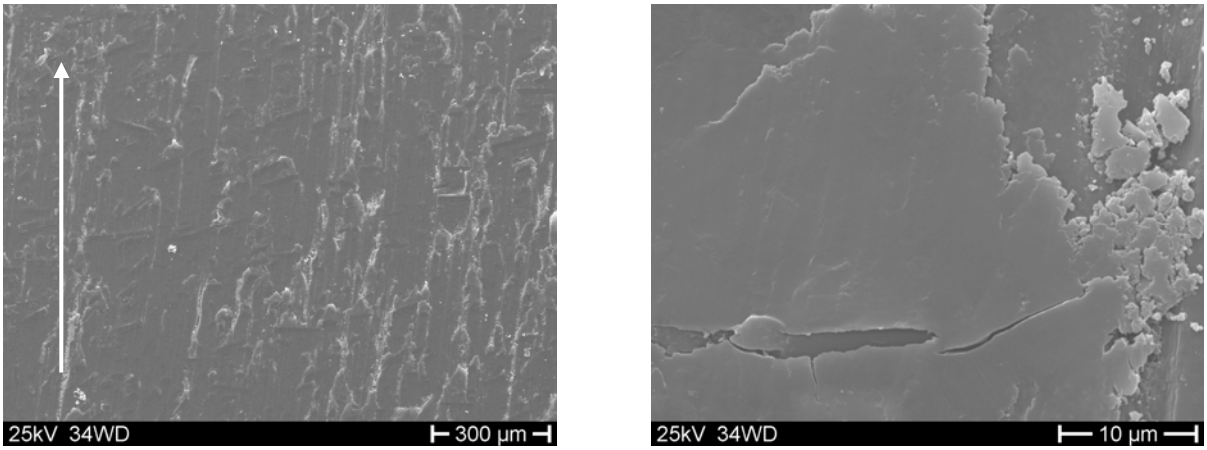

(a) (b)

Figure 5.31: (a) SEM micrographs of the worn surfaces of the composite nano-TiO_2+graphite+SCF/PEI at 12MPa and 1m/s, and (b) magnified view of a patch of worn debris. The Arrow represents the sliding direction.

most unchanged. Therefore, brittle fracture of the PEI matrix in the fibre/matrix interfacial region is greatly restricted at elevated temperature. This restriction causes fibres to remain in the matrix. As a result, the wear process is rather mild, resulting in a high load-carrying capacity.

The worn surface of the nanocomposite under 12MPa and 1m/s is shown in Fig. 5.31. The surface is relatively smooth and some debris patches are noticed. With a magnified view, it can be seen that a patch is formed with smaller wear debris, which might be generated by the mild abrasion induced by the hard nanoparticles [77].

5.2.3 Wear at Enhanced Sliding Velocity

Fig. 5.32 presents the results for the two composites worn under various sliding velocities at a constant pressure of 4MPa. The frictional coefficient (cf. Fig. 5.32a) of the composition without nanoparticles does not exhibit clear dependence on the sliding velocity, whereas that of the nanocomposite obviously reduces with the increase of velocity. However, this is not the case for the depth wear rate (cf. Fig. 5.32b). A higher sliding velocity includes a very high wear rate for the composition without nanoparticles, whereas the nanocomposite presents a relatively low wear rate for the whole speed range between 1 and 3 m/s.

With SEM examination of worn surfaces, obvious viscous flow of PEI matrix is observed due to the very high contact temperature sliding under 4MPa and 3m/s (cf. Fig. 5.33). In this situation, the wear rate is greatly increased because the reinforced fillers can no longer contribute to wear resistance. For the nanocomposite, the reduced frictional coefficient effectively restricts the increase of the contact temperature, therefore, resulting in very good wear resistance even at very high sliding velocity, i.e. 3m/s. A relative smooth worn surface is obtained (cf. Fig. 5.34).

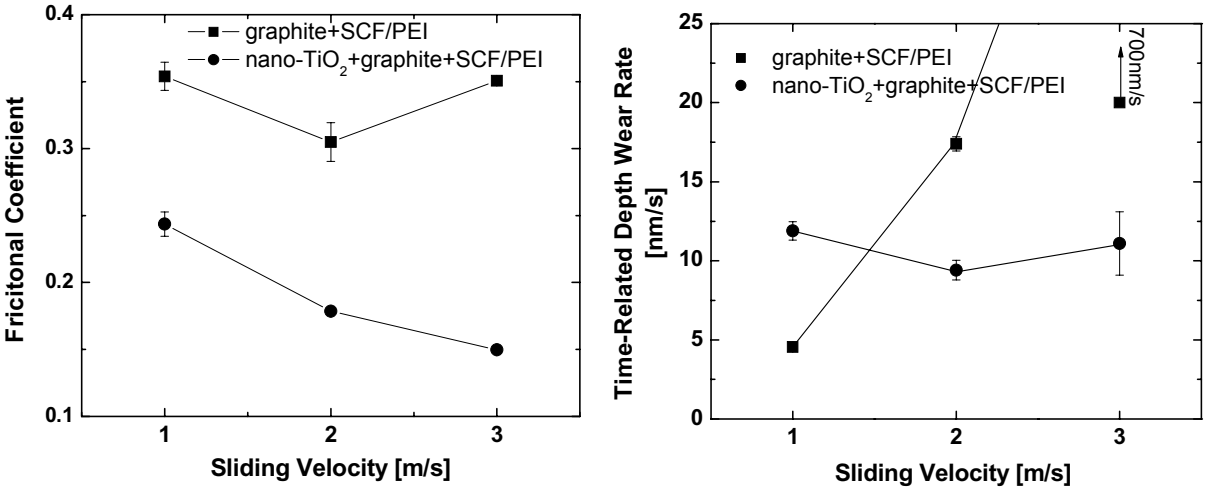

Figure 5.32: (a) Friction coefficient and (b) time-related depth wear rate as a function of sliding velocity. The contact pressure was kept constant of 4MPa.

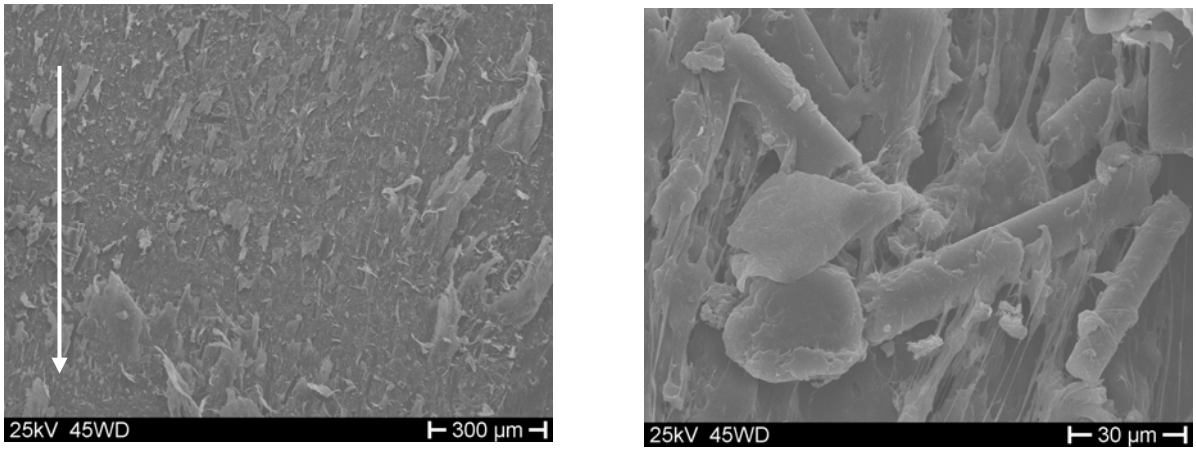

Figure 5.33: (a) SEM micrographs of the worn surfaces of the composite graphite+ SCF/PEI without nanoparticles at 4MPa and 3m/s, and (b) magnified view of viscous flow of PEI matrix. The Arrow represents the sliding direction.

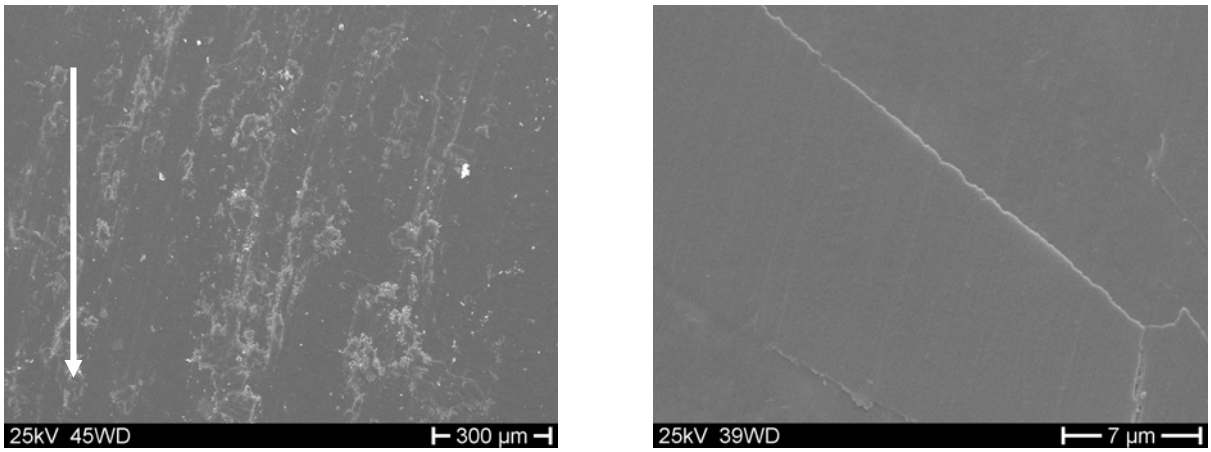

(a) (b)

Figure 5.34: (a) SEM micrographs of the worn surfaces of the composite nano-TiO_2+graphite +SCF/PEI at 4MPa and 3m/s, and (b) the magnified view of the worn fibres. Arrow line represents the sliding direction.

5.2.4 Surface Observations of Counterparts

In the case of sliding wear of polymers against steel counterparts, the friction component resulting from adhesion equals the product of the real contact area and the shear strength of the plastic (softer) material [128]. Therefore, once the mechanical properties of soft polymer are considered to be constant, the frictional coefficient is mostly determined by the proportion of the normal load to the real contact area. However, the actual relationship between them is very complex and is greatly influenced by a number of interactions, e.g. the mechanical properties of the polymer, the surface roughness of the contact bodies, the sliding conditions and the real contact temperature during sliding. In the present study, in order to understand the sliding performance of the composites with and without nanoparticles under various pressures, surface profiles of the counterparts resulted were investigated.

Fig. 5.35 gives the surface profiles of the metallic counterparts worn by the composite without nanoparticles at different pressures. It is clear that the roughness of the worn counterparts increases notably with the increase of the applied pressure. This indicates that, with the increased contact pressure, the real contact area is accordingly enlarged due to plastic deformation of the polymer matrix consequently resulting in increased friction force. This increase leads to two contrary effects to the fric-

tional coefficient. On the one hand, the contact temperature is elevated owing to frictional heating, which can cause an increase of the frictional coefficient. For instance, when the contact temperature approaches the *Tg* of the matrix, the real contact area would be greatly increased due to the marked decrease in stiffness. On the other hand, the higher friction force causes a smoothing effect on the counterpart by removing its asperities, generating uniform distribution of the real contact pressure. As

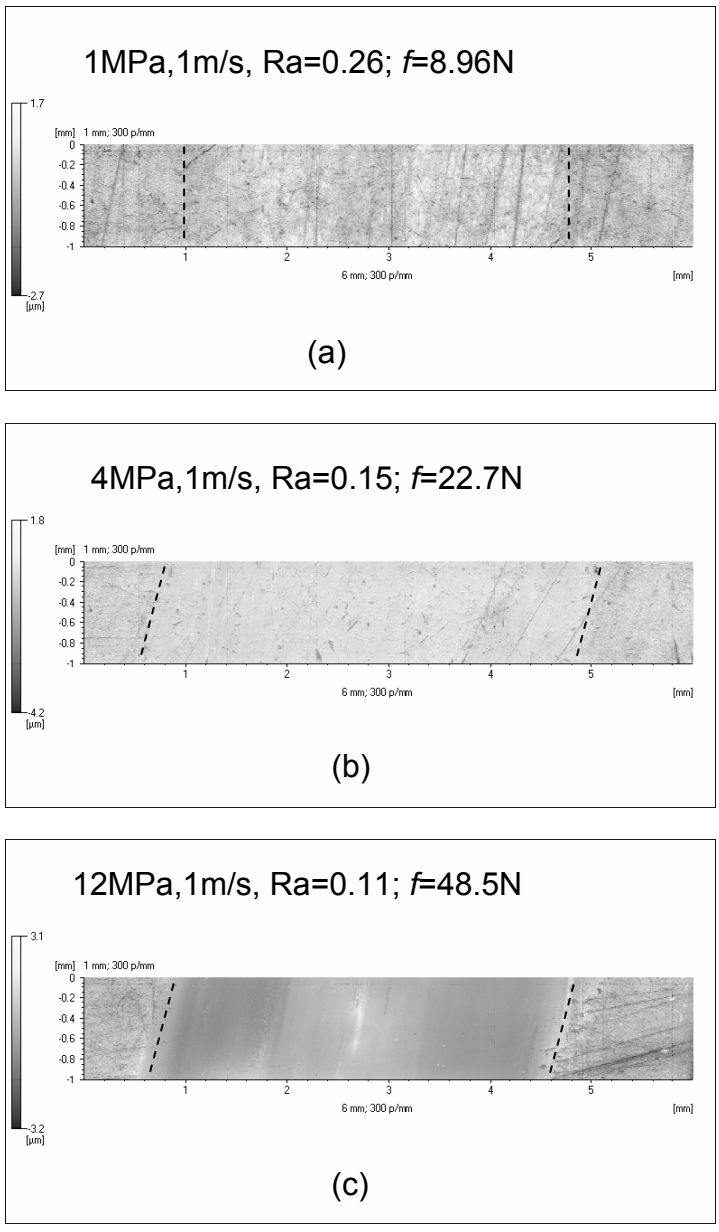

Figure 5.35: Surface profiles of worn region on the steel counterpart surface measured under a contact pressure of (a) 1MPa, (b) 4MPa, and (c) 12MPa of the composite without nano-TiO_2. The sliding velocity was kept constant at 1m/s. The corresponding *pv* condition, surface roughness of the worn region (*Ra*) and the friction force between contact bodies (*f*) are shown.

a result, the plastic deformation at contact spots would be reduced and thus restricted the increase of the real contact area [139]. Therefore, due to an observable smoothing effect, the frictional coefficient is decreased with the increase of contact pressure from 1 to 8 MPa. However, it increases again under very high pressure (12MPa) because the marked increase in the contact temperature becomes dominant over the real contact area and the frictional coefficient.

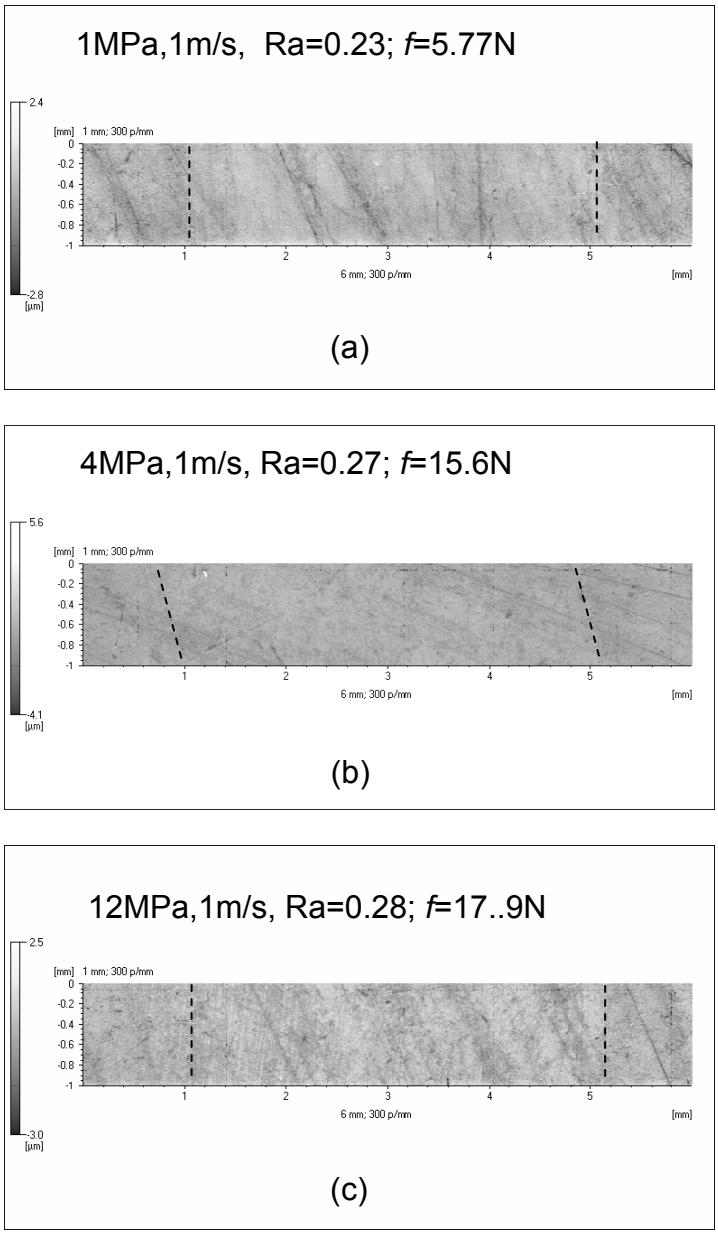

Figure 5.36: Surface profiles of worn region on the steel counterpart surface measured under a contact pressure of (a) 1MPa, (b) 4MPa, and (c) 12MPa of the composite with nano-TiO_2. The sliding speed was kept constant at 1m/s. The corresponding *pv* condition, surface roughness of the worn region (*Ra*) and the friction force between contact bodies (*f*) are shown.

For the nanocomposite, however, no obvious relationships between surface profiles and frictional coefficient can be observed. As shown in Fig. 5.36, the surface roughness of counterparts worn by the nanocomposite under different pressures is almost unchanged. At the same time, the frictional force is clearly lower than that of the composition without nano-TiO_2, especially under high pressures. The rolling effect of nanoparticles may dominate the sliding performance [74,77]. Meanwhile, these phenomena also indicate different contact/friction mechanisms for the composites studied without and with nanoparticles.

6 Wear Modelling of Polymer Nanocomposites Based on Energy Considerations

Wear has been the subject of much scientific and empirical investigation, owing to its widespread and pervasive economic consequences. Considerable efforts have been expended on the development of theories and deterministic models. However, there is still no way for the prediction of the wear behaviour of the materials, with confidence or certainty even if all of their physical and chemical properties have been independently established [82, 83]. It is now agreed by tribologists that tribological properties are generally not real material parameters, but depend on the tribo-system in which the materials have to function [97, 99,140]. Further, the friction process is a complex energy process [97, 99,141]. The main energy terms come from deformation and fracture work [97, 141,142]. The former is stored within the material as dislocation and finally appears as thermal energy. The latter generates new surfaces associated with wear debris. Although the quantitative determination of the energy distribution is very difficult, valuable indications for research may be derived from a qualitative consideration of tribo-systems, even those composed of diverse materials, operating under various conditions.

In this chapter, the friction process in the steady stage is characterized by the friction power intensity q_f, which is defined as,

$$q_f=\mu p v \ [\mathrm{w/m^2 s}] \tag{6.1}$$

in which μ is the frictional coefficient. p is the pressure applied and the v is the sliding velocity. The correlations between friction power intensity and contact temperature, as well volumetric wear rate are examined. In particular, using this energetic approach, the influences of sliding velocity and load on the contact/wear mechanisms are systematically investigated. The study is expected to make some contribution to understanding the fundamental mechanisms controlling friction and wear, as well as the effects of composition and sliding conditions on these mechanisms.

In order to establish a calculable model of the wear process, an artificial neural network (ANN) approach is applied to experimental data. ANN has been proved to be a powerful mathematical tool for simulating various engineering applications [108,115,143]. With an adequate dataset, ANN has also been successfully applied to predicting the wear properties of polymer composites (reviewed in Chapter 1). However, owing to the complex relationship between wear performance and input parameters (e.g. volume content of fillers and selected mechanical properties), a large dataset with sufficient information is necessary for the training of such an ANN [109]. However, using simple energy-based models, satisfactory ANN predictive quality could be reached with a relatively small dataset. In particular, the relatively simple construction of a trained ANN with quite fast computing speed shows potential, which will certainly be useful for prediction in online monitoring in practical applications.

6.1 Energetic Concept of Friction

During a friction process, nearly all the energy dissipated by friction appears as heat, which then flows into the rubbing bodies. The local increase in temperature significantly influences on both friction and wear behaviours. Numerous papers have been published relating to the temperature rise at local contact asperities. In general, two temperatures are of interest. The first is the mean or bulk surface temperature T_b, which appears a few tens of microns below the actual contact surface. The second is the local or flash temperature T_f, which occurs transiently at the tip of the individual contacting asperities and is almost always higher than T_b. In the present work, the formulation of bulk temperature for polymer composites sliding against a steel counterpart is developed. As well, the flash temperature is considered in term of the maximum attainable flash temperature occurring at the real contact area.

6.1.1 Calculation of the Contact Temperature

6.1.1.1 Bulk Temperature

Fig. 6.1 is a schematic configuration of the pin-on-disk, for which the temperature calculation is performed. According to our experiments, the pin is a polymer compos-

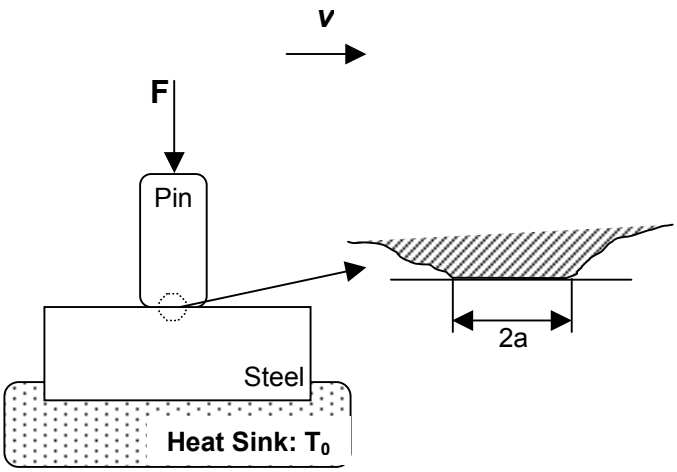

Figure 6.1: The pin-on-disk configuration for which the temperature calculations are performed.

ite specimen and the disk is a polished steel disk (German Standard 100Cr6). As stated in Chapter 1, frictional heat is divided by two rubbing bodies (cf. equation 1.4). However, in this case, almost all the generated heat would flux into the steel disk because the thermal conductivity of steel (e.g. the thermal conductivity of DIN 100Cr6 is about 58$Wm^{-1}K^{-1}$ [144]) is much higher than that of polymers (e.g. the thermal conductivity of PA66 is 0.23~0.25 $Wm^{-1}K^{-1}$ [145]). Therefore, the equation can be simplified as

$$T_b - T_0 = \frac{l_{disk}}{k_{disk}} q_f \tag{6.2}$$

k_{disk} is the thermal conductivity of the disk. l_{disk} is the equivalent depth for heat source to heat sink, which depends on whether the heat flux is transient or steady state. In order to determine the equivalent depth l_{disk}, the Pelcet parameter is introduced [101-103],

$$L_P = \frac{va}{2\kappa} \tag{6.3}$$

where *a* is the length of heat source in moving direction (Fig. 6.1) and κ is the thermal diffusivities of the disk,

$$\kappa = \frac{k}{\rho c} \tag{6.4}$$

which is determined by the material properties k (thermal conductivity), ρ (density) and c (specific heat capacity). L_P is normally interpreted as the ratio of the two times: $t_1=a^2/2\kappa$, which represents the time taken for the frictional heat to diffuse to a depth below the surface equal to the contact length a, and $t_2=a/v$, which is the duration for the heat applied to any point on the surface [101-103,146]. When L<1, the heat source is stationary and the contact temperature is determined by equation 1.3. Under high-speed conditions (L>5), however, heat flow is transient and the heat conduction occurs mainly perpendicular to the contact surface. The equivalent depth is determined by [147],

$$l_{disk} = \frac{a}{\sqrt{L_P}} \tag{6.5}$$

Therefore, the temperature is given by [102,146],

$$\Delta T_b = \mu P v \left(\frac{a}{vk\rho c} \right)^{1/2} \tag{6.6}$$

or,

$$q_f = k'(T_b - T_0)\ ,\ k' = \left(\frac{vk\rho c}{a} \right)^{1/2} \tag{6.7}$$

Here, k' is described as the factor of thermal diffusion of the system. Accordingly, the factor k' is mostly determined by the thermal conductivity of the disk, the sliding velocity and the real contact area.

To calculate the parameter L_P, it is necessary to determine the real contact area, which is generally much lower that the nominal contact area. For example, Friedrich et al [139] measured the real contact area between fibre-reinforced PEEK and steel counterpart at static condition under 10MPa. They found that the real contact area was only 2.9~10% of the nominal contact area, depending on fibre orientation. During the sliding process, this value should be increased due to the increase of contact temperature. In the present case, the sectional area of all the pin specimens is 4×4 mm^2. The pressures range from 1 to 12MPa, with the contact temperature ranging from room temperature to over 100^{o}C. Therefore the real contact area is conserva-

tively estimated as ~%5 of the nominal contact area and thus a=900μm. With the typical value for the steel, κ=14.2×10^{-6}m^2/s [147, 148] and v=1m/s, L_P=31 is obtained. Therefore, equation 6.7 for high-speed conditions is used to interpret the experimental results.

6.1.1.2 Flash Temperature

As mentioned earlier, the flash temperature refers to the temperature rise at the peaks of the contacting asperities with a very short duration [102]. This temperature can have a critical influence on friction and wear characteristics. However, due to the great difficulty to characterize the real contact state, e.g. the size and distribution of asperities, the accurate calculation of T_f is actually very difficult [149]. Several models have been developed to estimate the maximum attainable flash temperature [101,102, 150-152]. Based the temperature distribution in contact area, Archard [101, 102] proposed a relatively simple way to estimate the overall maximum attainable temperature T_{max} over the whole contact area,

$$T_{\max} = 16.4 T_b \tag{6.8}$$

which can be reasonably treated as the flash temperature. On the other hand, the surface temperature cannot increase indefinitely even when the sliding conditions are made more severe. For polymers, it is possible to put the limit of T_{max} or T_f in relation to certain significant temperature parameters such as the temperature of glass transition, heat distortion, softening point, melt point of crystals, decomposition temperature, etc [153,154]. When this boundary temperature level has been attained, the wear rate of the material would be very high due to serious deterioration of the mechanical properties. Therefore, this is also commonly the upper limit of operating conditions for tribo-materials.

6.1.2 Applications: Interpreting Frictional Heating Experiments

The test device used in the investigation is a pin-on-disk apparatus (Fig. 2.1 in Chapter 2). The applied pressure varies from 1MPa to 12MPa and the sliding velocity from 1m/s to 3m/s. Six compositions with distinct matrix systems are particularly consid-

ered: SCF+PTFE+graphite/epoxy with and without nano-TiO_2 (cf. Chapter 4), SCF+PTFE+graphite/PA6,6 with and without nano-TiO_2 (cf. Chapter 5) and SCF+PTFE+graphite/PEI with and without nano-TiO_2 (cf. Chapter 5). The test results are summarized in Table 6.1. For convenience, the materials are symbolized as [nano-TiO_2/PTFE/graphite/SCF] in volume content of each filler. The values of time-related depth wear rate, frictional coefficient and contact temperature, are all mean

Table 6.1: Wear results of various polymer composites tested by a pin-on-disk apparatus under different sliding conditions.

Composition		*pv* factor	Frictional Coefficient μ	Contact Temperature T_b [°C]	Maximum Attainable Flash Temperature $T_{max}=1.64T_b$ [°C]	Time-Related Depth Wear Rate W_t [nm/s]	Factor of Thermal Diffusion $k'=\mu pv/(T_b-T_0)$ [$Wmm^{-2}s^{-1}K^{-1}$]
Epoxy Based Composites	[0/5/5/15]	1MPa, 1m/s	0.59	34.07	55.87	0.81	0.042
		2MPa, 1m/s	0.78	67.98	111.49	4.16	0.033
		4MPa, 1m/s	0.63	82.78	135.76	17.12	0.037
		1MPa, 0.5m/s	0.47	25.95	42.56	0.27	0.039
		1MPa, 2m/s	1.08	62.27	102.12	6.28	0.049
	[5/5/5/15]	1MPa, 1m/s	0.49	29.74	48.78	0.89	0.050
		4MPa, 1m/s	0.33	50.99	83.62	3.92	0.043
		8MPa, 1m/s	0.21	57.24	93.87	9.79	0.044
		12MPa, 1m/s	0.14	60.65	99.46	11.36	0.042
		4MPa,2m/s	0.21	54.90	90.04	8.68	0.048
		4MPa, 3m/s	0.20	67.20	110.21	16.80	0.050
	[5/10/0/15]	1MPa, 1m/s	0.50	29.41	48.23	0.86	0.053
		4MPa, 1m/s	0.33	52.33	85.81	4.49	0.041
		8MPa, 1m/s	0.26	69.12	113.35	13.65	0.042
		12MPa, 1m/s	0.18	74.92	122.87	15.13	0.040
		4MPa, 2m/s	0.30	71.45	117.17	21.16	0.047
		4MPa, 3m/s	0.23	78.57	128.86	27.71	0.047
	[5/0/10/15]	1MPa, 1m/s	0.38	25.97	42.59	0.64	0.063
		4MPa, 1m/s	0.21	38.84	63.69	3.27	0.045
		8MPa, 1m/s	0.13	44.12	72.36	12.32	0.044
		12MPa, 1m/s	0.09	43.14	70.75	11.47	0.045
		4MPa, 2m/s	0.15	40.91	67.09	12.28	0.056
		4MPa, 3m/s	0.16	55.77	91.46	31.73	0.053

Table 6.1 (continued)

PA 6,6 Based Composites	[0/0/5/15]	1MPa, 1m/s	0.60	30.57	50.14	0.53	0.056
		2MPa, 1m/s	0.57	46.07	75.56	1.59	0.044
		4MPa, 1m/s	0.69	94.98	155.77	11.70	0.037
		8MPa, 1m/s	0.35	97.38	159.70	135.00	0.036
		2MPa, 2m/s	0.78	97.67	160.18	19.50	0.040
		2MPa, 3m/s	0.62	115.80	189.91	34.40	0.039
	[5/0/5/15]	1MPa, 1m/s	0.44	26.66	43.72	0.50	0.066
		2MPa, 1m/s	0.34	33.21	54.47	1.43	0.052
		4MPa, 1m/s	0.26	45.55	74.71	3.21	0.041
		8MPa, 1m/s	0.22	64.69	106.10	26.10	0.039
		2MPa, 2m/s	0.34	42.94	70.43	2.52	0.059
		2MPa, 3m/s	0.38	62.36	102.27	20.10	0.054
PEI Based Composites	[0/0/5/15]	1MPa, 1m/s	0.56	30.81	50.52	0.77	0.052
		4MPa, 1m/s	0.35	52.58	86.23	4.55	0.044
		8MPa, 1m/s	0.22	58.96	96.70	5.81	0.045
		12MPa, 1m/s	0.25	98.80	162.03	16.12	0.038
		4MPa, 2m/s	0.30	73.95	121.28	17.38	0.045
		4MPa, 3m/s	0.35	126.26	207.07	704.62	0.040
	[5/0/5/15]	1MPa, 1m/s	0.36	25.87	42.43	0.30	0.061
		4MPa, 1m/s	0.24	42.54	69.76	11.95	0.043
		8MPa, 1m/s	0.12	42.39	69.52	12.95	0.044
		12MPa, 1m/s	0.09	47.04	77.14	15.41	0.041
		4MPa, 2m/s	0.16	43.49	71.32	9.41	0.054
		4MPa, 3m/s	0.14	43.75	71.75	11.06	0.068

values during the steady state of the friction process. Also, each result is an average value of at least three experimental data. As given in the table, the value of the factor thermal diffusion k' is calculated by $k'=\mu pv/(T_b-T_0)$, in which $T_0=20^oC$. The maximum attainable flash temperature is estimated by bulk temperature according to equation 6.8. It is interesting to notice that the time related depth wear rate of PA66 based composites with and without nanoparticles clearly increases when the T_{max} exceeds the T_g of PA66, which is 77°C. Further, a very high wear rate is obtained by the PEI based composite without nanoparticles when the T_{max} is very close to the T_g of PEI (~233°C). These reasonable results also validate the estimation of the flash temperature in the real contact area.

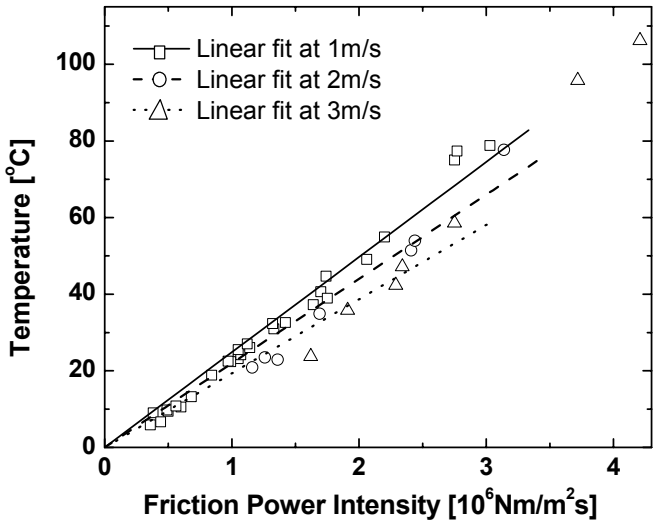

Figure 6.2: Contact temperature in the steady stage as a function of the friction power intensity under different sliding conditions.

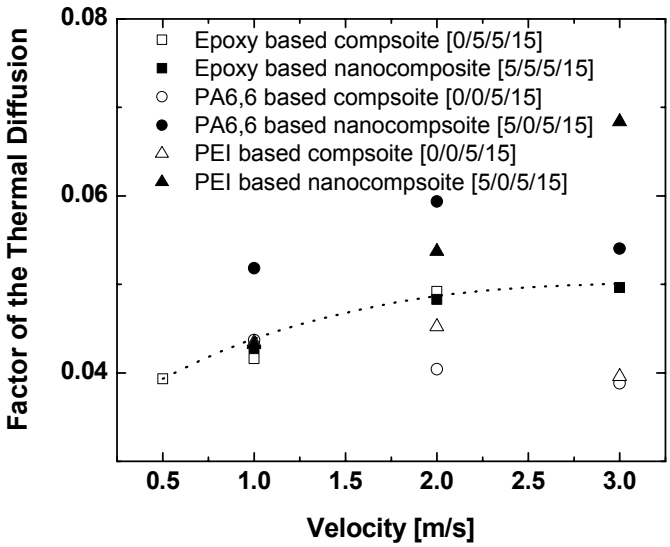

Figure 6.3: Variation of the factor of thermal diffusion at different sliding velocities with a constant pressure of 4MPa.

Fig. 6.2 depicts contact temperature as a function of friction power intensity. It is clear that the contact temperature is almost linearly proportional to q_f but nearly independent of the composite materials involved. The slope of the curve decreases with the increase of pressure sliding velocity as a whole, which is consistent with the equation 6.7. On the basis of this equation, the influence of sliding conditions on heat conduction is further investigated in detail. In particular, the effects of fillers on contact state and consequently heat conduction are also discussed.

6.1.2.1 Influence of Sliding Conditions

Fig. 6.3 shows the factor of the thermal diffusion *k'* at different sliding velocities. It is obvious that the *k'* is increased with an increase of velocity as a trend. However, the slope of the curve decreases at high velocities. This can be explained by the increase of the thickness of the transfer film layer (TFL) due to the temperature rise at the velocities evaluated [7]. As mentioned earlier, the thermal conductivity of polymers is much lower than that of steel. Therefore, the thick TFL acts as a thermal barrier and counteracts the effects of the high velocity to a certain extent. This phenomenon is observed more when the maximum attainable flash temperature is close or above the glass transition temperature T_g of the thermoplastic matrices. In this case, the viscosity of the thermoplastic matrices in local contact is increased noticeably, resulting in a continuous and thick transfer film layer on the steel counterpart. As a result, the factor *k'* could be even decreased at higher velocities (cf. Table 6.1).

When the pressure is increased, the real contact area normally grows until it equals the nominal contact area. According to Equation 6.7, *k'* would be decreased. This assumption is well supported by the experimental results, as shown in Fig. 6.4a. The *k'* of all materials decreases noticeably as the pressure increases from 1MPa to

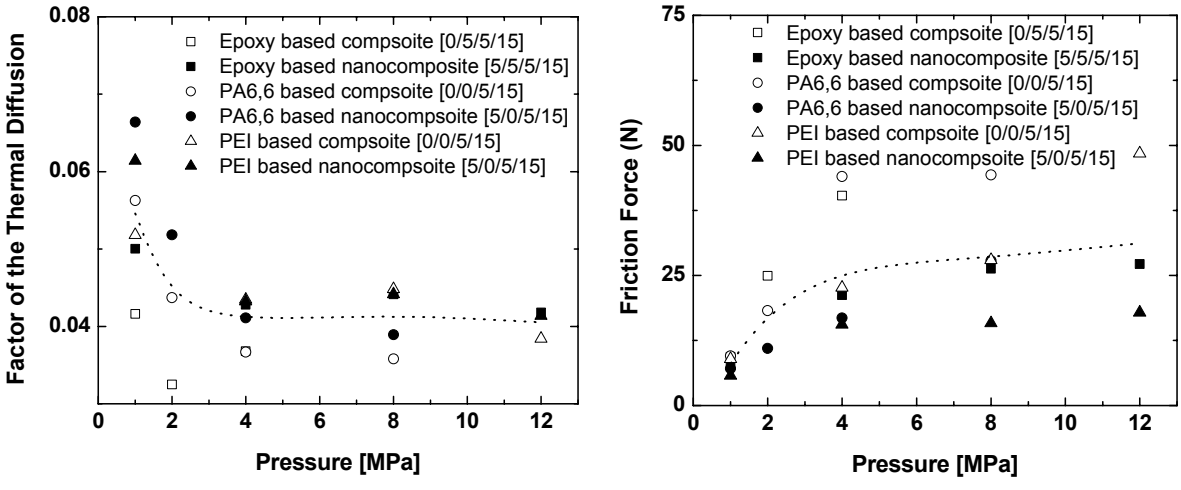

(a) (b)

Figure 6.4: (a) Variation of the factor of thermal diffusion and (b) friction force of materials under different pressures with a constant velocity of 1m/s.

4MPa. However, the slope is much reduced under higher pressures, which implies a smaller increase of the real contact area as it is very close to the nominal contact area. Fig. 6.4b shows the friction force ($f=\mu p$) of materials under different pressures. For a plastically deforming specimen against a hard counterpart, it was assumed that the friction force is linearly proportional to the real contact area and ultimate shear strength of material [155]. It is clear that the change of friction force is consistent with that of *k'* under various pressures.

It was noticed that the friction force and contact temperature for the PA66 based composite without nanoparticles increases from 4MPa, 1m/s to 8MPa, 1m/s. However, the wear loss of the material increases significantly. This can be attributed to attainment of the upper bound of the surface temperature (the most likely position is the softening point [153]). In this case, the softened polymer cannot sustain the higher friction force/work anymore, and a slight increase of pressure may cause greatly increased wear loss. Accordingly, the value of *pv* may be taken as the maximum allowable value for the operation of the material. For the PEI based nanocomposite, almost unchanged friction force and contact temperature are observed from 4MPa to 12MPa. However, it is evident that the contact temperature is much lower than the limit of T_{max} and the wear rate of the material is relatively stable. As indicated in Chapter 5, the friction behaviour of the material was governed by the rolling effect of the nanoparticles. This positive rolling effect effectively restricts the increase of friction under higher pressures and thus the friction/wear performance remains stable within a certain range of *pv* conditions. Meanwhile, these phenomena also confirm very different contact/friction mechanisms for the composites studied without and with nanoparticles, respectively.

6.1.2.2 Influence of Nanoparticles

As shown in Figs. 6.3 and 6.4, with the same matrix materials, the *k'* for the composites with nanoparticles is always a little higher than for those without nanoparticles under the same sliding conditions. This may be the effect of the three-body contact model due to the additional nanoparticles generating points contact instead of the

surfaces contact. As a result, the real contact area is decreased and *k'* is higher. Another possible reason is the change in the proportion of friction work caused by particle abrasion: that is the energy needed to bring about material loss is increased, while plastic and/or elastic deformation is correspondingly restricted. Consequently, contribution of the friction work to heat is reduced and the *k'* is nominally decreased. The relationship between friction work and the wear loss is considered later in this chapter.

6.1.2.3 Influence of Solid Lubricants

In Chapter 4, the influence of two solid lubricants, PTFE and graphite, was investigated with three different materials, "epoxy nanocomposite only with PTFE", "epoxy nanocomposite only with graphite" and "epoxy nanocomposite with both graphite and PTFE". On basis of micro-hardness measurements, it was proposed that the graphite was conducive of a lower frictional coefficient with a thinner transfer film. This assumption is also validated by the thermal diffusion characteristics. Fig. 6.5 compares the factor *k'* of three composites at different sliding velocities with a constant pressure of 4MPa. As shown in the figure, the composite with PTFE always displays the lowest *k',* with the thickest transfer film. In contrast, the *k'* of composite only with

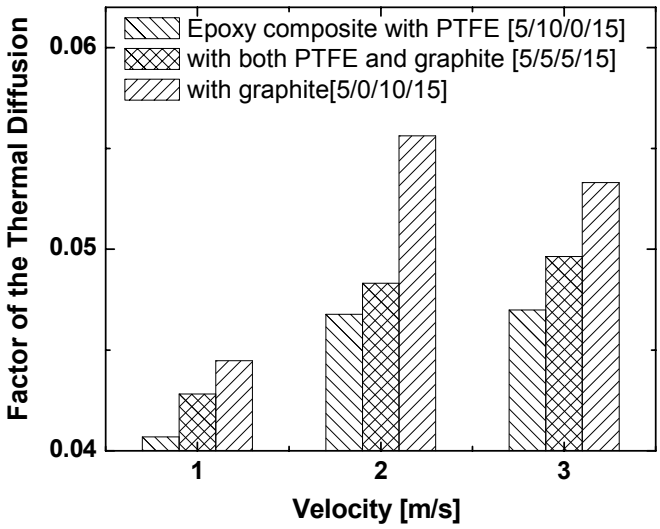

Figure 6.5: The influence of solid lubricants on the factor of thermal diffusion of epoxy based nanocomposites at different sliding velocities with a constant pressure of 4MPa.

graphite is always the highest, with the thinnest transfer film. As a whole, the *k'* of materials increases with the increase of sliding velocity.

6.2 Expressing Wear Rate, Based on Dissipated Energy

6.2.1 Analysis of Wear Mechanism Based on Energy Considerations

The friction process is very complex, involving asperity interaction and deformation, debris interaction and ploughing and adhesion. During the steady stage, however, the global roughness and the physical properties of contacting bodies remain statistically invariable. It follows that each frictional component maintains a fixed proportional contribution to the total [140]. When the sliding condition changes, this fixed proportion can be still expected if the contact state and the mechanical properties of contact bodies are unchanged. Based on such hypothesises, attempts have been made to correlate the volumetric wear loss with the total dissipated friction work, and the correlation has been found to be linear for various materials under different sliding conditions [97, 156-158]. The slope is determined by the mechanical properties of the material contributing or resisting the wear damage. It has been indicated that that energy dissipation concept can provide a good estimation for determining the wear rate of materials, which needs to take into consideration materials properties, sliding conditions etc. For short-fibre reinforced polymer composites, it is the short fibres that mostly undergo the bearing load during the sliding process. In this case, the physical properties of the contact bodies (short fibres and steel counterpart) remained relatively invariable unless the threshold of contact temperature (e.g. the T_g) was reached, which may then result in significant changes in the properties of the polymer matrix and lead to severe fibre removal. Therefore, it is possible to establish the relationship between dissipated energy and the wear loss of materials. Since all the specimens involved in this work had the same section area, the time-related depth wear rate was used to represent the volumetric wear rate in the steady stage.

Fig. 6.6 shows the time-related depth wear rate of various materials as a function of friction power intensity. The materials mentioned above were simply categorized as

two types: composites with or without nanoparticles. In addition, the wear results of neat PA66 and of PA66 filled with small nanoparticles (<50nm) only under different sliding conditions, are also given for comparison. All the wear results of the materials are summarized in Table 6.2. As shown in the figure, the slope of the curves increases at higher friction work. This is due to deterioration of the mechanical properties of the materials at the evaluated contact temperature. However, it is clear that the different material systems show distinct relationships between wear behaviour and dissipated energy.

For the composites without nanoparticles, those reinforced by SCF and solid lubricant(s) show very similar wear behaviours in response to friction work. This can be explained by the fact that wear processes of the materials are mainly governed by the wear/removal processes of short carbon fibre, and thus there is similar energy consumption in the sliding process. However, there are some energy/temperature thresholds above which the wear loss is significantly increased, as shown by the discontinuous changes of the curves. For example, very high wear loss occurred in the PA 6,6 based composite at 8MPa, and also for the PEI based composite at 4MPa, 3m/s (cf. Table 6.1).

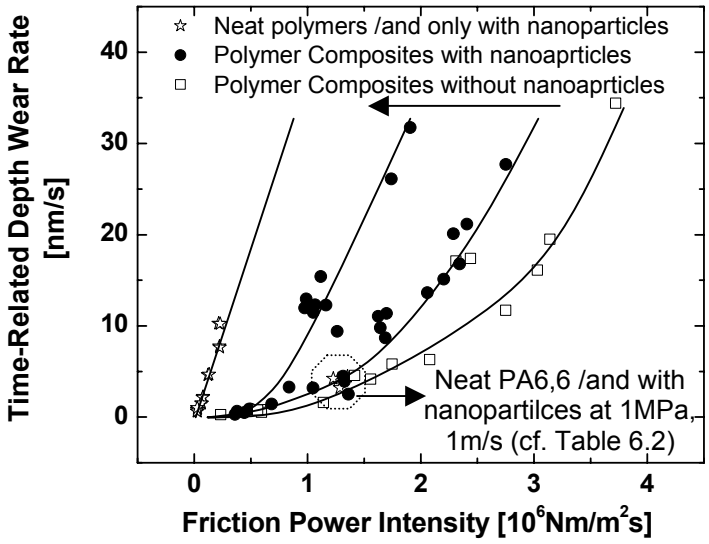

Figure 6.6: Time-related depth wear rate of various polymer composites as a function of friction power intensity.

With additional nanoparticles, the slopes of the curves increase due the change of contact mechanisms, i.e. three-body abrasion induced by hard particles. The schematic models of adhesive and abrasive wear are shown in Fig. 6.7. Strong adhesion occurs for combinations of like materials, e.g. polymer vs. polymer (transfer film), particularly when plastic deformation between contacting asperities takes place [14]. Adhesion can be reduced with the presence of additional hard particles, which result in two-body and/or three-body abrasive wear. In this case, the hard asperities/particles indent in the softer surface, engendering very high surface stress in the local contact area (Fig. 6.7b). As a result, wear debris is generated by cracks propagated in the sub-surface, combined with a micro-cutting or micro-ploughing process. Due to the different stress distribution in the real contact area, the portion of the

Table 6.2: Wear results of neat PA66 and PA66 filled with nanoparticles only, tested by a pin-on-disk apparatus under different sliding conditions.

Composition		*pv* factors	Frictional Coefficient μ	Contact Temperature T_b [°C]	Maximum Attainable Flash Temperature $T_{max}=1.64\times T_b$ [°C]	Time-Related Depth Wear Rate W_t [nm/s]	Factor of Thermal Diffusion $k'=\mu pv/(T_b-T_0)$ [$Wmm^{-2}s^{-1}K^{-1}$]
PA 6,6 Based Composites	Neat Polymer	1MPa-1m/s	1.29	50.43	82.71	3.20	0.0255
		2MPa-0.2m/s	0.54	25.87	42.43	10.26	0.0083
		1MPa-0.2m/s	0.61	23.60	38.71	4.62	0.0052
		0.5MPa-0.2m/s	0.66	22.27	36.52	0.15	0.0030
		1MPa-0.05m/s	0.58	21.01	34.45		0.0014
	+1vol.%TiO_2 [21nm]	1MPa-1m/s	1.27	53.93	88.45	4.20	0.0236
		1MPa-0.2m/s	0.66	24.03	39.40	4.69	0.0055
		0.5MPa-0.2m/s	0.78	22.42	36.77	0.22	0.0035
		1MPa-0.05m/s	0.65	21.38	35.06		0.0015
	+1vol.%SiO_2 [12nm]	1MPa-1m/s	1.23	49.61	81.36	4.21	0.0247
		2MPa-0.2m/s	0.56	26.11	42.82		0.0086
		0.5MPa-0.2m/s	0.76	22.19	36.39	0.21	0.0034
		1MPa-0.05m/s	0.55	21.16	34.70		0.0013
	+1vol.%Al_2O_3 [13nm]	0.5MPa-0.2m/s	0.65	22.18	36.37	0.15	0.0029
		2MPa-0.2m/s	0.56	25.88	42.44		0.0087
		1MPa-0.05m/s	0.51	21.08	34.57		0.0012
	+0.5vol.%TiO_2 [21nm, with surface treatment]	1MPa-1m/s	1.35	53.81	88.24	4.43	0.0252
		2MPa-0.2m/s	0.57	25.69	42.13		0.0089
		1MPa-0.05m/s	0.57	21.13	34.66		0.0014

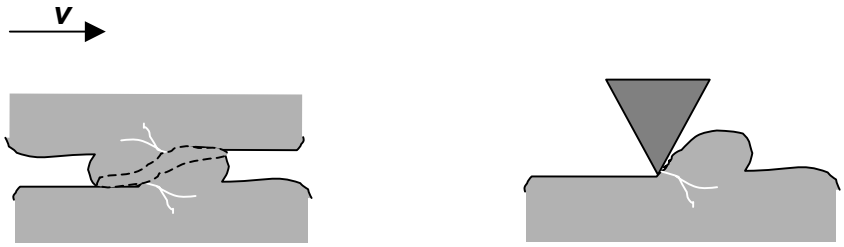

Figure 6.7: Schematic contact models of (a) adhesion and (b) abrasion.

energy directly towards the wear process of abrasion is generally higher than that of adhesion even with the same nominal contact pressure. Thus, the ratio of fracture energy and accordingly wear loss to the total friction work/power is increased. Besides, in this case, deterioration of the mechanical properties of the nanocomposite owing to weak interfacial bonding between particles and matrices can also result in an increase of the ratio. This model can also explain the observation that wear loss in the nanocomposites is sometime a little higher than in the composites without nanoparticles, although the friction coefficient, i.e. friction work of the nanocomposite is always lower in the same sliding conditions. For example, the PEI based nanocomposite demonstrated a higher wear rate than that without nanoparticles at 4MPa, and 8MPa 1m/s, as reported in Chapter 5. However, it is evident that the wear performance of nanocomposites is more complex and cannot be modelled by a single curve, which is further discussed in the next section.

The highest slope was obtained by the neat PA66 and the PA66 composite only with small nanoparticles particularly with relatively low *pv* factors, due to the relatively weak mechanical properties of the materials without fibre reinforcement. Moreover, on the basis of SEM observations, it was proposed that the wear processes of the materials were mostly governed by abrasive wear mechanisms without continuous transfer films under relatively lower *pv* conditions. In this case, the mechanical properties of the materials were almost invariable and the linearity between dissipated energy and wear loss was quite good. However, under the higher *pv* conditions e.g. 1MPa, 1m/s, the contact temperature was greatly increased and even above the T_g of PA66 (cf. Table 6.2). A thin transfer film was developed on the counterface and engendered the adhesive wear. As a result, friction force was greatly increased with

the increase in the real contact area, while the ratio of dissipated energy to wear loss was remarkably decreased, which is consistent with the model proposed above.

6.2.2 Possible Wear Mechanisms of Nanocomposites

Fig. 6.8 compares the time-related depth wear rate of various nanocomposites as a function of friction power intensity. As a whole, the epoxy based nanocomposites with PTFE ([5/5/5/15] and [5/10/0/15]) and the PA66 based nanocomposite demonstrated lower wear loss with the same friction work. In comparison with other materials, it is easier for these compositions to develop a continuous and thicker transfer film, which restricts the abrasive wear caused by hard counterpart or particles. Therefore, the ratio between the fracture work and total friction dissipated work is decreased and thus the slope is lower. This assumption is also supported by the micro-observation presented earlier. It was noticed that the nano-grooves on the fibre surface caused by particle abrasion were remarkably reduced for the nanocomposite with PA66 matrix ([5/0/5/15]) in comparison with that with epoxy matrix ([5/0/5/15]) at the similar sliding conditions. In addition, Fig. 6.9 compares the wear rate of three epoxy-based nanocomposites with different contents of the solid lubricants at different velocities. It

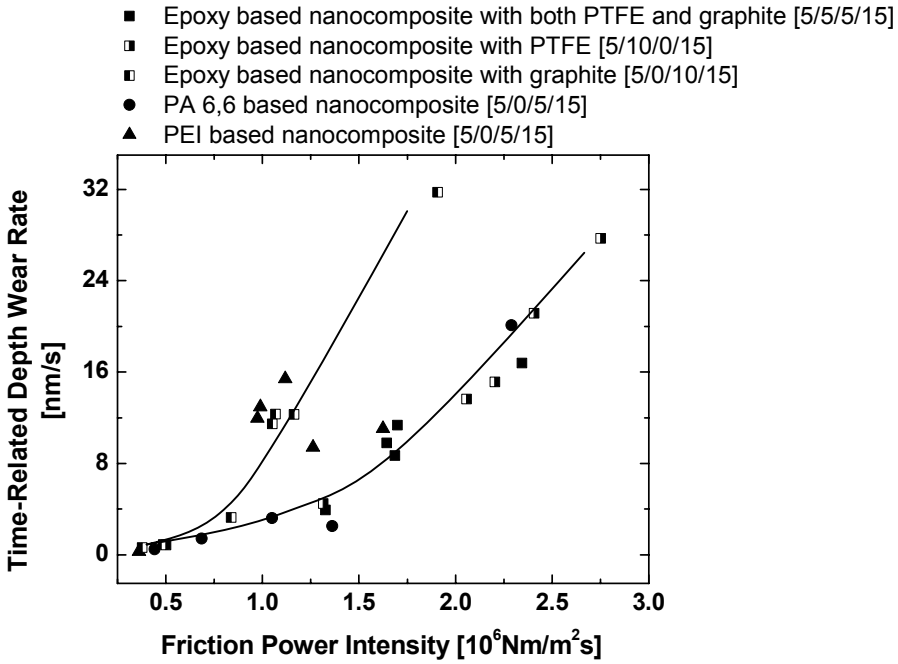

Figure 6.8: Time-related depth wear rate of various polymer based composites with nanoparticles as a function of friction power intensity

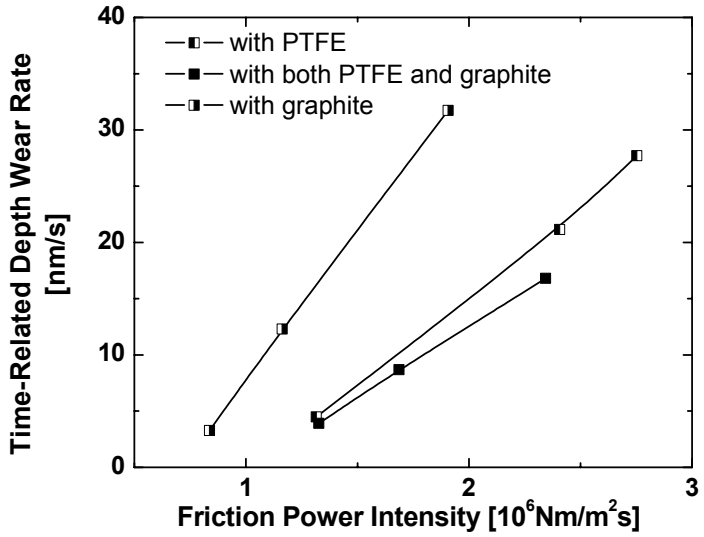

Figure 6.9: The influence of solid lubricants on the time-related depth wear rate of epoxy based nanocomposites corresponding to friction power intensity

is evindent that the composites with both lubricants achieved optimal wear behaviours as demonstrated by the lowest slope, which is consistent with the hypothesis proposed in Chapter 4.

Therefore, friction heat flux and the characterization of frictional work, i.e. the distribution of dissipated energy, are greatly influenced by the contact state depending on the sliding conditions. Although an accurate quantitative solution is difficult to achieve due to the difficulty in determining the material properties in the real contact area, qualitative analysis is possible using energy-based models. The validity of the models is well supported by experimental data with various materials under different sliding conditions. Analysis using the energy procedure may also provide useful information for understanding of the contact mechanisms controlling the friction and wear performance of the tribo-system. Moreover, simple models can provide an easy way for validation or evaluation of the wear mechanisms that have been proposed, usually on the basis of micro-observation of worn surfaces.

6.3 Applying ANN in Wear Prediction

6.3.1 General Remarks

In order to develop a quantitative solution for the wear problems, an ANN approach is applied to experimental data. The process of creating ANNs for materials research was summarized by Zhang et al [109] in terms of following stages:

1) Database collection: analysis and pre-processing of the data.
2) Training of the neural network: this includes the training algorithms and parameters of the network.
3) Testing of the trained network to evaluate its performance.
4) Use of trained ANNs for simulation and/or prediction.

It has been indicated that the predictive quality of ANNs can generally be improved by enlarging the training datasets and by optimizing the network construction, which includes choice of learning rules, ANN structure, etc. [115]. In this work, Bayesian regularization [109] (BR) was selected as a training algorithm, which is appropriate for determining the optimal regularization parameters in an automated fashion. The ANN configuration used was of one hidden layer, and the neurons in the layer were optimized based on the datasets involved. The coefficient of determination B (equation 1.7) was used to evaluate the ANN quality. To avoid any artificial influence in selecting the test data, a random technique was applied in the selection, and the entire process was repeated independently 50 times. The trained ANNs were applied to the two different wear datasets. Firstly, on the basis of the energy procedure, an attempt was made to use the ANN to predict the wear performance of three polymer composites with different matrices i.e. epoxy, PA66 and PEI under different sliding conditions. Secondly, a series of epoxy-based composites were considered. The sliding wear measurements and characteristic properties of the materials were used to train and test the neural network. The importance of the material properties to wear resistance was ranked.

6.3.2 ANN Prediction Using an Energetic Procedure

It has been indicated that the size of the ANN training dataset is a sensitive question in practical application. To reduce the amount of data required, much effort has been expended on the investigating the influence of various ANN architectures and input parameters [109,115]. In general, for wear problems, a large number of inputs are normally used, including the wear conditions, the volume contents of fillers and the related mechanical properties of the composites, etc. These parameters are selected on the basis of the rule-of-mixtures for composite materials and the wear models characterized by selected mechanical properties. However, the formulations for these models are normally very complex. In particular, it is difficult to determine the actual mechanical properties in the real contact area during the sliding process. Therefore, a large dataset is inevitably required to provide sufficient information for the ANN to learn the complex relationships between input parameters and wear output(s). Using the energetic procedure, however, the input parameters can be significantly reduced according to relatively simple models. As a result, a better result can be expected with relatively small dataset [143].

Fig. 6.10 shows the prediction results for the wear parameters (i.e. frictional coefficient and time-related depth wear rate) using the energy approach compared to that using volume contents and sliding conditions, based on the dataset given in Tables 2.1 and 2.2. In all cases, the number of neurons in the hidden layer is 20. It is clear that the quality of prediction is greatly improved when based on energy considerations. It should be stated that the input parameters such as volume contents and sliding conditions are independent of experimental results. Therefore, they can be used to predict an optimum design of composite materials for specific applications without the need for too many experiments. For example, the wear maps of Epoxy nanocomposite [5/5/5/15] at various sliding conditions can be easily generated by a well-trained ANN using the dataset of Tables 2.1 and 2.2 as shown in Fig. 6.11. With the energy procedure, because the contact temperature can be easily measured during sliding process and the sliding conditions are controlled by the experimenter, the established network based on energy consideration is particularly useful in condition monitoring of on-line systems.

6.3.3 Correlation with Wear Mechanisms Based on Importance Analysis

Although ANNs are a purely phenomenological method and do not directly produce a mechanistic understanding of the process being modelled, importance analysis of the ANN inputs is possible [109, 115]. Ranking the importance of material properties to wear characteristics could provide some useful information about which properties have a stronger relationship to wear in each case.

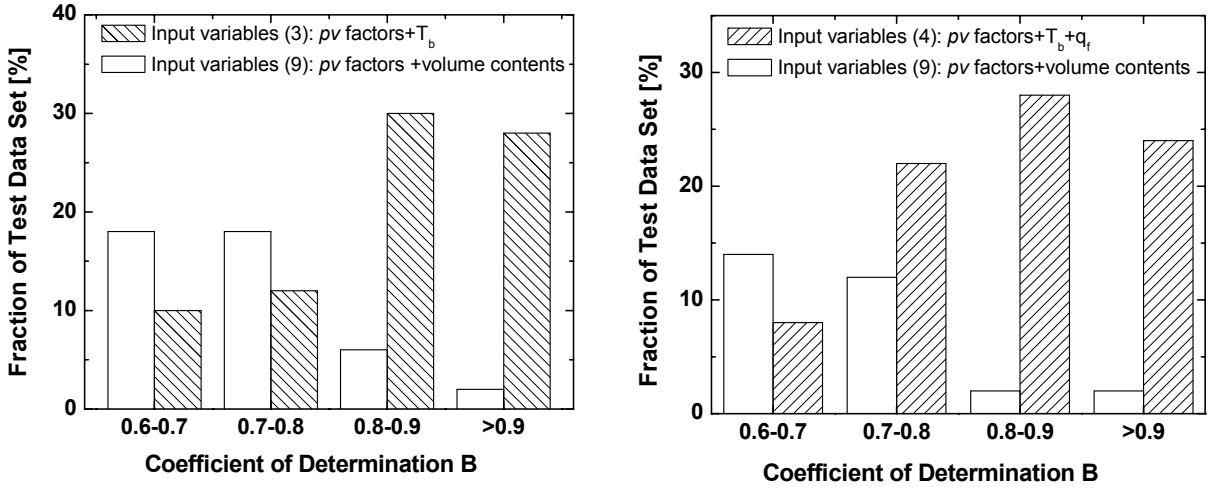

Figure 6.10: Comparison of the quality of ANNs in predicting the wear performance, i.e. (a) frictional coefficient and (b) time-related depth wear rate, using only contact temperature and sliding conditions as the input variables, with that using the volume contents of materials and sliding conditions.

Table 6.3: Wear results of a series of epoxy based composites tested by a block-on-ring apparatus at 1MPa, 1m/s.

Samples No.	***Composition***					***Material Properties***					***Wear Result***
	Matrix	PTFE	Graphite	SCF	TiO_2	Density	Modulus [MPa]	3-P-B (MPa)	Elongation (%)	Charpy (kJ/m^2)	Wt [nm/s]
1	100	0	0	0	0	1.14	2089.98	149.45	8.03	15.21	25.50
2	90	10	0	0	0	1.14	1785.38	65.38	3.83	10.55	7.07
3	90	0	10	0	0	1.23	3634.20	93.40	2.72	13.58	0.69
4	90	0	0	10	0	1.18	3462.43	105.27	3.41	19.58	4.58
5	80	10	10	0	0	1.24	2643.07	63.80	2.65	8.55	0.84
6	80	10	0	10	0	1.19	2290.28	68.88	3.77	12.59	0.75
7	80	0	10	10	0	1.28	4000.60	73.13	1.87	9.78	1.21
8	70	10	10	10	0	1.36	3749.13	70.03	1.77	6.59	0.58

Table 6.3 (continued)

9	85	5	5	5	0	1.20	2794.80	76.68	2.92	11.49	1.25
10	75	5	5	15	0	1.28	3958.13	75.28	1.94	11.11	1.13
11	75	5	15	5	0	1.33	4325.73	83.25	2.01	6.17	1.81
12	75	15	5	5	0	1.36	3680.37	66.25	1.87	6.17	0.63
13	70	5	9	16	0	1.27	1893.90	59.65	3.35	6.12	0.94
14	70	10	5	15	0	1.36	4208.50	76.18	1.87	5.85	0.64
15	72	10	12	5	0	1.35	3704.48	68.75	2.00	9.27	0.80
16	73	12	10	5	0	1.31	2361.30	53.30	2.19	9.35	0.88
17	70	5	15	10	0	1.37	4726.15	81.15	1.72	7.81	0.68
18	72	13	5	10	0	1.31	2596.88	55.83	2.11	10.39	0.80
19	95	0	5	0	0	1.18	3089.02	95.45	3.63	19.43	18.62
20	85	0	15	0	0	1.27	3953.03	81.22	2.37	11.23	1.30
21	95	0	0	5	0	1.16	2975.59	99.10	4.21	18.29	4.08
22	85	0	0	15	0	1.21	3614.24	82.28	2.86	13.18	1.41
23	80	0	0	20	0	1.23	4094.20	82.53	2.55	13.88	4.64
24	75	0	10	10	5	1.42	4725.43	96.35	2.16	8.33	0.52
25	85	0	5	5	5	1.35	3091.40	83.40	2.84	13.27	0.51
26	75	0	5	15	5	1.39	4055.18	80.68	2.10	9.61	0.44
27	65	0	15	15	5	1.48	4535.63	74.33	1.66	7.70	0.32
28	80	0	10	5	5	1.40	3972.05	90.00	2.47	10.32	0.61
29	70	0	10	15	5	1.42	4828.30	84.30	1.74	7.66	0.41
30	100	0	0	0	0	1.13	2338.80	149.53	9.77	26.87	9.06
31	68	0	15	15	2	1.40	4910.03	57.57	1.28	2.45	0.50
32	62	0	15	15	8	1.55	6155.68	80.10	1.42	7.08	0.77
33	62	0	13	15	10	1.61	6583.40	46.58	0.74	2.93	0.52
34	88	0	5	5	2	1.26	3148.30	77.95	3.06	11.96	1.46
35	82	0	5	5	8	1.44	3921.87	81.27	2.35	11.47	1.79
36	100	0	0	0	0	1.14	2780.55	76.25	3.69	67.06	112.14
37	67	0	7	21	5	1.45	5764.35	83.50	1.45	6.19	0.53
38	61	0	9	25	5	1.46	7829.10	65.52	0.91	4.83	1.93
39	65	15	0	15	5	1.47	7263.03	73.80	1.06	5.75	1.08
40	70	10	0	15	5	1.31	3488.60	71.16	2.37	8.69	1.31
41	66	0	15	15	4	1.54	6872.06	83.44	1.33	6.46	0.17
42	64	0	15	15	6	1.58	7013.87	71.13	1.09	4.85	0.12
43	75	15	0	5	5	1.28	2194.67	56.52	3.22	10.49	1.01
44	85	5	0	5	5	1.27	2669.02	77.85	3.43	9.45	0.63
45	86	0	5	5	4	1.41	4011.05	87.47	2.36	11.33	1.16
46	84	0	5	5	6	1.47	4321.64	91.91	2.40	12.32	0.64
47	77	0	5	15	3	1.34	5028.56	83.15	1.88	10.28	6.63
48	77	0	5	15	3	1.33	4822.83	83.33	1.83	11.12	6.99
49	75	0	10	10	5	1.42	5159.43	77.53	2.48	9.12	1.09
50	85	0	5	5	5	1.36	4132.23	74.10	2.61	12.49	13.40
51	70	10	10	10	0	1.33	3654.07	55.20	2.18	5.42	0.80
52	100	0	0	0	0	1.17	2188.85	82.48	6.67	61.27	113.89
53	85	5	5	5	0	1.24	3057.08	59.83	3.09	9.97	1.07
54	75	0	10	10	5	1.44	4897.55	95.23	2.34	7.73	5.08
55	85	0	5	5	5	1.38	3438.40	84.05	3.22	13.91	47.30
56	70	10	10	10	0	1.38	3328.98	60.90	2.07	7.84	0.92

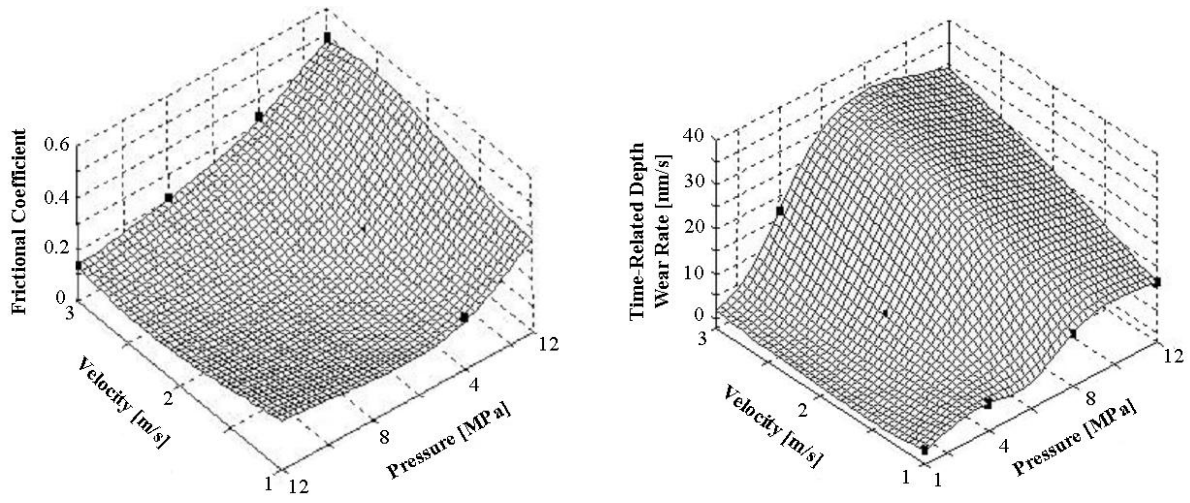

(a) (b)

Figure 6.11: Wear map for epoxy based nanocomposite [5/5/5/15] sliding against steel in a pin-on-disk apparatus: (a) frictional coefficient and (b) time-related depth wear rate. Squares are experimental data whereas the 3D-plane was calculated by a trained ANN.

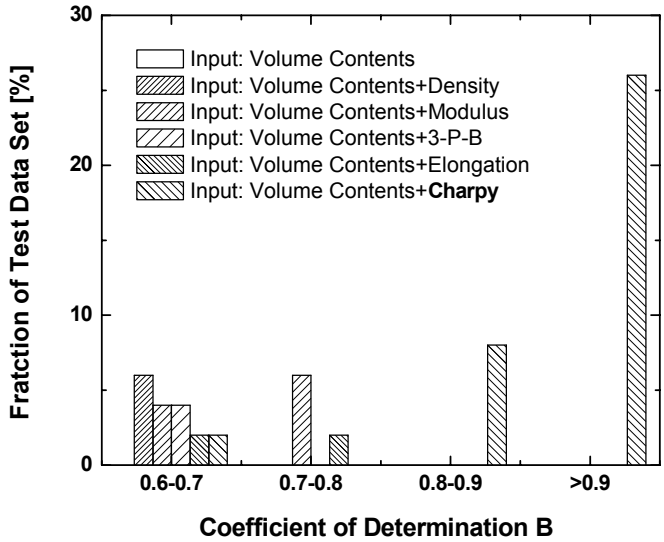

Figure 6.12: Ranking the importance of the input variables to wear loss of epoxy-based composites by ANN

A total dataset of 56 wear measurements is summarized in Table 6.3. All the wear rates of materials were obtained from a block-on-ring machine. To investigate the correlation between sliding wear rate and characteristic properties of these materials, each of properties was used with the volume contents of the composites only. The prediction results are shown in Fig. 6.12. The configuration of ANN applied is

9-[25]-1. It is clear that fracture behaviours (i.e. charpy results) display the strongest dependence on sliding wear of epoxy composites. This is consistent with the proposition that crack generation and propagation are the dominating damage mechanisms of brittle epoxy material in the sliding process (refer to Chapter 4). Therefore, it can be claimed that: “Importance analysis by ANN attempts to investigate the possible correlation between some simple measured parameters (e.g. charpy) to more complex properties (e.g. wear), which will be of additional help to materials research for mechanistic understanding.” [109].

7. Summary and Outlook

In the present work, inorganic nanoparticles TiO_2 (300nm) were employed to further improve the wear resistance of various polymer composites reinforced by traditional fillers such as short carbon fibres and solid lubricants. It was found that a combination of nanoparticles and short carbon fibres could achieve a significant improvement in the tribological performance of both thermosetting and thermoplastic composites. In addition, this concept allowed the use of these materials under more extreme wear conditions, i.e. higher normal pressures and higher sliding velocities. Results and conclusions obtained during the study are summarized in the following paragraphs. Suggestions for future investigation are also presented.

The tribological performance of epoxy-based composites filled with short carbon fibres, graphite, PTFE and nano-TiO_2 in different proportions and combinations was systematically studied under different sliding conditions. The following conclusions were drawn:

- The frictional coefficient of fibre-reinforced epoxy composites was significantly reduced by the addition of nano-TiO_2, and the contact temperature was consequently decreased under all test conditions. As a result, the wear resistance of the epoxy composites was clearly improved through the incorporation of nanoparticles, especially under high contact pressure and high sliding speed. Reduction of the basic wear factor k^* and enhancement of the load-carrying capacity were achieved, which can promote the use of such materials for applications entailing more severe wear conditions.
- On the basis of SEM and AFM observations, a positive rolling effect of the nanoparticles between the material pairs was proposed. This rolling effect helps to reduce the frictional coefficient during sliding, and accordingly reduces shear stress and contact temperature. This rolling effect also protects the short carbon fibres from more severe wear mechanisms, especially in high sliding pressure and speed situations.

- Both solid lubricants exhibited positive contributions to the development of transfer films, and thereby greatly reduced the wear rate of composites. Due to different molecular structures of two lubricants, the characteristics of the transfer films were also different. The composite with PTFE generally produced a relatively thicker transfer film, resulting in a shorter running-in stage. However, graphite was conducive to lower stable frictional coefficient and wear rate, especially under high pressures.

With optimized filler content from the earlier research, the wear behaviour of nano-TiO_2 filled thermoplastic composites PA66, PEI and PEEK, incorporated additionally with short carbon fibres and graphite flakes, were studied under different sliding conditions, respectively. In particular, the following conclusions were drawn:

- The specific wear rates of neat plastic polymers were noticeably reduced when the polymers were filled with conventional fillers SCF and graphite. In comparison with short fibre reinforced epoxy composites, the wear damage in the interfacial region of fibre/thermoplastic matrix was slight due to the ductile nature of the thermoplastic matrix material. As a result, a relatively high load carrying capacity could be commonly obtained by thermoplastic composites. However, the severe fibre removal and rapid increase of wear rate may occur when the contact temperature is increased up to the T_g of the matrix.
- With the addition of nano-TiO_2, the frictional coefficient and contact temperature of the composites were further decreased, especially with very high *pv* products. As a result, the “limiting *pv*” of the nanocomposites was clearly improved.
- With further investigation, it was found that the fibre removal was changed with the change of frictional coefficient. An increase of frictional coefficient exacerbated fibre removal and thus resulted in a higher specific wear rate. Moreover, te reduction of friction caused by the rolling effect of nanoparticles was prevailing in both the running-in stage and the steady stage.
- The tribological performance of the short-fibre reinforced, high temperature resistant polymers e.g. PEI was significantly enhanced under extreme sliding conditions by the addition of nanoparticles. Accordingly, the wear resistance of the materials was clearly improved.

In order to establish the relationships between frictional energy and contact temperature, as well the time-related depth wear rate, an energy-based procedure was proposed. The model is not intended to yield precise numerical results for the friction coefficient or wear rate, rather to determine the dependence of friction behaviour on contact state, which is greatly influenced by sliding conditions and various fillers. The validity of the model is well justified by the experimental results. On the other hand, the simple energy-based models also provided an easy way to evaluate the hypothesis of wear mechanisms. Further more, an ANN approach was applied to the experimental data to develop a quantitative solution for the wear problem. On the basis of the energy procedure, sliding conditions and contact temperature were used as the input variables. Owing to the relatively simple relationship, satisfactory results were obtained from the small dataset with a quite fast computing speed, which is vitally important for practical applications of ANN predictions, particularly in monitoring the condition of on-line systems.

Outlook

To understand the mechanisms in the sliding wear of inorganic particle-filled polymers, a nano-rolling model, caused by nanoparticles acting as third bodies, was proposed to account for the reduction of frictional coefficient. However, three-body abrasion is very complex and depends on many variables, including particle characteristics such as size, hardness and shape, and properties of the counterparts such as surface topography and lubricating conditions, and sliding conditions. The presence of so many factors, and the interactions among them, makes full characterization of the roles of these factors in friction and wear very difficult. Nevertheless, there is still a lack of fundamental understanding of the nano-rolling mechanism. This means that systematic investigation of all of the relevant characteristics and properties of nanoparticles is still a matter of further research. In particular, the following two questions should to be first concerned:

- What is the size effect of nanoparticles in their interaction with the surface profile (or roughness) of the counterparts?

- What is the influence of the mechanical characteristics (e.g. hardness) of particles on rolling mechanisms in relation to the properties of the counterparts?

The knowledge obtained will significantly advance current lubrication principles in tribology and may offer a promising novel route to the design of tribo-materials.

8. Literature

[1] Hirano, F.: Technological progress of tribology and its philosophical background, Tribology International 28 (1995) 11-13.

[2] Tichy, J.A., Meyer, D.M.: Review of solid mechanics in tribology, International Journal of Solids and Structures 37 (2000) 391-400.

[3] Czichos, H.: Introduction on friction and wear, in: K. Friedrich (Ed.), Friction and Wear of Polymer Composites, Elsevier Science Publishers, B.V. (1986) pp.1-23.

[4] Friedrich, K.: Wear of reinforced polymers by different abrasive counterparts, in: K. Friedrich (Ed.), Friction and Wear of Polymer Composites, Elsevier Science Publishers, B.V. (1986) pp.233-287.

[5] Kukureka, S.N., Hooke, C.J., Rao, M., Liao, P., Chen, Y.K.: The effect of fibre reinforcement on the friction and wear of polyamide 6,6 under dry rolling-sliding contact, Tribology International 32 (1999) 107-116.

[6] Bijwe, J., Rajesh, J.J., Jeyakumar, A., Ghosh, A., Tewari, U.S.: Influence of solid lubricants and fibre reinforcement on wear behaviour of polyethersulphone, Tribology International 33 (2000) 697-706.

[7] Bahadur, S.: The development of transfer layers and their role in polymer tribology, Wear 245 (2000) 92-99.

[8] Donnet, C., Erdemir, A.: Historical developments and new trends in tribological and solid lubricant coatings, Surface and Coatings Technology, 180-181 (2001) 76-84.

[9] Teer, D. G.: New solid lubricant coatings, Wear 251 (2001) 1068-1074.

[10] Friedrich, K., Zhang, Z., Klein, P.: Wear of polymer composites, in Stachowiak G.W. (Ed.) Wear - Materials, Mechanisms and Practice, as part of "Handbook of Measuring System Design" edited by Sydenham P. and Thorn R., John Wiley & Sons (2005) pp. 269-290.

[11] Zhang, Z., Friedrich, K.: Tribological characteristics of micro- and nanoparticle filled polymer composites, in K. Friedrich, S. Fakirov, Z. Zhang (Ed.), Polymer Composite - from Nano- to Macro-Scale, Springer (2005) pp. 169-185.

[12] Karger-Kocsis, J., Zhang, Z.: Structure-property relationships in nanoparticles/ semicrystalline thermoplastic composites, in Balta Calleja JF, Michler G. (Ed.) Mechanical properties of polymers based on nanostructure and morphology, CRC Press, New York (2005) pp.547-596.

[13] Blau, P.J., Budinski, K.G.: Development and use of ASTM standards for wear testing, Wear 225-229 (1999) 1159-1170.

[14] Stachowiak, G.W., Batchelor, A.W.: Engineering Tribology, 2nd ed, Butterworth-Heinemann, Woburn (2001) pp.619-667.

[15] Kato, K.: Wear in relation to friction - a review, Wear 241 (2000) 151-157.

[16] Tewari, U.S., Bijwe, J.: Recent development in tribology of fibre reinforced composites with thermoplastic and thermosetting matrices, in K. Friedrich (Ed.), Advances in Composites Tribology, Elsevier Science Publishers, B.V. (1993) pp.159-207.

[17] Häger, A.M., Davies, M.: Short-fibre reinforced, high-temperature resistant polymers for a wide field of tribological applicants, in K. Friedrich (Ed.), Advances in Composites Tribology, Elsevier Science Publishers, B.V. (1993) pp.104-157.

[18] Voss, H., Friedrich, K.: On the wear behaviour of short-fibre-reinforced PEEK composites, Wear 116 (1987) 1-18.

[19] Friedrich, K., Lu, Z., Hager, A.M.: Recent advances in polymer composites' tribology, Wear 190 (1995) 139-144.

[20] Bonfield, W., Edwards, B.C., Markham, A.J., White, J.R.: Wear transfer films formed by carbon fibre reinforced epoxy resin sliding on stainless steel, Wear 37 (1976) 113-121.

[21] Jain, V.K.: Investigation of the wear mechanism of carbon-fibre-reinforced acetal, Wear 92 (1983) 279-292.

[22] Zhang, H., Zhang, Z.: Comparison of short carbon fibre surface treatments on epoxy composites. II. Enhancement of the wear resistance. Composites Science and Technology 64 (2004) 2031-2038.

[23] Tsukizoe. T., Ohmae, N.: Friction and wear performance of unidirectionally oriented glass, carbon, aramid and stainless steel fibre-reinforced plastics, in: K. Friedrich (Ed.), Friction and Wear of Polymer Composites, Elsevier Science Publishers B.V. (1986) pp.205-231.

[24] Friedrich, K.: Wear models for multiphase materials and synergistic effects in polymeric hybrid composites, in K. Friedrich (Ed.), Advances in Composite Tribology, Elsevier Science Publishers, B.V. (1993) pp.209-273.

[25] Vaziri, M., Spurr, R.T., Stott, F.H.: An investigation of the wear of polymeric materials, Wear 122 (1988) 329-342.

[26] Cenna, A.A., Dastoor, P., Beehag, A., Page, N.W.: Effects of graphite particle addition upon the abrasive wear of polymer surfaces, Journal of Materials Science 36 (2001) 891-900.

[27] Tanaka, K.: Effects of various fillers on the friction and wear of PTFE-based composites, in K. Friedrich (Ed.), Friction and Wear of Polymer Composites, Elsevier Science Publishers, B.V. (1986) pp.137-174,

[28] Bahadur, S., Tabor, D.: The wear of filled polytetrafluoroethylene, Wear 98 (1984) 1-13.

[29] Khedkar, J., Negulescu, I., Meletis, E.I.: Sliding wear behavior of PTFE composites, Wear 252 (2002) 361-369.

[30] Gao, J.: Tribochemical effects in formation of polymer transfer film, Wear 245 (2000) 100-106.

[31] Bahadur, S., Gong, D.: The role of copper compounds as fillers in the transfer film formation and wear of nylon, Wear 154 (1992) 207-223.

[32] Bahadur, S., Kapoor, A.: The effect of ZnF_2, ZnS and PbS fillers on the tribological behavior of nylon 11, Wear 155 (1992) 49-61.

[33] Voort, J.V., Bahadur, S.: The growth and bonding of transfer film and the role of CuS and PTFE in the tribological behavior of PEEK, Wear 181-183 (1995) 212-221.

[34] Yu, L., Bahadur, S.: An investigation of the transfer film characteristics and the tribological behaviors of polyphenylene sulfide composites in sliding against tool steel, Wear 214 (1998) 245-251.

[35] Zhao, Q., Bahadur, S.: A study of the modification of the friction and wear behavior of polyphenylene sulfide by particulate Ag_2S and PbTe fillers, Wear 217 (1998) 62-72.

[36] Zhao, Q., Bahadur, S.: The mechanism of filler action and the criterion of filler selection for reducing wear, Wear 225-229 (1999) 660-668.

[37] Schwartz, C.J., Bahadur, S.: The role of filler deformability, filler-polymer bonding, and counterface material on the tribological behavior of polyphenylene sulfide (PPS), Wear 251 (2001) 1532-1540.

[38] Yu, L., Yang, S., Wang, H., Xue, Q.: An investigation of the friction and wear behaviors of micrometer copper particle- and nanometer copper particle-filled polyoxymethylene composites, J. Appl. Polym. Sci. 77 (2000) 2404-2410.

[39] Schwartz, C.J., Bahadur, S.: Studies on the tribological behavior and transfer film-counterface bond strength for polyphenylene sulfide filled with nanoscale alumina particles. Wear 237 (2000) 261-273.

[40] Bahadur, S., Sunkara, C.: Effect of transfer film structure, composition and bonding on the tribological behaviour of polyphenylene sulfide filled with nano particles of TiO_2, ZnO, CuO and SiC, Wear 258 (2005) 1411-1421.

[41] Friedrich, K., Flöck, J., Váradi, K., Néder, Z.: Experimental and numerical evaluation of the mechanical properties of compacted wear debris layers formed between composite and steel surfaces in sliding contact, Wear 251 (2001) 1202-1212.

[42] Chang, L., Zhang, Z.: Tribological properties of epoxy nanocomposites: III. Influence of solid lubricants - PTFE powders and graphite flakes, Wear (2004) to be submitted.

[43] Bhushan, B.: Nano- to microscale wear and mechanical characterization using scanning probe microscopy, Wear 251 (2001) 1105-1123.

[44] Randall, N. X., Bozet, J.L.: Nanoindentation and scanning force microscopy as a novel method for the characterization of tribological transfer films, Wear 212 (1997) 18-24

[45] Randall, N. X., Harris, A.: Nanoindentation as a tool for characterising the mechanical properties of tribological transfer films, Wear 245 (2000) 196-203.

[46] Adams, M.J., Allan, A., Briscoe, B.J., Doyle, P.J., Gorman, D.M., Johnson, S.A.: An experimental study of the nano-scratch behaviour of poly(methyl methacrylate), Wear 251 (2001) 1597-1583.

[47] Bahadur, S., Gong, D., Anderegg, J.W.: Studies of worn surfaces and the transfer film formed in sliding by CuS-filled and carbon fiber-reinforced nylon against a steel surface, Wear 181-183 (1995) 227-235.

[48] Bahadur S., Polineni, V.K.: Tribological studies of glass fabric-reinforced polyamide composites filled with CuO and PTFE, Wear 200 (1996) 95-104.

[49] Wang, J., Gu, M., Bai, S., Ge, S.: Investigation of the influence of MoS_2 filler on the tribological properties of carbon fiber reinforced nylon 1010 composites, Wear 255 (2003) 774-779.

[50] Minami, M., Suzuki, M., Nishimura, M.: Evaluation of tribological characteristics of PTFE composite transfer film in ultra-high vacuum, Tribological Transaction 36 (1993) 95-103.

[51] Suzuki, M., Prat, P.: Synergism of an MoS_2 sputtered film and a transfer film of a PTFE composite, Wear 225-229 (1999) 995-1003.

[52] Rong, M., Zhang, M., Liu, H., Zeng, H., Wetzel, B., Friedrich, K.: Microstructure and tribological behavior of polymeric nanocomposites, Industrial Lubrication & Tribology 53 (2001) 72-77.

[53] Zhang, M., Rong, M., Shu, L., Wetzel, B., Friedrich, K.: Effect of particle surface treatment on the tribological performance of epoxy based nanocomposites, Wear 253 (2002) 1086-1093.

[54] Xue, Q., Wang, Q.: Wear mechanisms of polyetheretherketone composites filled with various kinds of SiC, Wear 213 (1997) 54-58.

[55] Wang, Q., Xue, Q., Liu, H., Shen, W., Xu, J.: The effect of particle size of nanometer ZrO_2 on the tribological behaviour of PEEK, Wear 198 (1996) 216-219.

[56] Xing, X.S., Li, R.K.Y.: Wear behavior of epoxy matrix composites filled with uniform sized sub-micron spherical silica particles, Wear 256 (2004) 21-26.

[57] Wang, Q., Xu, J., Shen, W., Liu, W.: An investigation of the friction and wear properties of nanometer Si_3N_4 filled PEEK, Wear 196 (1996) 82-86.

[58] Wang, Q., Xue, Q., Shen, W.: The friction and wear properties of nanometer SiO_2 filled polyetheretherketone, Tribology International 30 (1997) 193-197.

[59] Wang, Q., Xu, J., Shen, W., Xue, Q., The effect of nanometer SiC filler on the tirbological behavior of PEEK, Wear 209 (1997) 316-321.

[60] Wang, Q., Xue, Q., Shen, W. and Zhang, J.: The friction and wear properties of nanometer ZrO_2-filled polyetheretherketone, J. Appl. Polym. Sci. 69 (1998) 135-141.

[61] Wang, Q., Xue, Q., Liu, W., Chen, J.: The friction and wear characteristics of nanometer SiC and polytetrafluoroethylene filled polyetheretherketone, Wear 243 (2000) 140-146.

[62] Avella, M., Errica, M.E., Martuscelli, E.: Novel PMMA/$CaCO_3$ nanocomposites abrasion resistant prepared by an in situ polymerization process, Nano Lett. 1 (2001) 213-217.

[63] Zhang, M., Rong, M., Yu, S., Wetzel, B., Friedrich, K.: Improvement of tribological performance of epoxy by the addition of irradiation grafted nano-inorganic particles, Macromol. Mater. Eng. 287 (2002) 111-115.

[64] Shi, G., Zhang, M., Rong, M., Wetzel, B., Friedrich, K.: Friction and wear of low nanometer Si_3N_4 filled epoxy composites, Wear 254 (2003) 784-796.

[65] Shi, G., Zhang, M., Rong, M., Wetzel, B., Friedrich, K.: Sliding wear behavior of epoxy containing nano-Al_2O_3 particles with different pretreatments, Wear 256 (2003) 1072-1081.

[66] Wetzel, B., Haupert, F., Friedrich, K., Zhang, M., Rong, M.: Impact and wear resistance of polymer nanocomposites at low filler content, Polymer Engineering and Science 42 (2002) 1919-1927.

[67] Wetzel, B., Haupert, F., Zhang, M.: Epoxy nanocomposites with high mechanical and tribological performance, Composites Science and Technology 63 (2003) 2055-2067.

[68] Sreekala, M.S., Eger, C.: Property improvements of an epoxy resin by nanosilica particle reinforcement, in K. Friedrich, S. Fakirov, Z. Zhang (Ed.) Polymer Composites - from Nano- to Macro- Scale, Springer (2005) pp.91-105.

[69] Li, F., Hu, K., Li, J., Zhao, B.: The friction and wear characteristics of nanometer ZnO filled polytetrafluoroethylene, Wear 249 (2002) 877-882.

[70] Sawyer, W.G., Freudenberg, K.D., Bhimaraj, P., Schadler, L.S.: A study on the friction and wear behavior of PTFE filled with alumina nanoparticles, Wear 254 (2003) 573-580.

[71] Zhang, Z., Haupert, F., Friedrich, K.: Enhancement of the wear resistance of polymer composites by nano-fillers, German Patent 103 29 228.4-43 (2005).

[72] Zhang, Z., Breidt, C., Chang, L., Haupert, F., Friedrich, K.: Enhancement of the wear resistance of epoxy: short carbon fibre, graphite, PTFE and nano-TiO_2, Compos. Part A 35 (2004) 1385-1392.

[73] Chang, L., Zhang, Z., Breidt, C., Friedrich, K.: Tribological properties of epoxy nanocomposites: I. Enhancement of the wear resistance by nano-TiO_2 particles, Wear 258 (2005) 141-148.

[74] Chang, L. and Zhang, Z.: Tribological properties of epoxy nanocomposites: II. A combinative effect of short carbon fibre and nano-TiO_2, Wear (2005) in press.

[75] Rapoport, L., Bilik, Y., Feldman, Y., Homyonfer, M., Cohen, S.R. and Tenne, R.: Hollow nanoparticles of WS_2 as potential solid-state lubricants, Nature 387 (1997) 791-793.

[76] Rapoport, L., Leshchinsky, V., Lapsker, I., Volovik, Y., Nepomnyashcy, O., Lvovsky, M., Popovitz-Biro, R., Feldman, Y., Tenne, R.: Tribological properties of WS_2 nanoparticles under mixed lubrication, Wear 255 (2003) 785-793.

[77] Chang, L., Zhang,Z., Zhang, H., On the sliding wear of nanoparticles filled polyamide 66 composites, Composites Science and Technology (2005), in press.

[78] Xian, G., Zhang, Z.: Tribological behaviour of micro- and nano-particles filled polyetherimide composites, Journal of Applied Polymer Science (2005) in press.

[79] Chang, L. and Zhang, Z.: Wear of nanoparticles filled polyetherimide composites, Tribology International, (2005) in press.

[80] Burwell, J.T. and Strang, C.D.: On the empirical law of adhesive wear, Journal of Applied Physics, 23 (1952) 18-28.

[81] Godet, M., Berthier, Y. and Lancaster, J., Vincent, L.: Wear modelling: using fundamental understanding or practical experience? Wear 149 (1991) 325-340.

[82] Meng, H.C., Ludema, K.C.; Wear models and predictive equations: their form and content, Wear 181-183 (1995) 443-457.

[83] Williams, J.A.: Wear modelling: analytical, computational and mapping: a continuum mechanics approach, Wear 225-229 (1999) 1-17.

[84] Burwell, J.T.: Survey of possible wear mechanisms, Wear 1 (1957)119-141.

[85] Gates, J.D.: Two-body and three-body abrasion: a critical discussion, Wear 214 (1998) 139-146.

[86] Iams, J.A., Hyncica, A.M.: Mechanisms of abrasive wear in lubricated contacts, Wear (1992) 152 57-74.

[87] Dwyer-Joyce, R.S., Sayles, R.S., Ioannides, E.: An investigation into the mechanisms of closed three-body abrasive wear, 175 Wear (1994) 133-142.

[88] Adachi, K., Hutchings, I.M.: Wear-mode mapping for the micro-scale abrasion test, Wear 255 (2003) 23-29.

[89] Xuan, J.L., Hong, I.T., Fitch, E.C.: Hardness effect on three-body abrasive wear under fluid film lubrication, Journal of Tribology 111 (1989) 35-40.

[90] Stachowiak, G.B., Stachowiak, G.W.: The effects of particle characteristics on three-body abrasive wear, Wear 249 (2001) 201-207.

[91] Trezona, R.I., Allsopp, D.N., Hutchings,I.M.: Transitions between two-body and three-body abrasive wear: influence of test conditions in the microscale abrasive wear test, 225-229 Wear (1999) 205-214.

[92] Stack, M.M., Mathew, M.: Micro-abrasion transition of metallic materials, Wear 255 (2003) 14-22.

[93] Kahlman, L.c Hutchings, I.M.: Effect of particulate contamination in grease-lubricated hybrid rolling bearings, Tribology Transaction 42 (1999) 842-850.

[94] Rapoport, L., Feldman, Y., Homyonfer, M., Cohen, H., Sloan, J., Hutchinson, J.L., Tenne, R.: Inorganic fullerene-like material as additives to lubricants: structure-function relationship, Wear 225-229 (1999) 975-982.

[95] Shakhvorostov, D., Poehlmann, K., Scherge, M.: An energetic approach to friction, wear and temperature, Wear 257 (2004) 124-130

[96] Sherif, H.A., Abu Omar, T.M.: Mechanism of energy dissipation in mechanical system with dry friction, Tribology International 37 (2004) 235-244.

[97] Huq, M.Z., Celis, J.-P.: Expressing wear rate in sliding contacts based on dissipated energy, Wear 252 (2002) 375-383.

[98] Rodkiewicz, C.M. and Wang, Y.: A dry wear model based on energy considerations, Tribology International, 27 (1994) 145-151

[99] Rymuza, Z.: Energy concept of the coefficient of friction, Wear 199 (1996) 187-196

[100] Holm, R.: Calculation of the temperature development in a contact heated in the contact surface, and application to the problem of the temperature rise at a sliding contact, Journal of Applied Physics 19 (1948) 361-366

[101] Archard, J.F.: The temperature of rubbing surfaces, Wear 2 (1959) 438-455.

[102] Archard, J.F., Rowntree, R.A.: The temperature of rubbing bodies: Part 2, the distribution of temperatures, Wear 128 (1988) 1-17.

[103] Ashby, M.F., Abulawi, J. and Kong, H.S.: Temperature maps for frictional heating in dry sliding, Tribology Transactions, 34 (1991) 577-587

[104] Wang, Y., Rodkiewicz, C.M.: Temperature maps for pin-on-disk configuration in dry slding, Tribology International27 (1994) 259-266

[105] Fouvry, S., Duó, P., Perruchaut, Ph.: A quantitative approach of Ti-6Al-4V fretting damage: friction, wear and crack nucleation, Wear 27 (2004), 916-929.

[106] Swingler, K.: Applying Neural Networks: A Practical Guide, Academic Press, Burlington, USA, 1996.

[107] Lee, J.A., Almond, D.P., Harris, B.: The use of neural networks for the prediction of fatigue lives of composite materials, Composites Part A: Applied Science and Manufacturing 30 (1999) 1159-1169.

[108] Bhadeshia, H.K.D.H.: Neural networks in materials science, ISIJ International, Vol.39 (10), Special Issue on “Application of Neural Network Analysis in Materials Science", 1999, 966-979.

[109] Zhang, Z., Friedrich, K.: Artificial neural networks applied to polymer composites: a review, Composites Science and Technology 63 (2003) 2029-2044.

[110] Jones, S.P., Jansen, R., Fusaro, R.L.: Preliminary investigation of neural network techniques to predict tribological properties, Tribology Transactions 40 (1997) 312-320.

[111] Rutherford, K.L., Hatto, P.W., Davies, C., Hutchings, I.M.: Abrasive wear resistance of TiN/NbN multi-layers: measurement and neural network modeling, Surface and Coatings Technology 86-87 (1996) 472-479.

[112] Myshkin, N.K., Kwon, O.K., Grigoriev, A.Ya., Ahn, H.-S., Kong, H.: Classification of wear debris using a neural network, Wear 203-204 (1997), 658-662.

[113] Zhang, M.Q., Lu, Z.P., Friedrich, K.: On the wear debris of polyetheretherketone: fractural dimensions in relation to wear mechanisms, Tribology Int. Vol. 30 No. 2 (1997) 87-102.

[114] Velten, K., Reinicke, R., Friedrich, K.: Wear volume prediction with artificial neural networks, Tribology International 33 (2000) 731-736.

[115] Zhang, Z., Friedrich, K., Velten, K.: Prediction of tribological properties of short fibre composites using artificial neural networks, Wear 252 (2002) 668-675.

[116] Zhang, Z., Friedrich, K.: Artificial neural network in polymer composites, Proceedings of the Third Asian-Australasian Conference on Composite Materials (ACCM-3), July 15-17, 2002, Auckland, New Zealand, edited by D. Bhattacharyya et.al., published by the Department of Mechanical Engineering, University of Auckland, ISBN 0-86869-019-8, pp.105-118.

[117] Zhang, Z., Barkoula, N.-M., Karger-Kocsis, J., Friedrich, K.: Artificial neural network predictions on erosive wear of polymers, Wear 255 (2003) 708-713.

[118] Eliezer, Z., Schulz, C.J., Barlow, J.W.: Friction and wear properties of an epoxy-steel system, Wear 46 (1978) 397-403.

[119] Hokao, M., S. Hironaka, Y. Suda, Y. Yamamoto, Friction and wear properties of graphite/ glassy carbon composites, Wear 237 (2000) 54-62.

[120] Kishore, Sampathkumaran, P., Seetharamu, S., Vynatheya, S., Murali, A., Kumar, R.K.: SEM observations of the effects of velocity and load on the sliding wear characteristics of glass fabric-epoxy composites with different fillers, Wear 237 (2000) 20-27.

[121] Kishore, Sampathkumaran, P., Seetharamu, S., Murali, A., Kumar, R. K.: On the SEM features of glass-epoxy composite system subjected to dry sliding wear, Wear 247 (2001) 208-213.

[122] Bassani, R., Levita, G., Meozzi, M., Palla, G.: Friction and wear of epoxy resin on inox steel: remarks on the influence of velocity, load and induced thermal state. Wear 247 (2001) 125-132.

[123] Lee, G.Y., Dharan, C.K.H., Ritchie, R.O.: A physically-based abrasive wear model for composite materials, Wear 252 (2002) 322-331.

[124] Chung, D.D. L.: Graphite, Journal of Materials Science 37 (2002) 1475-1489.

[125] Shimbo, M., Ochi, M., Ohoyama, N.: Frictional behavior of cured epoxide resins, Wear 91 (1983) 89-101.

[126] Deutsche norm: Prüfung metallischer Werkstoffe, Universalhärteprüfung (Testing of Metallic Materials: Universal Hardness Test), DIN 50359-1, 1997.

[127] Watanabe, M., Karasawa M. and Matsubara, K.: The frictional properties of nylon, Wear 12 (1968) 185-191.

[128] Velde, F.V.D. and Baets, P.D.: The friction and wear behaviour of polyamide 6 sliding against steel at low velocity under very high contact pressures, Wear 209 (1997) 106-114.

[129] Byett, J.H. and Allen, C.: Dry sliding wear behavior of polyamide 66 and polycarbonate composites, Tribology International 25 (1992) 237-246.

[130] Apichartpattanasiri, S., Hay, J.N. and Kukureka, S.N.: A study of the tribological behavior of polyamide 66 with varying injection-moulding parameters, Wear 251 (2001) 1557-1566.

[131] Watanabe, M. and Yamaguchi, H.: The frictional and wear properties of nylon, Wear 110 (1986) 379-388.

[132] Rajesh, J.J., Bijwe, J. and Tewari, U.S.: Abrasive wear performance of various polyamides, Wear 252 (2002) 769-776.

[133] Reinicke, R., Haupert F. and Friedrich, K.: On the tribological behaviour of selected, injection moulded thermoplastic composites, Composites: Part A 29A (1998) 763-771.

[134] Bijwe, J. and Tewari, U.S., Vasudevan, P.: Friction and wear studies of polyetherimide composites, Wear 138 (1990) 61-67.

[135] Bijwe, J., Indumathi, J., Rajesh, I.J., Fahim, M.: Friction and wear behavior of polytherimide composites in various wear modes, Wear 249 (2001) 715-726.

[136] Bijwe, J., Indumathi, J., Ghosh, A.K.: On the abrasive wear behaviour of fabric-reinforced polyetherimide composites, Wear 253 (2002) 768-777.

[137] Visconti, I.C., Langella, A. and Durante, M.: The wear behaviour of composite materials with epoxy matrix filled with hard powder, Applied Composite Material 8 (2001) 179-189.

[138] Kim, K.-Y., Ye, L.: Interlaminar fracture toughness of CF/PEI composites at elevated temperature: roles of matrix toughness and fibre/matrix adhesion, Composites: Part A 35 (2004) 477-487.

[139] Váradi, K., Néder, Z., Friedrich, K., Flöck, J.: The real contact area between composite and steel surfaces in sliding contact, Composites Science and Technology 61 (2001) 1853-1862.

[140] Zhang, J., Moslehy, F.A. and Rice, S.L.: A model for friction in quasi-steady-state sliding, Part I, Derivation and Part II Numerical results and discussion Wear 149 (1991) 1-25.

[141] Blau, P.J.: The significance and use of the friction coefficient, Tribology International, 34 (2001) 585-591.

[142] Uetz, H. and Foehl, J.: Wear as an energy transformation process, Wear, 49 (1978) 253-264.

[143] Kadi, H.EL, Al-Assaf, Y.: Energy-Based fatigue life prediction of fibre-glass/epoxy composites using modular neural network, Composite 57 (2002) 85-89.

[144] Kalin, M., Vizintin, J.: Comparison of different theoretical models for flash temperature calculation under fretting conditions. Tribology International 34 (2001) 831-839.

[145] Kohan, M.I.: Nylon plastic handbook, Hanser/Gardner Publications, Inc. Cincinnati, pp. 344, 1995.

[146] Ettles, C.M.McC.: Heat generation and friction in rotating bands, ASLE Tran. 29 (1986) 312-320.

[147] Ertz, M., Knothe, K.: A comparison of analytical and numerical methods for the calculation of temperatures in wheel/rail contact, Wear 253 (2002) 489-508.

[148] Gupta, V., Hahn, G.T., Bastias, P.C., Rubin, C.A.: Calculation of the frictional heating of the locomotive wheel attending rolling plus sliding, Wear 191 (1996) 237-241.

[149] Kalin, M.: Influence of flash temperatures on the tribological behaviour in low-speed sliding: a review, Materials Science and Engineering A, 374 (2004) 390-397.

[150] Tian, X., Kennedy, F.E.: Maximum and average flash temperature in sliding contacts, ASME Journal of Tribology 116 (1994) 167-174.

[151] Greenwood, J.A., Alliston-Greiner, A.E.: Surface temperature in a fretting contact, Wear 155 (1992) 269-275.

[152] Marscher, W.D.: A critical evaluation of the flash-temperature concept. ASLE Transactions, 25 (1982) 157-161.

[153] Ettles, C.M., Hardie, C.E.: The friction of some polymers and elastomers at high values of pressure X velocity, ASME Trans. Journal of Tribology 110 (1988) 678-684.

[154] Tripathy, B.S., Furey, M.J.: Tribological behavior of unidirectional graphite-epoxy and carbon-PEEK composites, Wear 162-164 (1993) 385-396.

[155] Heilmann, P., Rigney, D.A.: An energy-based model of friction and its application to coated systems, Wear 72 (1981) 195-217.

[156] Liskiewicz, T., Fouvry, S.: Development of a friction energy capacity approach to predict the surface coating endurance under complex oscillating sliding conditions, Tribology International 38 (2005) 69-79.

[157] Fouvry, S., Kapsa, P., Vincent, L.: Quantification of fretting damage, Wear 200 (1996) 186-205.

[158] Larbi, B.C. Cherif, A., Tarres, M.A.: Improvement of the adhesive wear resistance of steel by nitriding quantified by the energy dissipated in friction, Wear 258 (2005) 712-718.

9 List of Own Publications

Refereed journal papers

1. Chang, L., Zhang, Z., Breidt, C., Friedrich, K.: Tribological properties of epoxy nanocomposites: I. Enhancement of the wear resistance by nano-TiO_2 particles, Wear 258 (2005) 141-148.
2. Chang, L., Zhang, Z., Breidt, C.: Temperature dependence on impact resistance of short fiber/particle reinforced epoxy, Applied Composite Materials 11 (2004) 1-15.
3. Chang, L., Zhang, Z.: Tribological properties of epoxy nanocomposites: II. A combinative effect of short carbon fibre and nano-TiO_2, Wear (2005) in press.
4. Chang, L., Zhang, Z., Zhang, H.: On the sliding wear of nanoparticles filled polyamide 6,6, Composites Science and Technology (2005) in press.
5. Chang, L., Zhang, Z., Zhang, H. and Friedrich, K.: Effect of nanoparticles on the tribological behaviour of short carbon fibre reinforced poly(etherimide) composites, Tribology International (2005) in press.
6. Zhang, Z., Breidt, C., Chang, L., Friedrich, K.: Wear of PEEK composites related to their mechanical performances, Tribology International, 37 (2004) 271-277.
7. Zhang, Z., Breidt, C., Chang, L., Haupert, F., Friedrich, K.: Enhancement of the wear resistance of epoxy: short carbon fibre, graphite, PTFE and nano-TiO_2, Composites A 35 (2004) 1385-1392.
8. Breidt, C., Chang, L., Zhang, Z.: Tribologische und Mechanische Eigenschaften von Nanopartikelverstarkten Verbundwerkstoffen, Tribologie und Schmierungstechnik 52 (2005) 14-17.
9. Breidt, C., Zhang, Z., Chang, L.: Haupert F: Mechanische Eigenschaften und tribologisches verhalten verstärkter Epoxidharze: Modifizierung durch Graphit, Kohlenstofffasern und PTFE resp.Nanopartikel,Tribologie und Schmierungstechnik 4 (2003) 15-17.

10. Chang, L., Zhang, Z.: Tribological properties of epoxy nanocomposites: III. Influence of solid lubricants - PTFE powders and graphite flakes, revised version to be submitted to Wear.

11. Chang, L., Zhang, Z.: Friction characteristics and wear processes in sliding contacts based on energy consideration, to be submitted to Wear

12. Chang, L., Zhang, Z., Zhang, H.: On the sliding behaviors of nanoparticles filled high temperature resistant polymers, in preparation.

Conference/symposium proceedings

13. Chang, L., Zhang, Z., Zhang, H.: Enhancement of the tribological properties of fibre-reinforced polyamide 66 by TiO_2 nanoparticles, IVW-Kolloquium 2004, IVW-Schriftenreihe Band 48, 5.-6. Oktober 2004, pp. 183-188.

14. Chang, L., Zhang, Z., Zhang, H.: Tribological properties of TiO_2 particle filled polyetherimide composites, Europe/China Symposium on Reinforced Polymers, June 29-July 2, 2004, the Ecole des Mines in Nancy, France, CD-ROM.

15. Chang, L., Zhang, Z., Zhang, H.: The enhancement of the tribological properties of fibre-reinforced polyamide 6,6 by TiO_2 nanoparticles, 11th European Conference on Composite Materials (ECCM 11), May 31- June 3, 2004, Rhodes, Greece, CD-ROM.

16. Chang, L., Zhang, Z., Zhang, H.: Enhancement of nano-TiO_2 particle filled high temperature resistant polymers, 2005 China International Conference on Nanoscience and Technology (ChinaNano2005), June 9 - 11, 2005 Beijing, China.